

# Numerical stabilization for multidimensional coupled convection-diffusion-reaction equations

***Citation for published version (APA):***

Hernandez, H. A. (2017). *Numerical stabilization for multidimensional coupled convection-diffusion-reaction equations: applications to continuum dislocation transport*. [Phd Thesis 1 (Research TU/e / Graduation TU/e), Mechanical Engineering]. Technische Universiteit Eindhoven.

***Document status and date:***

Published: 13/09/2017

***Document Version:***

Publisher's PDF, also known as Version of Record (includes final page, issue and volume numbers)

***Please check the document version of this publication:***

- A submitted manuscript is the version of the article upon submission and before peer-review. There can be important differences between the submitted version and the official published version of record. People interested in the research are advised to contact the author for the final version of the publication, or visit the DOI to the publisher's website.
- The final author version and the galley proof are versions of the publication after peer review.
- The final published version features the final layout of the paper including the volume, issue and page numbers.

[Link to publication](#)

***General rights***

Copyright and moral rights for the publications made accessible in the public portal are retained by the authors and/or other copyright owners and it is a condition of accessing publications that users recognise and abide by the legal requirements associated with these rights.

- Users may download and print one copy of any publication from the public portal for the purpose of private study or research.
- You may not further distribute the material or use it for any profit-making activity or commercial gain
- You may freely distribute the URL identifying the publication in the public portal.

If the publication is distributed under the terms of Article 25fa of the Dutch Copyright Act, indicated by the "Taverne" license above, please follow below link for the End User Agreement:

[www.tue.nl/taverne](http://www.tue.nl/taverne)

***Take down policy***

If you believe that this document breaches copyright please contact us at:

[openaccess@tue.nl](mailto:openaccess@tue.nl)

providing details and we will investigate your claim.

# Numerical stabilization for multidimensional coupled convection-diffusion-reaction equations

*Applications to continuum dislocation transport*

PROEFSCHRIFT

ter verkrijging van de graad van doctor aan de Technische Universiteit  
Eindhoven, op gezag van de rector magnificus prof.dr.ir. F.P.T. Baaijens,  
voor een commissie aangewezen door het College voor Promoties, in het  
openbaar te verdedigen op woensdag 13 september 2017 om 14:00 uur

door

Héctor Hernández

geboren te Irapuato, Mexico

Dit proefschrift is goedgekeurd door de promotoren en de samenstelling van de promotiecommissie is als volgt:

voorzitter:	prof.dr. L.P.H. de Goeij
1 <sup>e</sup> promotor:	prof.dr.ir. M.G.D Geers
2 <sup>e</sup> promotor:	prof.dr.ir. T.J. Massart (Université libre de Bruxelles (ULB))
copromotor:	dr.ir. R.H.J. Peerlings
leden:	prof.dr. J.G.M. Kuerten
	prof.dr.rer.nat. R. Svendsen (RWTH Aachen University)
	prof.dr.ir. G. Degrez (Université libre de Bruxelles (ULB))
	prof.dr.ir. H. Deconinck (Université libre de Bruxelles (ULB))

Het onderzoek dat in dit proefschrift wordt beschreven is uitgevoerd in overeenstemming met de TU/e Gedragscode Wetenschapsbeoefening.

*A mis padres Mónico y María Elena*  
*A mis hermanas Ana y Carmen*



A catalogue record is available from the Eindhoven University of Technology Library.  
ISBN: 978-90-386-4346-5

Cover design by Anastasija Mass.  
Printed by Gildeprint, Enschede, The Netherlands.

© Copyright, 2017, Hector Alonso Hernandez Velazquez.

All rights reserved. No part of this publication may be reproduced, stored in a retrieval system, or transmitted, in any form or by any means, electronic, mechanical, photocopying, recording or otherwise, without prior permission of the author.

The research described in this thesis has been funded by the European Commission through an *Erasmus Mundus* grant in the framework of the *Simulation in Engineering and Entrepreneurship Development* program.

# Abstract

Partial differential equations having diffusive, convective and reactive terms appear naturally in the modeling of a large variety of processes of practical interest in several branches of science such as biology, chemistry, economics, physics, physiology and materials science. Moreover, in some instances several species or components interact with each other requiring to solve strongly coupled systems of convection-diffusion-reaction equations. Of special interest for us is the numerical treatment of the advection dominated continuum dislocation transport equations used to describe the plastic behavior of crystalline materials.

Analytical solutions for such equations are extremely scarce and practically limited to linear equations with homogeneous coefficients and simple initial and boundary conditions. Therefore, resorting to numerical approximations is the most affordable and often the only viable strategy to deal with such models. However, when classical numerical methods are used to approximate the solutions of such equations, even in the simplest one dimensional case in the steady state regime for a single equation, instabilities in the form of node to node spurious oscillations are found when the convective or reactive terms dominate over the diffusive term.

To address such issues, stabilization techniques have been developed over the years in order to handle such transport equations by numerical means, overcoming the stability difficulties. However, such stabilization techniques are most often suited for particular problems. Additionally, no extensive work has been carried out for systems of coupled equations. The reason for this immaturity is the lack of a maximum principle when going from a single transport equation towards systems of coupled equations.

The main aim of this work is to present a stabilization technique for systems of coupled multidimensional convection-diffusion-reaction equations based on coefficient perturbations. These perturbations are optimally chosen in such a way that certain compatibility conditions analogous to a maximum principle are satisfied. Once the computed perturbations are injected in the classical Bubnov-Galerkin finite element method, they provide smooth and stable numerical approximations.

Such a stabilization technique is first developed for the single one-dimensional convection-diffusion-reaction equation. Rigorous proof of its effectiveness in rendering

unconditionally stable numerical approximations with respect to the space discretization is provided for the convection-diffusion case via the fulfillment of the discrete maximum principle. It is also demonstrated and confirmed by numerical assessments that the stabilized solution is consistent with the discretized partial differential equation, since it converges to the classical Bubnov-Galerkin solution if the mesh Péclet number is small enough. The corresponding proofs for the diffusion-reaction and the general convection-diffusion-reaction cases can be obtained in a similar manner. Furthermore, it is demonstrated that this stabilization technique is applicable irrespective of whether the advective or the divergence form is used for the spatial discretization, making it highly flexible and general. Subsequently the stabilization technique is extended to the one-dimensional multiple equations case by using the superposition principle, a well-known strategy used when solving non-homogeneous second order ordinary differential equations. Finally, the stabilization technique is applied to mutually perpendicular spatial dimensions in order to deal with multidimensional problems.

Applications to several prototypical linear coupled systems of partial differential equations, of interest in several scientific disciplines, are presented. Subsequently the stabilization technique is applied to the continuum dislocation transport equations, involving their non-linearity, their strongly coupled character and the special boundary conditions used in this context; a combination of additional difficulties which most traditional stabilization techniques are unable to deal with. The proposed stabilization scheme has been successfully applied to these equations. Its effectiveness in stabilizing the classical Bubnov-Galerkin scheme and being consistent with the discretized partial differential equation are both demonstrated in the numerical simulations performed. Such effectiveness remains unaffected when different types of dislocation transport models with constant or variable length scales are used.

These results allow envisioning the use of the developed technique for simulating systems of strongly coupled convection-diffusion-reaction equations with an affordable computational effort. In particular, the above mentioned crystal plasticity models can now be handled with reasonable computation times without the use of extraordinary computational power, but still being able to render accurate and physically meaningful numerical approximations.

# Contents

Abstract . . . . .	v
<b>1 Introduction</b>	<b>1</b>
1.1 Motivation . . . . .	1
1.2 Objectives . . . . .	3
1.3 Structure of the thesis . . . . .	4
<b>2 Stabilization of One-Dimensional Continuum Dislocation Transport</b>	<b>5</b>
2.1 Introduction . . . . .	6
2.2 Continuum model for dislocation transport . . . . .	7
2.2.1 Governing equations . . . . .	8
2.2.2 Boundary and initial conditions . . . . .	10
2.3 Stabilization by perturbation in finite element approximation . . . . .	11
2.3.1 Spatial discretization . . . . .	11
2.3.2 Stabilization by coefficient perturbation . . . . .	13
2.3.3 Accounting for non-linearity . . . . .	18
2.4 Computational assessment of the stabilization scheme . . . . .	19
2.4.1 Influence of the applied stress . . . . .	21
2.4.2 Influence of the mesh size . . . . .	22
2.4.3 Time evolution . . . . .	26
2.5 Conclusion and outlook . . . . .	29
<b>3 Stabilization of Coupled Convection-Diffusion-Reaction Equations</b>	<b>30</b>
3.1 Introduction . . . . .	31
3.2 Problem definition and finite element discretization . . . . .	34
3.3 Stabilization by coefficient perturbation . . . . .	36
3.3.1 Extension to systems of coupled equations . . . . .	36
3.3.2 Particularization to uncoupled sets of equations . . . . .	39
3.4 Applications and computational assessment . . . . .	40
3.4.1 Convection-diffusion system . . . . .	41
3.4.2 Diffusion-reaction system . . . . .	43
3.4.3 Convection-diffusion-reaction system . . . . .	46
3.5 Comparison with other techniques . . . . .	49
3.5.1 Convection-diffusion system . . . . .	52
3.5.2 Diffusion-reaction system . . . . .	52
3.5.3 Convection-diffusion-reaction system . . . . .	53
3.6 Conclusions and outlook . . . . .	55

<b>4</b>	<b>Applications to Coupled Continuum Dislocation Transport Equations</b>	<b>57</b>
4.1	Introduction . . . . .	58
4.2	Continuum model for dislocation transport . . . . .	60
4.2.1	Governing equations . . . . .	60
4.3	Computational assessment of the stabilization technique . . . . .	61
4.3.1	Influence of the applied stress . . . . .	64
4.3.2	Influence of the discretization . . . . .	66
4.3.3	Non-linear and time evolution adaptivity . . . . .	69
4.3.4	Models and length scale comparison . . . . .	73
4.4	Rearrangement of convection and diffusion matrices . . . . .	74
4.5	Conclusions and outlook . . . . .	76
<b>5</b>	<b>Multidimensional Extension</b>	<b>81</b>
5.1	Introduction . . . . .	82
5.2	Problem definition and finite element discretization . . . . .	84
5.2.1	Multidimensional extension of the stabilization technique . . . . .	86
5.3	Applications and computational assessment . . . . .	87
5.3.1	Convection-diffusion system . . . . .	89
5.3.2	Diffusion-reaction system . . . . .	93
5.3.3	Convection-diffusion-reaction system . . . . .	94
5.4	Comparison with other techniques . . . . .	98
5.4.1	Convection-diffusion system . . . . .	98
5.4.2	Diffusion-reaction system . . . . .	100
5.4.3	Convection-diffusion-reaction system . . . . .	100
5.5	Conclusions and outlook . . . . .	100
<b>6</b>	<b>Stabilized Two-dimensional Strain-Gradient Plasticity</b>	<b>104</b>
6.1	Introduction . . . . .	105
6.2	Two-dimensional dislocation transport . . . . .	106
6.3	Mechanical equilibrium . . . . .	107
6.4	Algorithmic coupling of transport and equilibrium problems . . . . .	108
6.5	Computational assessment . . . . .	109
6.5.1	Problem description . . . . .	111
6.5.2	Results . . . . .	112
6.6	Conclusions and outlook . . . . .	115
<b>7</b>	<b>Conclusions and Outlook</b>	<b>117</b>
7.1	Results discussion . . . . .	117
7.2	Further developments . . . . .	118
7.2.1	Numerical methods . . . . .	118
7.2.2	Crystal plasticity . . . . .	119
	Bibliography . . . . .	121

# Chapter 1

## Introduction

This chapter defines the motivation and objectives of the present work. This is done giving a general overview of the state of the art of the two main topics this work touches, namely *numerical stability for convection-diffusion-reaction equations* and *crystal plasticity based on continuum dislocation transport*. It also provides a summary of the work carried out during the research project which resulted in the present manuscript. The final section is entirely devoted to outlining the general structure of this thesis.

### 1.1 Motivation

Partial differential equations involving diffusive, convective and reactive terms appear naturally in the modelling of a large variety of processes of practical interest in several branches of science such as biology, chemistry, economics, physics, physiology and materials science. Moreover, in some instances several species or components interact with each other, leading to strongly coupled systems of convection-diffusion-reaction equations [3–6, 14, 15, 17, 18, 30, 37, 45, 70, 71, 84].

Of special interest in this thesis are the continuum dislocation transport equations used to describe the plastic behaviour of crystalline materials at the meso-scale. This interest originates in the fact that an accurate description of the plastic behaviour of materials is of paramount importance in materials science applications. For crystalline solids, inelastic effects have been taken into account at the level of single crystals by various types of crystal plasticity models. Among these, models based on dislocation transport equations are appealing because they establish a link with the true physical process underlying the plasticity, i.e. glide of dislocations [42]. For efficiency, these frameworks are formulated in terms of dislocation densities, rather than dislocations as individual entities, resulting in a continuum description. The resulting transport equations consist of a set of coupled, transient, and non-linear partial differential equations, involving spatial derivatives of the dislocation densities of both first and second order [21, 28, 31, 32, 32, 36, 66, 79, 85, 86].

Analytical solutions for convection-diffusion-reaction equations are extremely scarce and practically limited to linear equations with homogeneous coefficients and simple initial and boundary conditions, even in the single equation case. Therefore, resorting to numerical approximations is the most affordable and often the only viable strategy to deal with these models. However, when classical numerical methods are used to approximate the solutions, even in the simplest one dimensional case, in the steady state regime, for a single equation, instabilities in the form of node to node spurious oscillations are found when the convective or reactive terms dominate over the diffusive term [26, 63, 73, 76, 81, 82, 87].

To address these numerical instabilities for the single equation case, stabilization techniques have been developed over the years [7, 13, 23, 27, 33, 41, 43, 44, 56, 57, 60, 87]. The vast majority of these stabilization techniques, which have been developed in the context of the finite element method, focus on the numerical approximation of the Navier-Stokes equations or other sets of equations in fluid dynamics. Many of them borrow ideas originating from finite difference and finite volume methods [7, 23, 24, 44, 87]. However, such stabilization techniques are most often suited for particular problems. Additionally, no extensive work has been carried out for coupled systems of equations. The reason for this immaturity is the lack of a maximum principle when going from a single transport equation towards coupled systems of equations [1, 12, 62].

Despite the aforementioned progress in fluid dynamics, in solid mechanics in general, and in mechanics of materials in particular, extensive and fine tuned application of such stabilization techniques has been developed only recently. The numerical difficulties mentioned above are particularly cumbersome when working with continuum dislocation transport equations because of their intrinsic transient, non-linear and convection-dominated nature. Their mutual coupling and the special types of boundary conditions with which they are supplied add even more difficulty in their numerical approximation [31, 36]. Most simulations of continuum dislocation transport problems reported in the literature use extremely refined discretizations, thus largely avoiding the problem. Some results however appear to nevertheless show traces of spurious oscillations in the solutions, which may be associated to the instability problem caused by convection-like terms present in the systems of equations to be discretized [21, 85, 86]. The use of extremely fine discretizations is evidently not sustainable when going to more realistic multi-dimensional problems due to their high computational cost.

Important progress has been recently achieved by applying some well-known stabilization techniques like pure up-winding in the finite volume method context, Galerkin/least-squares, and exponential filtering for a spectral method to dislocation transport problems. It has been found in the first case that pure up-winding tends to cause over diffusion [50] while in the two latter cases the artificial diffusion is controlled by a damping parameter, which needs to be calibrated [20, 79]. A special effort is therefore required in order to transfer the concepts and techniques nowadays standard in the fluid dynamics community towards the mechanics of materials community. For these reasons, a specific stabilization technique fitting the special characteristics of the system of partial differential equations for dislocation transport must be developed.

## 1.2 Objectives

In view of the difficulties previously mentioned for general systems of coupled convection-diffusion-reaction equations, and in particular for the equations governing continuum dislocation transport, two main goals have been pursued during the development of this work as reported in the present thesis. The first main goal is to develop a stabilization technique for systems of coupled multidimensional convection-diffusion-reaction equations based on coefficient perturbations. These perturbations are optimally chosen in such a way that certain compatibility conditions analogous to a maximum principle are satisfied. Once the computed perturbations are injected in the classical Bubnov-Galerkin finite element method, they provide smooth and stable numerical approximations of a perturbed problem that resembles as much as possible the original problem at hand. It is important to remark that the main motivation for the development of this stabilization technique is its application to the continuum dislocation transport equations, in view of the difficulties encountered when dealing with them, especially the avoidance of extremely fine discretizations which in turn lead to excessively demanding computations. This application represents the second main goal of the present work.

While pursuing these two main goals, several issues having profound scientific significance can be clearly identified. They are captured in the following research questions, which this thesis aims to thoroughly answer.

1. Is it possible to construct an unconditionally stable numerical scheme with respect the spatial discretization which is efficient for both the advective and divergence forms of the convection-diffusion-reaction equation?
2. How to apply such a technique to the case of transient, non-linear and heterogeneous continuum dislocation transport equations?
3. How to cope with the different dislocation transport models available in the literature? In other words, is it possible to develop a stabilization technique being at the same time general but also highly versatile?
4. Is it possible to develop a methodology allowing the stabilization of systems of coupled convection-diffusion-reaction equations instead of only a single equation?
5. How to extend the stabilization technique to multi-dimensional domains?
6. How does the stabilization technique cope with two-dimensional crystal plasticity based on continuum dislocation transport?



## 1.3 Structure of the thesis

The remainder of this manuscript reflects the way in which the results have been obtained during the research project. This implies that the complexity of the problems addressed increases chapter by chapter.

- **Chapter 2.** The next chapter presents the development of a stabilization technique for the simplest of the situations of interest in this work, namely for the single one-dimensional convection-diffusion-reaction equation. Subsequently, the stabilization technique is applied to the convection dominated continuum dislocation transport equations and its performance is assessed through a thorough numerical assessment.
- **Chapter 3.** The stabilization technique is extended to the case of a system of coupled one-dimensional differential equations by using the superposition principle, a well-known strategy used when solving non-homogeneous second order ordinary differential equations by analytical means. Three problems coming from different scientific fields are considered in order to test the effectiveness of the stabilization technique in treating systems of coupled convection-diffusion-reaction equations.
- **Chapter 4.** Once the stabilization technique has been extended to coupled systems of equations, it is well suited for the numerical treatment of the continuum dislocation transport equations irrespective of the variables used or the modelling assumptions considered. This application is presented in this chapter. It is carried out using a set of field variables for which the stabilization technique originally developed in Chapter 2, prior to the rigorous extension to coupled systems of equations, cannot successfully be employed.
- **Chapter 5.** This chapter pursues the extension of the stabilization technique from one-dimensional to two-dimensional configurations. The three-dimensional case is also discussed in this chapter. Applications to several prototypical linear coupled systems of partial differential equations, of interest in several scientific disciplines, are presented.
- **Chapter 6.** The stabilization technique, already extended to coupled systems of equations in multi-dimensional domains, is next applied to the continuum dislocation transport equations this time coupled with the mechanical equilibrium equations in two-dimensional domains.
- **Chapter 7.** This closing chapter presents the main conclusions of this work. It also discusses some of the drawbacks still to be overcome and suggests directions for further improvement of the methodology and its analysis.

## Chapter 2

# Stabilization of One-Dimensional Continuum Dislocation Transport

---

### Abstract

Recent developments in plasticity modeling for crystalline materials are based on dislocations transport models, formulated for computational efficiency in terms of their densities. This leads to sets of coupled partial differential equations in a continuum description involving diffusion and convection-like processes combined with non-linearity. The properties of these equations cause the most traditional numerical methods to fail when applied to solve them. Therefore, dedicated stabilization techniques must be developed in order to obtain physically meaningful and numerically stable approximations. The objective of this chapter is to present a dedicated stabilization technique and to apply it to a system of dislocation transport equations in one dimension. This stabilization technique, based on coefficient perturbations, successfully provides unconditional stability with respect to the spatial discretization. Several of its favorable characteristics are discussed, providing evidence of its versatility and effectiveness through a thorough numerical assessment.

**keywords.-** Crystal plasticity, Dislocation transport, Stabilized finite element method.

---

---

This chapter is based on: [Hernández H.](#), Massart T.J., Peerlings R.H.J., and Geers M.G.D. 2015. *Towards an unconditionally stable numerical scheme for continuum dislocation transport*. Modelling and Simulation in Materials Science and Engineering, **23**, No. 8.

## 2.1 Introduction

The accurate description of the plastic behaviour of materials is of paramount importance in engineering applications. For crystalline solids, inelastic effects have been taken into account at the level of single crystals by various crystal plasticity models [66]. At a higher spatial resolution, plasticity in a single crystal can be modelled using dislocation transport equations [21, 32, 36].

For efficiency, such frameworks are formulated in terms of dislocation densities, rather than dislocations as individual entities, resulting in a continuum description. The transport equations consist of a set of coupled, transient, and non-linear partial differential equations, involving derivatives in space of both first and second order [31, 32]. The simultaneous presence of both order derivatives of transported densities complicates the numerical treatment of such systems of equations; especially when the first order convection-like term dominates the second order diffusion-like term.

When classical numerical schemes, such as centred finite differences or Bubnov-Galerkin finite elements, are used to approximate the solution of such transport problems (combining convection and diffusion), spurious and non-physical oscillations appear, rendering the numerical approximation unstable. Hence, stabilization approaches must be used in order to get physically meaningful and numerically stable approximations. In the wider finite element context, several stabilization techniques have been proposed; e.g. the Streamline Upwind Petrov-Galerkin method [7, 41], the Galerkin Least-Squares method [27], the bubble multi-scale stabilization method [60], the sub-grid method [33], and the finite calculus-based approach [56, 57]. The vast majority of these techniques deals mainly with convection dominated cases [23, 87]. The addition of a reaction term can also cause numerical instabilities by itself, even in the absence of convection. Alternative stabilization techniques have also been developed to deal with the general convection-diffusion-reaction equation with diffusion being the weakest transport mechanism [13, 43, 44].

In spite of the success of the existing stabilization techniques, the direct and straightforward application of the Streamline Upwind Petrov-Galerkin method, by far the most popular stabilization technique, does not remedy the instability of the numerical approximation for the system of equations treated in this chapter if applied as originally proposed [87]. This is associated with the non-standard way in which integration by parts in the weak form is performed; which is necessary in order to be able to apply physically meaningful boundary conditions, as will be explained in the sequel. However, significant progress has recently been made in order to overcome this difficulty [13, 23]. Some well-known stabilization techniques like pure up-winding in the finite volume method context and Galerkin/least-squares have been successfully applied to dislocation transport problems. It has been found in the former case that pure up-winding tends to cause over diffusion [50] while in the latter case the artificial diffusion is controlled by a damping parameter to be calibrated [79]. For these reasons, a specific stabilization technique fitting the special characteristics of the system of partial differential equations for dislocation transport must be developed.

The development of such a tailor-made stabilization technique and its application to the dislocation density transport equations is the aim of this chapter. This will be achieved by enforcing the discrete maximum principle [12, 73, 80], which is the translation of the continuous maximum principle related to the physics of the problem. This continuous maximum principle, in its simplest form, establishes that in the absence of sources and sinks (including reaction terms) the solution of a second order differential equation has no maxima other than at the boundaries [62]. Furthermore, it will also be shown, and confirmed numerically, that the stabilized finite element approximation converges to that of the classical Bubnov-Galerkin scheme if the mesh Péclet number is small enough. For transparency, we limit our development to the one-dimensional problem of parallel, infinite straight edge dislocations which glide under the influence of an applied shear stress. The approach followed can however easily be extended to more complex, multidimensional situations, since the main numerical difficulty, the convection-dominance, remains the same.

The chapter is organized as follows. In Section 2.2 the physical problem, illustrated through the shearing of an infinite crystal, is sketched. Its translation, based on some simplifying assumptions, into a system of partial differential equations is presented next. Special attention is paid to the formulation of boundary conditions; their physical meaning and the mathematical implications are discussed in detail. Section 2.3 is devoted to the numerical approximation of the system of partial differential equations by the finite element method, and to the development of a stabilization technique for the steady state linear convection-diffusion-reaction equation with constant coefficients in one spatial dimension. Unconditional stability and consistency of the stabilization technique for the convection-diffusion case are discussed. At the end of this section, the non-linearity in the second order derivative term is taken into account and its effect on the proposed stabilization technique is discussed. Section 2.4 assesses the stabilization technique through three numerical examples. The first one focuses on demonstrating the effectiveness of the stabilization technique, the second one investigates its consistency, and in the last example detailed results concerning the time evolution are presented. Finally, Section 2.5 presents the main conclusions of this chapter and discusses some future developments to be considered.

## 2.2 Continuum model for dislocation transport

The main focus of this chapter is the development of an efficient stabilization technique for modeling dislocation transport in a single crystal. In these models, the governing equations are typically written in terms of dislocations densities on glide planes. The total dislocation density on a particular plane is defined as the total length of dislocation line per unit crystal volume [36, 42]. We consider a single glide system with infinite parallel edge dislocations. Positive and negative dislocations densities, denoted respectively by  $\rho^+$  and  $\rho^-$ , rather than the more traditional total dislocation density  $\rho = \rho^+ + \rho^-$  and geometrically necessary dislocation density  $\kappa = \rho^+ - \rho^-$  are used. This choice is made since  $\rho^+$  and  $\rho^-$  have the same physical interpretation and therefore the same restrictions, e.g. both must be non-negative. Moreover, the final system of partial differential equations obtained when using positive and negative

dislocation densities shows a symmetric structure with respect to the terms differentiated in space. Interactions between dislocations of opposite sign such as annihilation, will not be taken into account for the sake of simplification. Positive and negative dislocations are therefore assumed to move on independent glide planes. As an idealization, an infinite medium is considered in the direction perpendicular to the glide planes and, it is subjected to a shear stress  $\tau$ . This configuration is depicted in Figure 2.1, together with the boundary conditions to be satisfied by the dislocation fluxes as described in detail later. Whereas this particular system is obviously simplified, it is expected that the stability analysis carried out here carries over to more general cases as well.

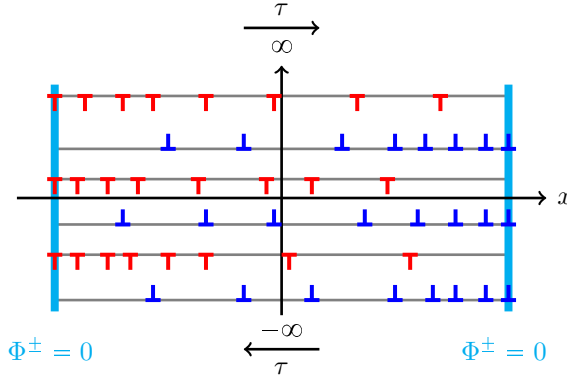


Figure 2.1: Positive and negative dislocations in independent glide planes bounded by impenetrable barriers.

The stress  $\tau$  causes the positive dislocations to pile-up at the right of the glide plane while negative dislocations do the same at the left. Typical solutions will exhibit boundary layers at the extremities of the spatial domain as shown with solid lines in Figure 2.2 for positive and negative dislocations densities in blue and red, respectively. Nevertheless, the numerical approximation of the solution by classical finite elements suffers from spurious oscillations, as shown with dashed lines in the same figure. The smooth and physically meaningful result can be obtained using stabilization techniques tailored to the system of equations under investigation, as will be developed in the sequel.

### 2.2.1 Governing equations

The system of equations describing the dislocation transport in the considered configuration can be written as the general conservation equation

$$\frac{\partial \rho}{\partial t} + \frac{\partial}{\partial x} (\Phi) = s, \quad (2.1)$$

where  $\rho$  is a generic dislocation density to be transported and conserved,  $\Phi$  is its flux and  $s$  is its corresponding source term.

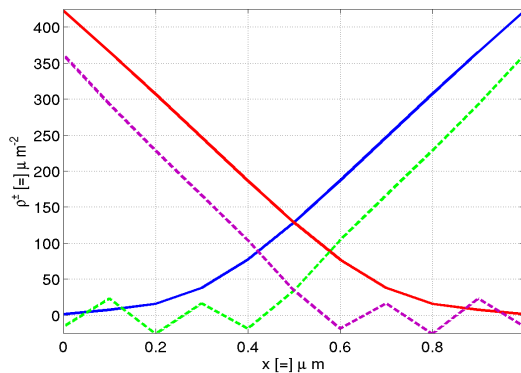


Figure 2.2: Pile-up of positive and negative dislocations densities. Classical finite element solutions (dashed) with spurious oscillations; smooth and non-negative stabilized solutions (solid).

This equation can be particularized for positive and negative dislocation densities to get the pair of conservation equations

$$\frac{\partial \rho^+}{\partial t} + \frac{\partial}{\partial x} (\Phi^+) = s^+, \quad (2.2)$$

$$\frac{\partial \rho^-}{\partial t} + \frac{\partial}{\partial x} (\Phi^-) = s^-, \quad (2.3)$$

with source terms  $s^+$  and  $s^-$  for positive and negative dislocations densities respectively. Note that one would generally have  $s^+ = s^-$  and that this source may depend on  $\rho^+$  and  $\rho^-$ . The corresponding fluxes can be expressed as

$$\Phi^+ = \rho^+ v^+, \quad \text{and} \quad \Phi^- = \rho^- v^-, \quad (2.4)$$

where  $v^+$  and  $v^-$  are the velocities of positive and negative dislocations. These velocities can be obtained by an averaging process along a single glide plane, of the Peach-Koehler forces experienced by each dislocation considering a constant drag coefficient  $B$ . This force originates from the externally applied forces and the forces induced by the interactions with other dislocations. After performing such averaging in the infinite medium considered here, the velocities can be expressed as [21, 31, 32]

$$v^\pm = \pm \frac{b\tau}{B} - \mathcal{L}^2 \frac{\bar{G}b^2}{6B} \left[ (b'_1 + b'_2) \frac{\partial \rho^\pm}{\partial x} + (b'_1 - b'_2) \frac{\partial \rho^\mp}{\partial x} \right]. \quad (2.5)$$

in which the first term is classical and the second accounts for the internal stress due to the presence of dislocation density gradients. In this expression,  $b$  is the Burgers vector length,  $\bar{G} = G/(2(1 - \nu))$  is a material constant and  $\tau$  is the externally applied shear stress. Finally  $\mathcal{L}$  denotes the length scale. Note that setting  $\mathcal{L} = h$ , with  $h$  being the glide plane vertical spacing, leads to constant length scale models. By setting  $\mathcal{L} = 1/\sqrt{\rho^+ + \rho^-}$  variable length scale models are obtained. Two constants,

$b'_1 = (2 + a)b_1$  and  $b'_2 = (2 - a)b_2$ , have been introduced in order to allow addressing several dislocation transport models presented in the literature. If only interactions between dislocation of the same sign are taken into account, then  $a = 0$ ; otherwise  $a = 1$ . Moreover, by taking  $b_1 = 1$  and  $b_2 = 1$ , models of the same type as the model presented in [21] are obtained. On the other hand, taking  $b_1 = 0$  and  $b_2 = 12/(2 - a)$  leads to models like the one presented in [32]. The superscript  $\pm$  is used to denote velocities of both positive and negative dislocations in a single expression. To compact subsequent manipulations the following constants are introduced

$$C_0 = \frac{b\tau}{B}, \quad \text{and} \quad C_1 = \frac{\bar{G}b^2}{12B}, \quad (2.6)$$

which allows expressing the positive and negative fluxes generically as

$$\Phi = \rho \left\{ \hat{C}_0 - C_1 \mathcal{L}^2 \left[ (b'_1 + b'_2) \frac{\partial \rho}{\partial x} + (b'_1 - b'_2) \frac{\partial \hat{\rho}}{\partial x} \right] \right\}, \quad (2.7)$$

in which the constant  $\hat{C}_0$  is simply  $C_0$  when used with Equation (2.2) and  $-C_0$  when used in Equation (2.3). Similarly  $\hat{\rho}$  is  $\rho^+$  when used with Equation (2.3) and  $\rho^-$  when used with Equation (2.2). With these conventions it is now possible to work directly on the general conservation Equation (2.1) without the need to refer to any particular form as in the Equations (2.2-2.3).

The substitution of the generic flux given by Equation (2.7) in the conservation Equation (2.1) leads to a system of two transient and non-linear partial differential equations for which analytical solutions are not available [75]. Therefore, a numerical approximation is required for which the finite element method will be used in the next section.

## 2.2.2 Boundary and initial conditions

From the physical viewpoint, two types of boundary conditions have to be considered. The first one consists of a free surface where dislocations can escape, causing their corresponding density to vanish, i.e.  $\rho^\pm = 0$ . This corresponds to Dirichlet boundary conditions for the conservation Equation (2.1). Conversely, in other cases the boundary corresponds to an impenetrable barrier for the dislocations, e.g. a grain or phase boundary. This situation is shown in Figure 2.1 and can be stated as  $\Phi^\pm|_\Gamma = 0$ . Note that this corresponds to a coupled mixed boundary condition since, as is clear from Equation (2.7), the corresponding dislocation density and the normal derivatives of both dislocation densities across the boundary are involved.

In order to mathematically close the system of partial differential equations describing the dislocation transport, it must be supplemented with proper initial conditions that correspond with a distribution of the positive and negative dislocation densities on the whole spatial domain at the initial time, i.e.  $\rho_0^\pm(\Omega) = \rho^\pm(\Omega, t = 0)$ .

## 2.3 Stabilization by perturbation in finite element approximation

This section focuses on the development of a stabilization technique in the context of the finite element method, fitting the special requirements and features of the system of partial differential equations for dislocation transport.

For the sake of simplicity, all the discussion and subsequent developments shall be carried out first using a generic linear conservation equation. The non-linearity in the second order derivative and its effects on the stabilization technique are discussed at the end of this section.

### 2.3.1 Spatial discretization

The point of departure is a linear conservation equation with a reaction term of the form

$$\frac{\partial u}{\partial t} + \frac{\partial}{\partial x} (F) + \gamma u = f, \quad (2.8)$$

where  $u$  is the physical quantity to be transported,  $F$  its corresponding flux,  $\gamma \in \mathbb{R}$  is the reaction coefficient and  $f \in \mathbb{R}$  the source term.

It will be assumed that the flux is composed of a diffusive and a convective contribution, corresponding to two different physical transport phenomena, i.e.

$$F = -\alpha \frac{\partial u}{\partial x} + \beta u, \quad (2.9)$$

where  $\alpha \in \mathbb{R}^+$  is the diffusion coefficient and  $\beta \in \mathbb{R}$  is the convection coefficient. Throughout this section all coefficients will be regarded as constants. The direct substitution of the flux given by Equation (2.9) in the general conservation Equation (2.8) leads to

$$\frac{\partial u}{\partial t} + \frac{\partial}{\partial x} \left( -\alpha \frac{\partial u}{\partial x} + \beta u \right) + \gamma u = f, \quad (2.10)$$

which will be referred to as the *divergence* form of the conservation equation due to the fact that integration over the whole domain gives, via the divergence theorem, the total flux across the boundary.

Expanding the spatial derivative on the terms composing the flux gives

$$\frac{\partial u}{\partial t} + \frac{\partial}{\partial x} \left( -\alpha \frac{\partial u}{\partial x} \right) + \beta \frac{\partial u}{\partial x} + \gamma u = f, \quad (2.11)$$

Equation (2.11) will be referred to as the *advective* form because of the direct interpretation of the first spatial derivative term which represents convection.



Multiplying Equation (2.8) by a weighting function  $w$ , and integrating over the whole spatial domain, one obtains the weak form

$$\int_{\Omega} w \frac{\partial u}{\partial t} d\Omega + \int_{\Omega} w \frac{\partial}{\partial x} (F) d\Omega + \int_{\Omega} w \gamma u d\Omega = \int_{\Omega} w f d\Omega, \quad (2.12)$$

By integrating by parts the second term in the left hand side one obtains

$$\int_{\Omega} w \frac{\partial u}{\partial t} d\Omega - \int_{\Omega} \frac{\partial w}{\partial x} F d\Omega + \int_{\Gamma} w F d\Gamma + \int_{\Omega} w \gamma u d\Omega = \int_{\Omega} w f d\Omega. \quad (2.13)$$

Note that integration by parts on the whole flux is seldom done in the context of a finite element solution for fluid problems. Instead, integration by parts is most often only performed on the terms differentiated up to the second order, i.e. the advective form (2.11) is preferred over the divergence form (2.10). Here, integration by parts is performed on the whole flux term in order to easily handle the boundary condition corresponding to an impenetrable wall, which involves the total flux at the boundary, and not only its diffusive part, i.e. the divergence form (2.10) will be used in what follows.

The boundary integral term in Equation (2.13), accommodates naturally the required essential and natural boundary conditions. The first case corresponds to Dirichlet boundary conditions on  $u$ , for which we choose the weighting function  $w$  to vanish at this portion of the boundary, that is  $w(\Gamma_D) = 0$ . The second type of boundary condition of interest is a homogeneous Robin boundary condition which prevents the flow of the conserved quantity  $u$  out the spatial domain; i.e.  $F(\Gamma_R) = 0$ . In both cases the boundary integral in Equation (2.13) vanishes and hence it will be omitted in the sequel.

To discretize Equation (2.13), the weighting function  $w$  and the transport variable  $u$  are expressed as linear combinations of their corresponding nodal values using trial and shape functions  $W_k$  and  $P_k$  associated with the  $n_e$  nodes within each finite element as follows

$$w = \sum_{k=1}^{n_e} W_k w_k \quad \text{and} \quad u = \sum_{k=1}^{n_e} P_k u_k. \quad (2.14)$$

After evaluation of the element integrals, the element matrices are assembled to obtain a global discretized system of the form

$$\mathbf{M} \dot{\mathbf{u}} + (\mathbf{D} + \mathbf{C} + \mathbf{R}) \mathbf{u} = \mathbf{f}, \quad (2.15)$$

where  $\mathbf{M}$  is the mass matrix,  $\mathbf{D}$  is the diffusion matrix,  $\mathbf{C}$  is the convection matrix and  $\mathbf{R}$  is the reaction matrix.  $\mathbf{u}$  is a vector containing the nodal values of the transported quantity to be approximated, where the superimposed dot implies differentiation in time. Finally  $\mathbf{f}$  takes into account the source term  $f$  and boundary conditions.

Using a Bubnov-Galerkin approach, with  $P_k = W_k$ , and after discretization in time of Equation (2.15) by a two-step finite difference scheme, physically meaningful solutions can be obtained when the coefficients related to convection  $\beta$  and reaction

$\gamma$  are small with respect to the diffusion coefficient  $\alpha$  on a sufficiently fine mesh. This corresponds to a diffusion dominated problem. Yet for many physical situations this diffusion dominance may not be present. For instance, in the absence of reaction ( $\gamma = 0$ ) and for a convection coefficient  $\beta$  that is not small compared to the diffusion coefficient  $\alpha$ , the problem is dominated by convection. In the latter case, oscillations appear when  $\beta$  is increased or when the mesh is coarsened, polluting the quality of the numerical approximation, a problem that becomes more pronounced as  $\beta$  increases [23, 24, 87].

### 2.3.2 Stabilization by coefficient perturbation

The oscillation phenomenon described in Section 2.3.1 is caused by the fact that the classical Bubnov-Galerkin method applied to the considered partial differential equations does not satisfy the discrete maximum principle [12, 43], which would guarantee uniform convergence of the finite element approximation. A stabilization technique is therefore required in order to get physically meaningful approximations.

Several of these stabilization techniques are available in the literature [7, 13, 27, 33, 41, 44, 56, 57, 60]. The vast majority developed in the context of the finite element method, focus on the numerical approximation of the Navier-Stokes or other set of equations in fluid dynamics. Many of these techniques borrow ideas originating from finite difference and finite volume methods [7, 23, 24, 44, 87].

The most extensively used technique, the Streamline-Upwind Petrov-Galerkin approach, denoted SUPG, is based on a modification of the weighting functions by the addition of a perturbation proportional to the gradient of the interpolation functions. The magnitude of the perturbation depends on the Péclet number, that measures the relative importance of convection over diffusion [7, 43]. Modifying the weighting functions proportional to the gradient of the interpolation functions in the present case, where integration by parts is applied on the whole flux, including first order terms, makes the SUPG technique inactive if applied in a straightforward manner, as implemented in [87]. This is due to the fact that this implementation of SUPG has been originally designed for problems in which integration by parts is applied only on the terms differentiated up to second order, i.e. when working with the advective form (2.11) as usually done in the finite element method for fluid related problems. When using integration by parts on the whole flux with the divergence form (2.10), one can note that if linear interpolation functions are used in one dimension, the SUPG modification of the weighting functions vanishes and has no significant effect.

To deal with the discretization of Equation (2.13), an alternative stabilization technique is developed next. It is based on adding a perturbation to the problem coefficients in order to obtain a numerical approximation free of oscillations. This is achieved by enforcing the numerical scheme to satisfy the discrete maximum principle [7, 12, 43]. Due to the complexity of the original problem at hand (involving non-linearity in both the first and second order spatial derivatives, with two different coupled variables in a transient state), the intended stabilization technique is first investigated for a simplified linear Dirichlet boundary value problem in divergence form

defined as follows

$$\frac{\partial}{\partial x} \left( -\alpha \frac{\partial u}{\partial x} + \beta u \right) + \gamma u = f \quad \text{in} \quad \Omega = (0, 1), \quad (2.16)$$

$$u(x=0) = u_0 \quad \text{and} \quad u(x=1) = u_1, \quad (2.17)$$

where  $\alpha \in \mathbb{R}^+$  is the diffusion coefficient,  $\beta \in \mathbb{R}$  is the convection coefficient, and  $\gamma \in \mathbb{R}^+$  is the reaction coefficient. Finally,  $f$  stands for a source term.

After discretization of Equation (2.16) with a Bubnov-Galerkin approach as in the previous section, using a uniform mesh with element length  $\ell$  and linear shape functions, the stencil corresponding to the  $i$ -th node, or more precisely the  $i$ -th row of the corresponding matrix equation, is given by

$$-\left(\frac{\alpha}{\ell} + \frac{\beta}{2} - \frac{\gamma\ell}{6}\right)u^{(i-1)} + \left(\frac{2\alpha}{\ell} + \frac{4\gamma\ell}{6}\right)u^{(i)} - \left(\frac{\alpha}{\ell} - \frac{\beta}{2} - \frac{\gamma\ell}{6}\right)u^{(i+1)} = \ell f_i. \quad (2.18)$$

In order to establish a stable numerical scheme, the stencil (2.18) must satisfy the discrete maximum principle [12, 43], which in turns requires that the coefficient matrix must be diagonally dominant by rows with non-positive off-diagonal entries [67, 80], that is

$$\sum_{j=1}^n a_{ij} \geq 0, \quad \forall \quad i = 1, \dots, n, \quad (2.19)$$

$$a_{ij} \leq 0, \quad \forall \quad i, j = 1, \dots, n; \quad i \neq j \quad (2.20)$$

$\mathbf{A} \in \mathbb{R}^{n \times n}$  being the coefficient matrix obtained after assembly of the element matrices. According to (2.19-2.20), the numerical scheme will be stable only if the physical coefficients and the element size satisfy the following inequality

$$\frac{\alpha}{\ell} - \frac{|\beta|}{2} - \frac{\gamma\ell}{6} \geq 0. \quad (2.21)$$

The starting point in the development of the stabilization technique is the fact that the numerical scheme presented above does not satisfy the discrete maximum principle, and is therefore unstable for the actual combination of physical coefficients  $\alpha$ ,  $\beta$ , and  $\gamma$  and element size  $\ell$ . Instead of enforcing Inequality (2.21) by mesh refinement, the solution will be approximated by a modified, though similar, problem to the one defined by Equations (2.16-2.17) for which it is known *a priori* that it is stable. By construction, the difference between these two problems lies exclusively in the value of the physical coefficients  $\alpha$ ,  $\beta$ , and  $\gamma$ ; the essential form of the differential operators, source terms and boundary conditions remain unchanged.

The modification of the physical coefficients defines a perturbed problem, as it will be referred to hereafter, with respect to the actual problem to approximate. According to this terminology we define the perturbed coefficients as

$$\tilde{c} = c + c^*, \quad \text{with} \quad c = \alpha, \beta, \gamma, \quad (2.22)$$

where the tilde is used to refer to the perturbed coefficients, and the asterisk to the coefficient perturbations.

The perturbed problem is now discretized as previously done for the original one, with the only difference that the perturbed coefficients are used instead. After assembly, the  $i$ -th stencil of the matrix equation is extracted and rearranging terms, one obtains

$$-\frac{\tilde{\alpha}}{\ell} \left( u^{(i-1)} - 2u^{(i)} + u^{(i+1)} \right) - \frac{\tilde{\beta}}{2} \left( u^{(i-1)} - u^{(i+1)} \right) + \frac{\tilde{\gamma}\ell}{6} \left( u^{(i-1)} + 4u^{(i)} + u^{(i+1)} \right) = \ell f_i. \quad (2.23)$$

The coefficient perturbations now have to be selected in a way that the stencil given by Equation (2.23) does satisfy the discrete maximum principle. As an additional constraint, the problem defined by these perturbations is required to be as close as possible to the original problem, i.e. the minimal perturbations have to be found that render the perturbed problem stable.

This minimization is achieved by resorting to the exact solution of the homogeneous differential equation associated to the convection-diffusion-reaction Equation (2.16)

$$u(x) = Ae^{\lambda_1 x} + Be^{\lambda_2 x}, \quad (2.24)$$

where the constants  $A$  and  $B$  depend only on the boundary conditions, and where  $\lambda_{1,2}$  are the roots of the characteristic polynomial defined by Equation (2.16) in the homogeneous case as given by

$$\lambda_{1,2} = \frac{\beta}{2\alpha} \pm \sqrt{\left(\frac{\beta}{2\alpha}\right)^2 + \frac{\gamma}{\alpha}}. \quad (2.25)$$

This exact solution is used by evaluating it at the three equidistant nodes, i.e. at  $x_{i-1}$ ,  $x_i$  and  $x_{i+1}$ , defining the finite element stencil (2.18)

$$u^{(i)} = Ae^{\lambda_1 x_i} + Be^{\lambda_2 x_i}, \quad \text{and} \quad u^{(i\pm 1)} = Ae^{\lambda_1 x_i} e^{\pm \lambda_1 \ell} + Be^{\lambda_2 x_i} e^{\pm \lambda_2 \ell}, \quad (2.26)$$

and injecting these evaluations in the perturbed stencil given by Equation (2.23), in order to recover the exact values at the nodes. After some elementary algebra, the following expression is obtained

$$\begin{aligned} & \frac{\tilde{\alpha}}{\ell} \{ Ae^{\lambda_1 x_i} [1 - \cosh(\lambda_1 \ell)] + Be^{\lambda_2 x_i} [1 - \cosh(\lambda_2 \ell)] \} + \\ & \frac{\tilde{\beta}}{2} \{ Ae^{\lambda_1 x_i} \sinh(\lambda_1 \ell) + Be^{\lambda_2 x_i} \sinh(\lambda_2 \ell) \} + \\ & \frac{\tilde{\gamma}\ell}{6} \{ Ae^{\lambda_1 x_i} [2 + \cosh(\lambda_1 \ell)] + Be^{\lambda_2 x_i} [2 + \cosh(\lambda_2 \ell)] \} = 0. \end{aligned} \quad (2.27)$$

Two independent equations can be obtained from this general expression. The first one is obtained by choosing suitable boundary conditions in order to get  $B = 0$ . By changing the boundary conditions such that  $A = 0$ , a second equation can be generated. Together, these two equations form an under-determined system for the

three perturbed coefficients, which reads as follows

$$\frac{\tilde{\alpha}}{\ell} [1 - \cosh(\lambda_1 \ell)] + \frac{\tilde{\beta}}{2} \sinh(\lambda_1 \ell) + \frac{\tilde{\gamma} \ell}{6} [2 + \cosh(\lambda_1 \ell)] = 0, \quad (2.28)$$

$$\frac{\tilde{\alpha}}{\ell} [1 - \cosh(\lambda_2 \ell)] + \frac{\tilde{\beta}}{2} \sinh(\lambda_2 \ell) + \frac{\tilde{\gamma} \ell}{6} [2 + \cosh(\lambda_2 \ell)] = 0. \quad (2.29)$$

Note that these two equations represent a linear system with three unknowns for which normalization (by pre-multiplication by its coefficient matrix transpose) is not useful due to its homogeneity. As a consequence it is not feasible to perturb the three physical coefficients at once. Therefore, one of the perturbations is arbitrarily set to zero and the others are determined by solving the remaining  $2 \times 2$  linear system.

In order to illustrate the effectiveness of this stabilizing scheme, a simplified version of Equations (2.16-2.17) is considered with  $\gamma = 0$ . This is the convection-diffusion problem, when convection is dominant. The stability condition for the original, non-perturbed problem according to Inequality (2.21) then reads

$$\text{Pe} \stackrel{\text{def}}{=} \frac{\beta \ell}{2\alpha} \leq 1, \quad (2.30)$$

where Pe is the mesh Péclet number. The roots of the characteristic polynomial associated with the partial differential equation are then

$$\lambda_1 = \lambda = \frac{\beta}{\alpha} \quad \text{and} \quad \lambda_2 = 0, \quad (2.31)$$

and therefore, the system of the two Equations (2.28-2.29) degenerates into a single equation that states the relationship to be satisfied among the perturbed convection and diffusion coefficients as

$$\frac{\tilde{\alpha}}{\ell} [1 - \cosh(\lambda \ell)] + \frac{\tilde{\beta}}{2} \sinh(\lambda \ell) = 0. \quad (2.32)$$

This under-determined equation is solved by setting one of the coefficient perturbations to zero, allowing to extract the other perturbation in terms of the actual convection and diffusion coefficients.

If the diffusion coefficient is perturbed, i.e. if  $\beta^* = 0$  is imposed, the diffusion perturbation is obtained as

$$\alpha^* = \alpha \text{Pe} [\coth(\text{Pe}) - \text{Pe}^{-1}]. \quad (2.33)$$

Note that Equation (2.33) resembles the well-known artificial diffusion formula used in the SUPG implementations [23, 24, 87]. Note that this function is strictly non-negative, has a single root when  $\text{Pe} = 0$ , and is symmetric around it. This means that, for unstable problems the diffusion is artificially increased to have a stable solution. If only diffusion is present in the original problem, the diffusion perturbation vanishes and the stabilization technique does not introduce any effect, as expected. Moreover,

the strictly positive character matches the fact that diffusion always acts in the same manner towards all directions. Finally, it can be verified that the discrete maximum principle is indeed fulfilled after perturbing the diffusion coefficient by evaluating Inequality (2.21) with the perturbed diffusion  $\tilde{\alpha}$  instead of the actual diffusion  $\alpha$ . This yields

$$\coth(\text{Pe}) \geq 1, \quad (2.34)$$

a condition that is always satisfied for any value of  $\text{Pe}$  by definition, which means that unconditional stability is guaranteed.

Note that another choice can be made for the perturbations by setting  $\alpha^* = 0$  and perturbing the convection coefficient. In this case the corresponding perturbation will be given by

$$\beta^* = \beta \text{Pe}^{-1} [\tanh(\text{Pe}) - \text{Pe}]. \quad (2.35)$$

Again, this function has a single root at  $\text{Pe} = 0$ . This time,  $\beta^*$  is odd in  $\beta$ . This agrees with the fact that convection is directional and can be reversed. This function introduces an artificial convection velocity but this time in the direction opposite to the actual physical velocity, i.e. it reduces the convective velocity. When choosing convection to be perturbed, evaluating Inequality (2.21) yields

$$\tanh(\text{Pe}) \leq 1, \quad (2.36)$$

which is also always satisfied.

Equations (2.34) and (2.36) confirm that the proposed methodology furnishes an unconditionally stable linear steady state convection-diffusion equation irrespective of the coefficients perturbed. The artificial diffusion formula used for the SUPG stabilization method can be obtained as a special case of the present stabilization technique. The proofs of unconditional stability for the diffusion-reaction case, with  $\beta = 0$ , can also be obtained by similar developments. The situation in which all three physical mechanisms are acting is more intricate, but it is possible to demonstrate that it is also unconditional stable. Details for the two latter cases have been omitted here for brevity.

Note that, after spatial discretization on a uniform mesh, the advective form given by Equation (2.10) and the divergence form given by Equation (2.11) both lead to the same stencil for the  $i$ th node. In other words, the  $i$ -th row of the coefficient matrix given by Equation (2.18) will be the same irrespective of the form chosen. Since the stabilization technique developed here is based precisely on the use of this stencil, the method proposed is useful irrespective of the form used in the spatial discretization.

As a closing remark for the present section, it is emphasized that the stability problem is inherent to the numerical scheme, and not to the physical problem, when applied on a particular mesh. When the mesh is refined, i.e.  $\ell \rightarrow 0$ , the magnitude of the coefficient perturbations go to zero, irrespective of the magnitude of the physical coefficients, as is clear from Equations (2.33-2.35) for the convection-diffusion case. The same applies to the diffusion-reaction and the convection-diffusion-reaction cases.

This means that the stabilized scheme proposed here is consistent since, as the mesh is sufficiently refined, perturbation is not required because the original problem is already stable.

### 2.3.3 Accounting for non-linearity

The terms involving the non-linearity in the conservation Equations (2.2-2.3) after substitution of the corresponding fluxes given by Equation (2.7) are non-standard with respect to those encountered in fluid dynamics applications. For instance, the Navier-Stokes Equations for Newtonian fluids include non-linearity in the convective term, which is first order in space [24]. Still in the fluids community, the equations modeling the fluid flow with a free surface through a porous medium or heat transfer with temperature dependent conductivity incorporate non-linear diffusion [2, 22, 46]. In the present case, the non-linearity is present in both the convective and diffusive terms.

The non-linearity in the second order, diffusion term is examined here, still in a simplified problem similar to the one given by Equation (2.16). The non-linear convection-diffusion-reaction equation in steady state regime then reads

$$-\alpha \frac{\partial}{\partial x} \left( u \frac{\partial u}{\partial x} \right) + \beta \frac{\partial u}{\partial x} + \gamma u = f \quad \text{in} \quad \Omega = (0, 1), \quad (2.37)$$

which after discretization using the Bubnov-Galerkin finite element method leads to the  $i$ -th stencil on a uniform mesh

$$-\left( \frac{u^{(i-1)}}{2} \frac{\alpha}{\ell} + \frac{\beta}{2} - \frac{\gamma \ell}{6} \right) u^{(i-1)} + \left( \frac{u^{(i)}}{2} \frac{2\alpha}{\ell} + \frac{4\gamma \ell}{6} \right) u^{(i)} - \left( \frac{u^{(i+1)}}{2} \frac{\alpha}{\ell} - \frac{\beta}{2} - \frac{\gamma \ell}{6} \right) u^{(i+1)} = \ell f_i. \quad (2.38)$$

Diagonal dominance, which has to be satisfied in order to fulfil the discrete maximum principle, requires

$$\gamma \ell - \frac{\alpha}{2\ell} \left( u^{(i-1)} - 2u^{(i)} + u^{(i+1)} \right) \geq 0, \quad (2.39)$$

while the remaining two conditions to be satisfied in order to fulfil Inequalities (2.19-2.20) now read

$$\frac{\alpha}{\ell} \frac{u^{(i-1)}}{2} - \frac{\beta}{2} + \frac{\gamma \ell}{6} \geq 0, \quad \text{and} \quad \frac{\alpha}{\ell} \frac{u^{(i+1)}}{2} + \frac{\beta}{2} + \frac{\gamma \ell}{6} \geq 0. \quad (2.40)$$

For the convection-diffusion case with  $\gamma = 0$ , from Inequality (2.39) it is required that

$$\frac{\partial^2 u}{\partial x^2} \approx \frac{u^{(i-1)} - 2u^{(i)} + u^{(i+1)}}{\ell^2} \leq 0. \quad (2.41)$$

and

$$C_{off} \stackrel{\text{def}}{=} \frac{\beta \ell}{u^{(m)} \alpha} \leq 1, \quad \text{with} \quad u^{(m)} = \min_{i \in \mathcal{I}} u^{(i)}, \quad (2.42)$$

$\mathcal{I} = \{ i \mid x_i \in \Omega \}$  being the set of nodes defining the finite element mesh, with  $u^{(m)}$  the minimum nodal value of the approximated solution in the spatial domain, and  $C_{off}$  the off-diagonal coefficient associated with the  $i$ -th stencil.

The analogy of condition (2.42) on  $C_{off}$  with the corresponding one for the Péclet number defined by Inequality (2.30) is obvious and allows defining a point-wise effective diffusion coefficient as

$$\alpha_e = \frac{1}{2} u^{(i)} \alpha. \quad (2.43)$$

Note that coercitivity and ellipticity of the second order differential operator is retained if  $u^{(i)} > 0$ , a condition that should be satisfied for dislocation density variables.

Using this effective diffusion coefficient in the stabilization technique defined in Section 2.3 allows one to extend it to the non-linear convection-diffusion-reaction Equation (2.37). This can be explained by the fact that the stabilization technique works in an element-wise fashion, that is, the stability problem is treated at each element independently, regardless of all other elements in the mesh, instead of trying to face the stability problem as a global one. The proposed stabilization technique can therefore be used on irregular meshes, an appreciable feature for future extensions to multidimensional problems. Moreover, spatially variable convection, diffusion, and reaction coefficients may also be considered.

This also ensures that in each element the perturbation introduced, which is responsible for a deviation from the original problem to the perturbed problem that is actually approximated, is the lowest possible ensuring stable numerical approximations. Furthermore, the magnitude of the perturbation decreases if the mesh is refined.

## 2.4 Computational assessment of the stabilization scheme

This section presents some numerical examples which illustrate the efficiency and consistency of the developed stabilization technique applied to the dislocation transport system given by Equations (2.2-2.3). In particular, a constant length scale model including interactions between dislocations of different sign is considered. Thus  $\mathcal{L} = h$  and  $a = 1$ . Additionally  $b_1$  and  $b_2$  have been both set equal to one.

In order to apply the stabilization technique based on the linear steady state convection-diffusion-reaction equation with constant coefficients and its non-linear extension to the dislocation transport equations, the generic flux of dislocations given by Equation (2.1) is directly substituted in the general dislocation density conservation Equation (2.2):

$$\frac{\partial \rho}{\partial t} + \frac{\partial}{\partial x} \left[ \left( \hat{C}_0 - 2C_1 h^2 \frac{\partial \hat{\rho}}{\partial x} \right) \rho - 4C_1 h^2 \rho \frac{\partial \rho}{\partial x} \right] = s, \quad (2.44)$$

in which terms acting as a convection-like coefficient and a diffusion-like coefficient can be identified as

$$\beta(\hat{\rho}) = \hat{C}_0 - 2C_1 h^2 \frac{\partial \hat{\rho}}{\partial x} \quad \text{and} \quad \alpha(\rho) = 4C_1 h^2 \rho. \quad (2.45)$$



This reveals the analogy between the dislocations transport Equation (2.1) and the convection-diffusion-reaction Equation (2.16), and therefore enables a direct application of the stabilization technique developed. Note that this analogy can always be established irrespective of the model's type used (as those presented in [21] or [32]), of the length scale selected (constant or variable) and irrespective of whether the interactions between dislocations of different sign are included or neglected.

To incorporate the transient character of the problem, the fully implicit backward Euler method has been used for time integration. This scheme is unconditionally stable with respect to time (step size  $\Delta t$ ) and the spectral properties of the matrices appearing in Equation (2.15), despite having only first order accuracy [2, 19, 38, 49, 63].

For all simulations, the Picard iterative method is used to deal with the non-linear system of equations obtained after discretization of the dislocation transport equations at each time step [51, 59, 63, 64]. The difference among two successive approximations is measured as

$$d^{(j)} = \|\rho_t^{(j)} - \rho_t^{(j-1)}\|_2, \quad (2.46)$$

where  $j$  is the iteration number, and the sub-index  $t$  is used to emphasize the current time step. The iteration is stopped as soon as the tolerance  $\epsilon_n = 10^{-6}$  is reached, that is,  $d^{(j)} < \epsilon_n$ . The initial guess is always taken as the final approximation at the previous time step:  $\rho_{t+\Delta t}^{(0)} = \rho_t^{(j)}$ .

At each non-linear iteration, a linear system of equations has to be solved. For this purpose the *BiCGStab* method has been used having in mind a future multidimensional extension of the framework which leads very large and sparse systems [67, 77, 78]. In all cases, the maximum number of allowed iterations is set equal to the size of the linear system, although the iteration process is stopped as soon as  $\|\mathbf{r}^{(k)}\|/\|\mathbf{b}\| < \epsilon_s = 10^{-6}$  is reached, with  $\mathbf{r}^{(k)}$  the  $k$ -th residual vector and  $\mathbf{b}$  the right hand side vector. The final approximation of the previous iteration is always taken as the initial guess for the linear solver. No preconditioning is used.

The physical parameters have been taken constant for the ease of comparison. The values used correspond to those presented by [50] and are comparable to those used in [21]. The domain considered has unit length  $L = 1 \mu m$ , and a single material has been used on the whole domain. Its properties are as follows;  $h = 0.1 \mu m$ ,  $b = 0.0003 \mu m$ ,  $B = 10^{-4} Pa s$ ,  $\nu = 1/3$ ,  $G = 25 GPa$ . The initial condition for all problems was chosen as  $\rho_0^\pm = 200 \mu m^{-2}$ . Finally, the time step is the same for all simulations and equals  $\Delta t = 10^{-1} \mu s$ .

Only the applied stress  $\tau$ , the mesh size  $\ell$ , and the final time  $T_f$  are modified during this study. Once they are chosen for a particular problem they are not changed, i.e. for a particular simulation the applied stress is constant over the whole domain which is discretized with a uniform mesh.

Even though the precise definition of a mesh Péclet number is not possible due to the non-linear nature of the dislocation transport problem, see Expression (2.45), for each simulation it is computed using the data corresponding to the initial condition, and according to Equation (2.30) as

$$\text{Pe} = \frac{C_0 \ell}{4C_1 \rho_0}, \quad (2.47)$$

where it has been assumed that  $\partial \hat{\rho} / \partial x = 0$  and  $\rho = \rho_0$  in the Equations (2.45). Note that this is the most conservative situation. As the computation evolves in time and dislocation transport takes place, negative dislocations pile up at the left boundary of the spatial domain and thus the corresponding spatial density gradient will be negative, which increases the magnitude of the convection-like term for positive dislocations  $\beta^+(\rho^-)$  as can be seen from the first Equation in (2.45). Likewise, positive dislocations pile up in the opposite direction, leaving the left part of the spatial domain causing a decrease of the diffusion-like term for positive dislocation density  $\alpha^+(\rho^+)$ , see the second Equation in (2.45). Thus, as the simulations advance in time it is expected that the stabilization technique will play a more prominent role, making this initial mesh Péclet number, as defined by Equation (2.47) only useful for comparative purposes.

### 2.4.1 Influence of the applied stress

In this first example, the focus is mainly on the effectiveness of the stabilization technique developed. To this aim, three different cases are computed, all using the same uniform coarse mesh of 50 linear elements. Only the applied stress is increased in each of the cases, taking the values  $\tau = 0.1, 1.0$ , and  $10.0$  GPa. Note that the last value ( $10.0$  GPa) is never encountered in a real physical situation, and is considered here for the purpose of investigating the effectiveness of the stabilization technique under extreme conditions. The corresponding initial mesh Péclet numbers are  $\text{Pe} = 0.2667, 2.6667$ , and  $26.6667$ .

Figure 2.3 shows the results in terms of positive and negative dislocation densities in blue and red respectively. The results obtained with the classical Bubnov-Galerkin method are depicted in the left column, while the right column shows the results with the stabilization technique. These numerical schemes are referred to as *classical* and *stabilized* respectively.

Note that even in the first case depicted in the top row of Figure 2.3, for a small applied stress with an initial Péclet number lower than unity, saw-tooth-like wiggles appear in the regions of the spatial domain where dislocations densities are close to zero. This effect pollutes the numerical approximation since the nodal densities at some points are negative, which has no physical meaning. The numerical approximation obtained with the stabilization scheme, as shown on the right, is smooth, non-negative, and free of any oscillation.

The results for the second case with  $\tau = 1.0$  GPa are shown in the middle row of Figure 2.3. In this case the initial mesh Péclet number is larger than one, and

this range matches practical applications. On the left, corresponding to the classical scheme, the oscillations are much larger than in the previous case, making the numerical approximation completely useless for any application. This effect is due to the fact that the convective character of the problem, evaluated in the initial condition, has been increased by one order of magnitude. In other words, the true mesh Péclet number in the pile-up regions is considerably higher than the estimate based on the initial data. The corresponding stabilized result is shown on the right in the middle row. It does not exhibit any wiggle or oscillation and the densities are non-negative on the whole space domain. As expected, the width of the boundary layer is decreased and dislocation densities reach higher values compared to the case with a lower applied stress.

By increasing the initial convection even more by one order of magnitude, the amplitude of the oscillations observed in the classical scheme continues to increase. These oscillations become so severe that the obtained numerical approximations for both positive and negative dislocation densities grow unboundedly. The corresponding plot for this case, shown at the left on the bottom row, depicts the approximation at an early time instance, the last at which a solution could still be obtained. Upon using the stabilized scheme, the numerical approximation is again non-negative and free of oscillations. Due to the high convection conjugated with the non-linearity, sharp inflections are obtained close to the boundary layers. Note that a solution obtained at earlier time than the ones corresponding for lower stresses is here depicted. At this time, the steady state has already been reached. This is due to the high applied stress leading to a quick formation of dislocation pile-up at the boundaries of the spatial domain.

### 2.4.2 Influence of the mesh size

The purpose of the second example is to illustrate the behavior of the stabilization technique under mesh refinement. Therefore, the element size  $\ell$  is progressively reduced and the applied stress is kept constant and equal to  $\tau = 0.01$  GPa. The choice of this limited stress value in this example is to prevent the sudden formation of boundary layers. The obtained numerical approximations at two different time instances are analyzed.

In each plot in Figure 2.4, the positive and negative dislocation densities profiles obtained with the classical Bubnov-Galerkin and the stabilized schemes appear together. Dashed lines are used for the classical Bubnov-Galerkin scheme, green for positive dislocations and purple for negative ones. Approximations obtained with the stabilized scheme are plotted with continuous lines, in blue for positive and red for negative dislocations. The results were obtained using meshes of 10, 50, 100, and 500 elements with linear shape functions. The plots at the left are those corresponding to  $t = 10^6 \mu s$  while the ones at the right are the corresponding snapshots at  $t = 10^7 \mu s$ .

Note that at  $t = 10^6 \mu s$ , the numerical approximations do not reveal any undesirable behavior irrespective of the scheme used. This is due to the fact that a low convection is present in the problem and more importantly, the fact that both dislocation densities

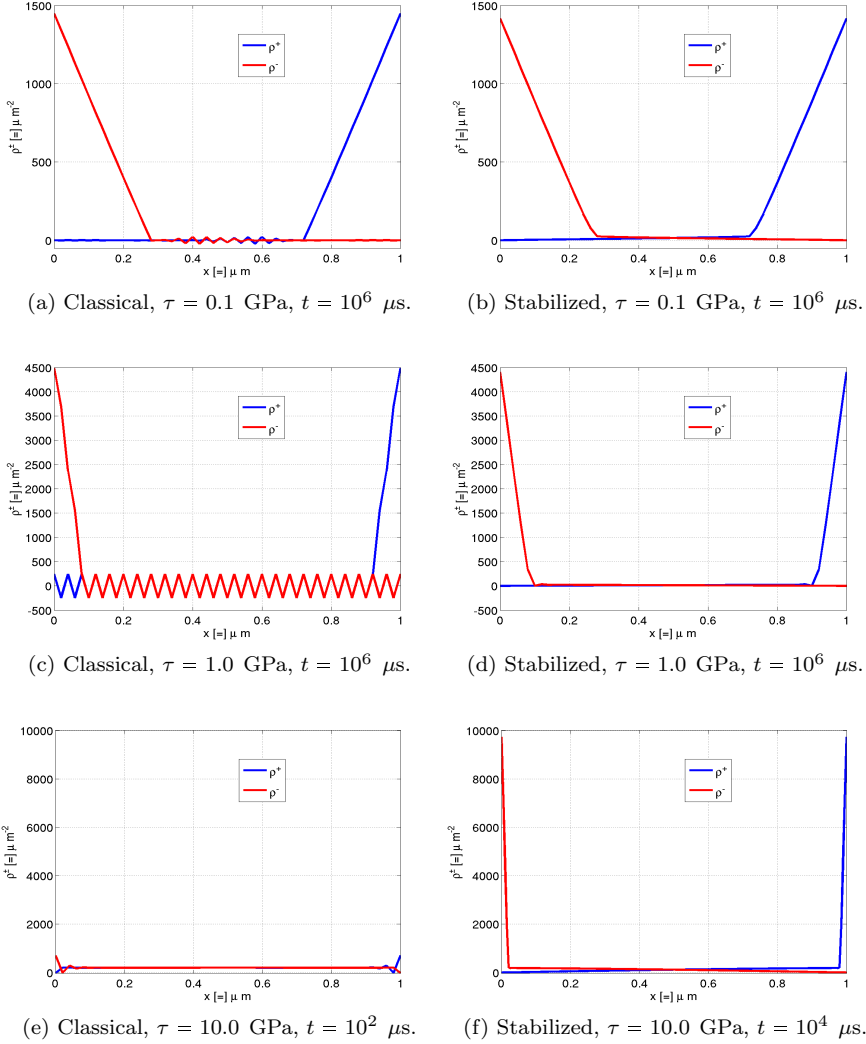


Figure 2.3: Comparison of positive and negative dislocation densities  $\rho^\pm$  obtained with the classical (left) and stabilized (right) scheme, increasing the applied stress  $\tau$  from top to bottom.

are far away from zero. Therefore, the effective diffusion (given by the first equation in (2.45)), does not decrease significantly and the problem remains diffusion dominated.

As the simulation evolves until  $t = 10^7$   $\mu$ s (right column in Figure 2.4), it is observed that dislocations pile-ups tend to form at the extremities of the spatial domain, thereby causing a decrease of the corresponding densities at the opposite boundary. This generates instabilities due to the reduction of the effective diffusion. This time all the results obtained with the classical Bubnov-Galerkin scheme become unstable even

when using the finest mesh, while the results obtained with the stabilized scheme all remain stable.

Results for other stress levels are omitted since they do not provide other information. Note that for some cases, none of the results obtained with the classical Bubnov-Galerkin scheme were free of spurious oscillations, while those obtained with the stabilized scheme were still smooth, non-negative, and free of oscillations.

These results confirm that the presented stabilization technique is effective when needed. If spurious oscillations are not present because the problem is not dominated by convection or the mesh is fine enough, the effect of the stabilization is negligible.

In terms of computing time, for the same discretization, the use of the stabilization technique practically doubles the elapsed time with respect to the Bubnov-Galerkin scheme for cases in which the latter still furnishes physically meaningful results. This increase does not depend significantly on mesh refinement or on the applied stress level. One nevertheless expects a significant gain in computational efficiency, because using the stabilization technique allows to coarsen the mesh drastically compared with the classical formulation.

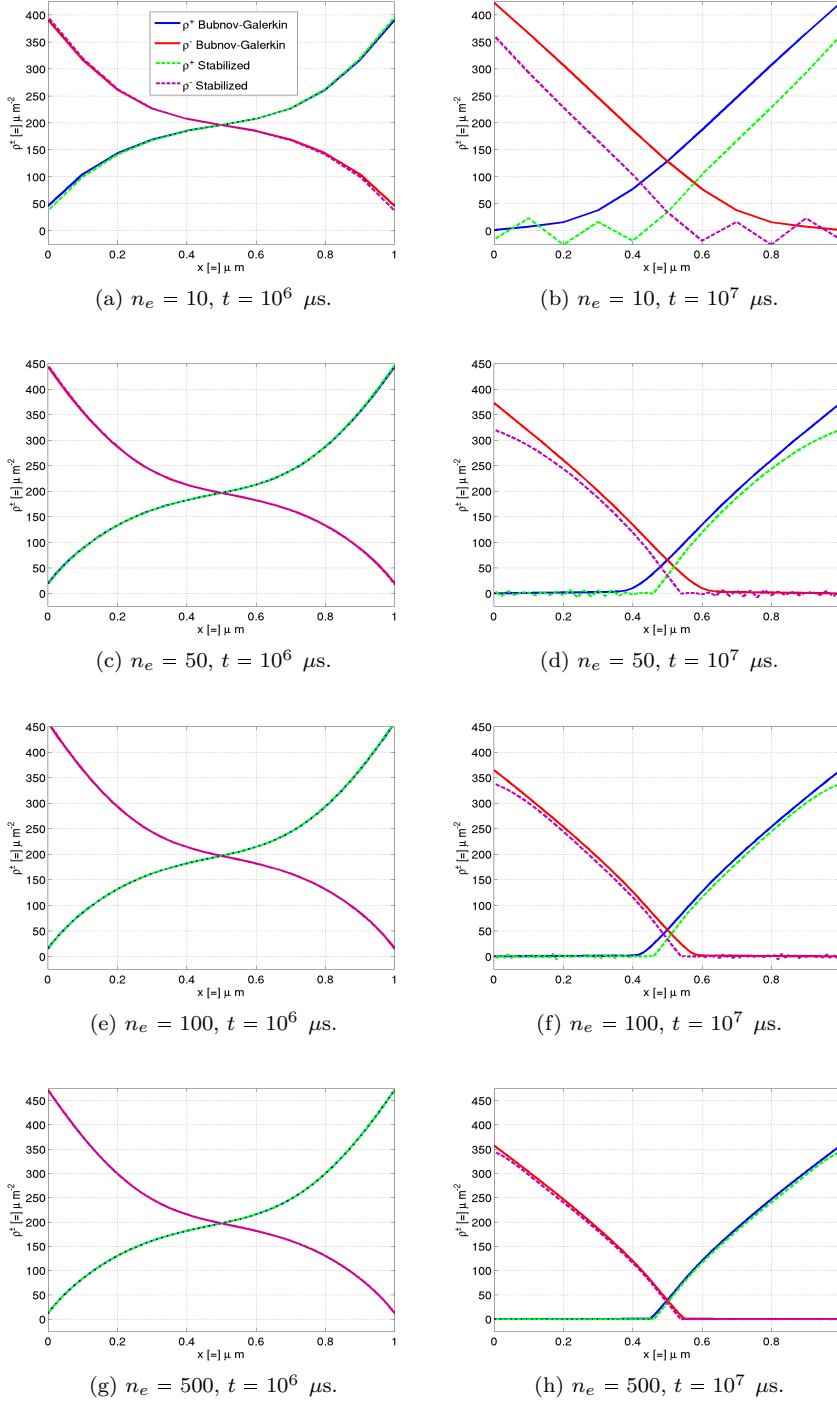


Figure 2.4: Positive and negative dislocations densities  $\rho^\pm$  obtained with the classical and stabilized scheme at two different time instances (left and right) with applied stress  $\tau = 0.01$  GPa, increasing the number of elements (top to bottom).

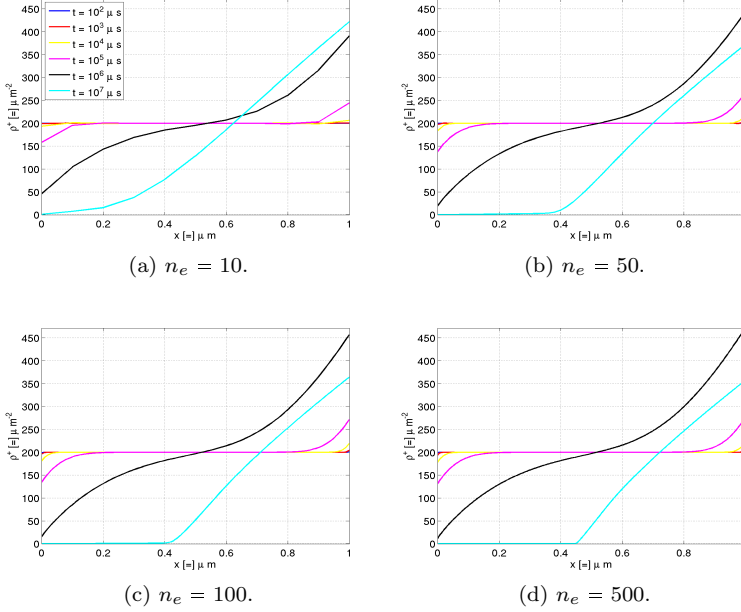


Figure 2.5: Comparison of positive dislocation density  $\rho^+$  evolution obtained with the stabilized scheme with applied stress  $\tau = 0.1$  GPa, increasing the number of elements from left to right and from top to bottom.

### 2.4.3 Time evolution

In this last subsection, the results for a single problem, with  $\tau = 0.1$  GPa, are presented in more detail. The goal here is to present numerical evidence of the characteristics of the proposed stabilization technique. For clarity, only the results corresponding to the positive dislocation density obtained with the stabilized scheme will be shown. The same four meshes used previously are analyzed, but now for several time instances. Snapshots from  $t = 10^2 \mu\text{s}$  up to  $t = 10^7 \mu\text{s}$  with one order of magnitude increments will be taken, to be depicted on a logarithmic time scale.

The evolution of the positive dislocation density is depicted in Figure 2.5 for the four meshes in each subfigure. As the mesh is refined, the sharp change at the dislocations pile-up are resolved more accurately.

Correspondingly, Figure 2.6 depicts for each mesh the time evolution of the Péclet number on a logarithmic scale. Note that at early stages of the computation, the Péclet number is practically constant on the whole spatial domain and given by Equation (2.47). Evidently, the Péclet number at early stages is reduced as the mesh is refined. As the computation evolves the Péclet number grows on those parts of the spatial domain where the positive dislocation density approaches zero. Since finer meshes are more accurate in these regions, these finer meshes also reveal the highest Péclet number values at the last computed time  $t = 10^7 \mu\text{s}$ .

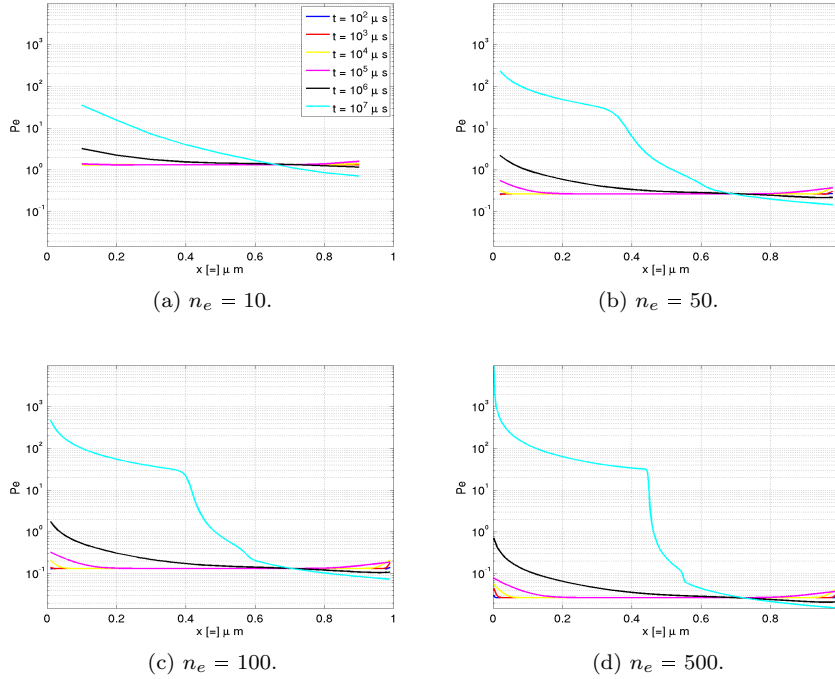


Figure 2.6: Comparison of Péclet number evolution with applied stress  $\tau = 0.1$  GPa, increasing the number of elements from left to right and from top to bottom.

The same information is shown in Figure 2.7, where each plot corresponds to a fixed time  $t$  with the Péclet number depicted on the whole spatial domain for the four meshes. The left subfigure corresponds to time  $t = 10^2 \mu s$ . The Péclet number for all the meshes is nearly constant, except at the boundaries with the finer mesh. This is due to the mesh's ability to resolve the boundary layers that start to emerge. The middle subfigure confirms this. The right subfigure, corresponding to time  $t = 10^6 \mu s$ , shows the tendency of the Péclet number to increase in those regions where the positive dislocation density approaches zero values and to decrease at the opposite boundary where the positive dislocation density grows, causing an increment of the effective diffusion. Note that all the maximum values of the Péclet number have surpassed the minimum Péclet number of the corresponding coarse mesh suggesting that the non-linearity of the system has a strong influence on the stability properties. Simple mesh refinement, which may become expensive from a computational viewpoint, cannot provide a satisfactory answer to the stability problem.

Finally, the magnitude of the perturbation  $|\beta^*|$  computed and used to stabilize the problem at hand for the four different meshes is provided in Figures 2.8 and 2.9. The magnitude of the required perturbation to get stability effectively vanishes as the mesh is refined for early stages of the computation as can be seen in Figure 2.8. As the computation evolves, refined meshes, able to resolve more accurately values



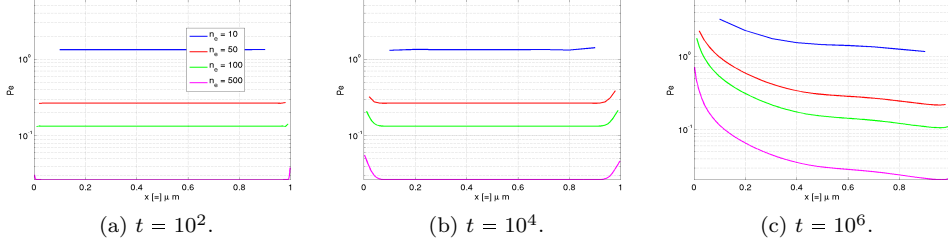


Figure 2.7: Comparison of the Péclet number on the spatial domain for the four meshes with applied stress  $\tau = 0.1$  GPa, increasing the time instance from left to right.

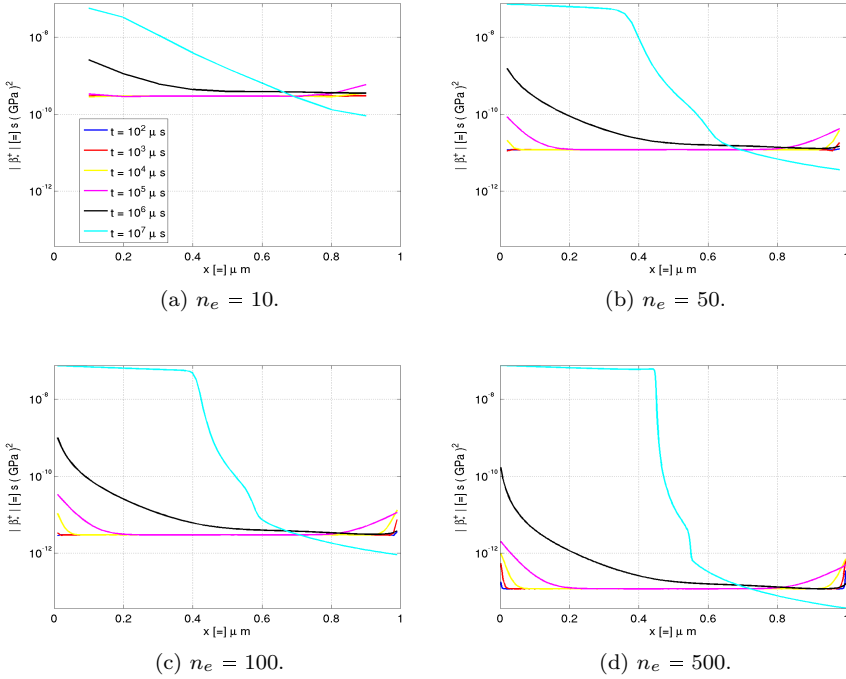


Figure 2.8: Comparison of the advection perturbation magnitude  $|\beta^*|$  evolution used to get stability with applied stress  $\tau = 0.1$  GPa, increasing the number of elements from left to right and from top to bottom.

of positive dislocation density approaching zero, reduce further the effective diffusion  $\alpha(\rho)$ . Figure 2.9 also confirms the fact that simple mesh refinement will not solve the instability problem by itself and more importantly, that the coefficient perturbation necessary to stabilize the problem decreases upon mesh refinement.

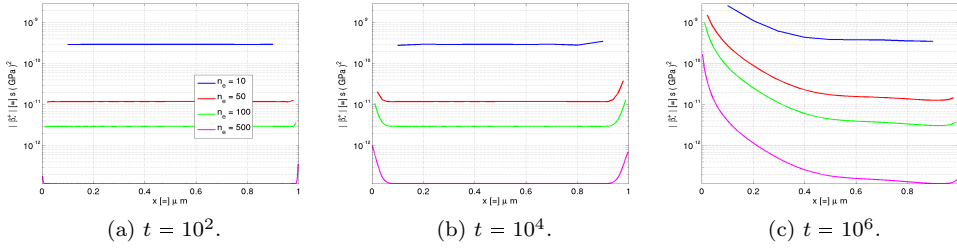


Figure 2.9: Comparison of the advection perturbation magnitude  $|\beta^*|$  on the spatial domain for the four meshes with applied stress  $\tau = 0.1$  GPa, increasing the time instance from left to right.

## 2.5 Conclusion and outlook

In this chapter a stabilization technique for the general steady state and linear convection-diffusion-reaction equation with constant coefficients has been developed. For the linear convection-diffusion case it has been explicitly demonstrated that the proposed technique leads to unconditionally stable solutions via the fulfilment of the discrete maximum principle, and that the stabilized scheme solution converges to the classical Bubnov-Galerkin solution if the mesh Péclet number is small enough. Although not shown in this chapter, the diffusion-reaction and the general convection-diffusion-reaction case are also endowed with these two properties; which together make the stabilized scheme convergent by the Lax equivalence theorem. Furthermore, this stabilization technique is applicable when either the advective or the divergence form has been used for the spatial discretization, making it highly flexible and general.

Although the dislocation density transport equations of interest in this chapter are transient, non-linear, and with variable coefficients, the proposed stabilization scheme has been successfully applied to these equations. Its effectiveness in stabilizing the classical Bubnov-Galerkin scheme and consistency have both been demonstrated in the numerical simulations performed. The effectiveness of the stabilization technique remains unaffected when different types of models, as those presented in [21] or in [32], are used, with constant or variable length scales. Moreover, the more commonly used total and geometrically necessary dislocations densities can be easily obtained from the positive and negative dislocations densities in a post-processing step.

It is noted that an error analysis could add a significant value to the proposed stabilization technique and should be investigated as future work. It is also planned to extend this stabilization technique to multidimensional configurations. Although the present chapter is mainly focused on parallel edge dislocations, more complex dislocation density transport models, such as those modeling screw and mixed dislocations and other phenomena as annihilation, will be investigated as well.

## Chapter 3

# Stabilization of Coupled Convection-Diffusion-Reaction Equations

---

### Abstract

Partial differential equations having diffusive, convective and reactive terms appear in the modelling of a large variety of processes in several branches of science. Often, several species or components interact with each other rendering strongly coupled systems of convection-diffusion-reaction equations. Exact solutions are available in extremely few cases lacking practical interest. Then, numerical approximation remains the best strategy for solving these problems. The properties of these systems of equations cause most traditional numerical methods to fail, with the appearance of violent and non-physical node to node oscillations in the solutions. Therefore, strategies must be developed in order to obtain physically meaningful and numerically stable approximations. Such stabilization techniques have been extensively developed for the single equation case in contrast to the multiple equations case. The objective of this chapter is to present a stabilization technique for coupled systems of convection-diffusion-reaction equations. Several of its attractive characteristics are discussed, providing evidence of its versatility and effectiveness through a thorough numerical assessment.

**keywords.-** Numerical instability, Stabilized finite element method, Convection-diffusion-reaction equations, Coupled systems.

---

---

This chapter is based on: [Hernández H.](#), Massart T.J., Peerlings R.H.J., and Geers M.G.D. 2016. *A Stabilization Technique for Coupled Convection-Diffusion-Reaction Equations*. In preparation.

### 3.1 Introduction

Partial differential equations including convection, diffusion, and reaction terms arise naturally in many branches of engineering and science. Analytical solutions of such equations are known in very few simple cases that generally lack practical interest, even if they do provide valuable mathematical, physical, or computational insights. Moreover, non-linearity, intricate boundary conditions, irregular geometries, heterogeneity in the space and time dependence of the transport coefficients complicate the situation even more, rendering the problem intractable by analytical tools. For this reason, numerical approximation methods remain the best strategy for solving such equations.

In recent decades, all well-known numerical techniques have been applied to solve such convection-diffusion-reaction equations. Finite differences, finite volumes, finite elements, spectral, or meshless methods, to name a few, are most common in the field.

These numerical techniques have been applied with different degrees of success. Some of them have excelled for some specific problems, while not obtaining satisfactory results, or even completely failing, for other problems. In this respect, a general purpose numerical methodology does not seem to be available yet. The vast majority of the above mentioned numerical methods are successful when convection, reaction, or a combination of both acting together, are largely dominated by diffusion, tending towards a *purely diffusive* process. The situation is drastically changed when either convection, reaction, or a combination of both overwhelms diffusion. In such situations, numerical instability arises when diffusion becomes less predominant for affordable meshes. The numerical approximations are usually plagued with spurious oscillations near boundary and internal layers, and can exhibit negative values even if the underlying partial differential equation only accepts non-negative solutions.

This stability problem is inherent to the numerical discretization scheme, and not to the underlying partial differential equation. When the discretization is refined the magnitude of the oscillations decreases or they even completely disappear, yielding a smooth numerical approximation.

This suggests that the lack of numerical stability and the subsequent oscillations appear because the discretization is too coarse to adequately capture all the physics of the governing transport mechanisms. This can also be interpreted as a lack of richness of the approximation space to fully capture the behaviour of the function underlying the solution of the continuous model. In several cases, the refinement required to get acceptable numerical approximations is so excessive that the approximation process becomes prohibitive in computational terms.

Over the years, ad hoc discretization strategies or stabilization techniques have been developed to overcome such difficulties. Finite difference method practitioners have defined several techniques in this respect, such as upwinding schemes, the use of high order schemes, or the use of fitted meshes [9, 25, 29, 52, 54]. Flux reconstruction, total variation diminishing techniques, high order schemes, essentially non-oscillatory

schemes, and their weighted version are now well established techniques in the finite volume method community [68, 72, 76]. Streamline upwind Petrov-Galerkin, Galerkin least-squares, discontinuous Galerkin schemes; bubble enrichment; algebraic sub-grid scale approaches, spurious oscillations at layers diminishing techniques, and boundary layer elements, among others, have been devised over the years in the finite element method community [7, 11, 13, 44, 56, 60].

These techniques exhibit different degrees of success, and many of them have not been designed for general purposes. Some are focused on the convection-diffusion case, while others were developed for the diffusion-reaction case. In the finite difference and the finite element method communities, most of the approaches use the advective form of the partial differential equation [23, 24, 73, 87]. On the other hand, the divergence form is preferred by the finite volume and spectral method communities [8, 26, 81, 82]. In view of the significant number of contributions dealing with these difficulties, one may get the misleading impression that these instability problems have been fully solved.

Yet, little attention has been paid to *systems* of convection-diffusion-reaction equations, although they also arise naturally in several branches of science such as bio-mechanics [18], combustion [5], computer science [30], ecology [45], economy [6], epidemiology [84], finance [17], groundwater pollution [4], heat transfer [70], neuroscience [3], physiology [37], seepage flow [71], solid mechanics [14] or turbulence [15]. The reason for this immaturity is the lack of a maximum principle when going from a single transport equation towards systems of coupled equations in the most general form [62].

In a contribution by Abrahamson, Keller, and Kreiss [1], a stabilization technique for systems of one dimensional convection-diffusion-reaction equations in steady state, i.e. a system of ordinary differential equations, has been proposed and successfully applied. This technique is a direct extension of a previously developed upwinding scheme for first order derivative terms [65, 69, 74, 83].

Additional progress in the approximations for systems of convection-diffusion-reaction equations until the late 1990's has been mainly made by the finite difference method community. The issue has been addressed by extending techniques previously used for discretizing a single equation. The most representative approaches consist of the use of upwind finite differences for the convective terms on layer adapted meshes according to the construction proposed by Shishkin and Bakhvalov [29, 48]. In these papers, theoretical developments have unravelled the conditions for a continuous maximum principle to be valid. In other cases compatibility conditions are derived and used instead. For finite volumes, the strategies have been similar. Discontinuous and high order approximations, upwinding and adaptive meshes were the most successful techniques to deal with coupled equations [16, 58]. In the finite element method context, streamline upwind Petrov-Galerkin, Galerkin least-squares, algebraic sub-grid scale with high order elements together with shock capturing techniques have been the most promising techniques [4, 5, 14]. In general, and within all these methodologies, the case of systems of equations has been traditionally tackled using techniques

previously successful in the case of a single equation. The same guiding strategy is followed in the present chapter.

The main aim here is to present a stabilization technique for a system of coupled convection-diffusion-reaction equations able to resolve the main shortcomings of the above mentioned stabilization techniques such as mesh fitting or the need to adapt the mesh, the requirement of high order or discontinuous approximations and the introduction of excessive diffusive up-winded differences. This methodology extends a recently proposed approach for a single equation, described in [34], to a general system of convection-diffusion-reaction equations. The methodology is conceptually based on perturbing the original partial differential equation, whose discretized form on a particular discretization is on beforehand known to yield an unstable approximation, by modifying its transport coefficients to obtain a well behaved numerical approximation without altering the physics [7, 43]. The required modification or perturbation is optimally determined as the smallest possible one that still guarantees stability. These perturbations are chosen in such a way that certain compatibility conditions analogous to a maximum principle are satisfied. Once the computed perturbations are injected in the classical Bubnov-Galerkin finite element method, they deliver smooth and stable numerical approximations.

Applications to several coupled systems of partial differential equations in one dimension arising from different phenomena are presented. These results demonstrate the use of the developed technique for simulating problems modeled by systems of convection-diffusion-reaction equations with an affordable computational effort. Examples showing the reliability of the approach are presented through several thorough and detailed numerical assessments.

The chapter is organized as follows. In Section 3.2 the basic terminology and notations are introduced. A particular effort has been made to homogenize the different conventions used in the literature due to the variety of phenomena for which coupled convection-diffusion-reaction equations are obtained. Subsequently, the classical Bubnov-Galerkin finite element discretization is introduced in the most traditional way and important issues on the treatment of the boundary conditions are discussed. Section 3.3 is devoted to the development of a stabilization technique for a steady state linear system of convection-diffusion-reaction equations with constant coefficients in one dimension. The particular case when the coupling coefficients vanish is discussed, at which the proposed stabilization technique collapses to previously proposed techniques designed for the case of a single equation. Unconditional stability and consistency of the stabilization technique for the special case of a single convection-diffusion equation is discussed. Section 3.4 assesses the stabilization technique through three numerical examples. The first one is of the convection-diffusion type, while the second one is of the diffusion-reaction type. Finally, the third problem is of convection-diffusion-reaction type with not only boundary layers as in the previous problems, but also internal layers. Finally, Section 3.6 presents the main conclusions of the chapter and discusses some future developments to be considered.

### 3.2 Problem definition and finite element discretization

In all generality, consider a system of  $m$  conservation equations with reaction terms of the form

$$\rho_{pq} \frac{\partial u_q}{\partial t} + \frac{\partial}{\partial x} (F_p) + \gamma_{pq} u_q = f_p, \quad (3.1)$$

where the use of repeated indices implies the traditional summation convention. The main variables to be approximated,  $u_q$  for  $q = 1, 2, \dots, m$ , are the physical quantities to be transported,  $F_p$  are their corresponding fluxes, and  $f_p \in \mathbb{R}$  are the source terms, both for  $p = 1, 2, \dots, m$ . The reaction coefficients  $\gamma_{pq} \in \mathbb{R}$ , for  $p, q = 1, 2, \dots, m$  will be referred to as *direct* when  $p = q$  and as *coupled* when  $p \neq q$ . Finally,  $\rho_{pq} \in \mathbb{R}^+$  are the mass coefficients, which are assumed to vanish when  $p \neq q$ .

The fluxes are composed of diffusive and convective contributions, i.e.

$$F_p = -\alpha_{pq} \frac{\partial u_q}{\partial x} + \beta_{pq} u_q. \quad (3.2)$$

Here  $\alpha_{pq} \in \mathbb{R}^+$  are the diffusion coefficients and  $\beta_{pq} \in \mathbb{R}$  are the convection coefficients. These diffusion and convection coefficients will also be referred to as *direct* or *coupled* using the above mentioned convention. Throughout this section all coefficients will be regarded as constants.

Substituting the flux given by Equation (3.2) in the general conservation Equation (3.1) leads to

$$\rho_{pq} \frac{\partial u_q}{\partial t} + \frac{\partial}{\partial x} \left( -\alpha_{pq} \frac{\partial u_q}{\partial x} + \beta_{pq} u_q \right) + \gamma_{pq} u_q = f_p. \quad (3.3)$$

which is the *divergence* form of the conservation equation due to the fact that integration over the whole domain involves, via the divergence theorem, the total flux across the boundary.

Since all the physical coefficients are regarded as constants, it is possible to expand the spatial derivative on the terms composing the flux to obtain

$$\rho_{pq} \frac{\partial u_q}{\partial t} - \alpha_{pq} \frac{\partial^2 u_q}{\partial x^2} + \beta_{pq} \frac{\partial u_q}{\partial x} + \gamma_{pq} u_q = f_p. \quad (3.4)$$

which is in turn the *advective* form because of the direct interpretation of the first order spatial derivative term representing convection.

With these conventions and assumptions it is possible to rewrite the system of equations (3.4) in matrix form as

$$\mathbf{M} \dot{\mathbf{u}} - \mathbf{A} \mathbf{u}'' + \mathbf{B} \mathbf{u}' + \mathbf{G} \mathbf{u} = \mathbf{f}, \quad (3.5)$$

where the superimposed dot implies differentiation in time while the prime denotes a derivative with respect to the spatial coordinate.  $\mathbf{M} = \text{Diag}(\rho_{11}, \rho_{22}, \dots, \rho_{mm})$

is the *matrix of mass coefficients* and  $\mathbf{A}$ ,  $\mathbf{B}$ , and  $\mathbf{G}$  are the *matrices of diffusion, convection, and reaction coefficients*, while  $\mathbf{u} = [u_1, u_2, \dots, u_m]^T$  is the *vector of unknowns*. Finally, the *source vector*  $\mathbf{f} = [f_1, f_2, \dots, f_m]^T$  gathers the  $m$  source terms. Care must be taken not to confuse the above matrices with the finite element matrices to be introduced afterwards.

For the sake of clarity in the notation, a single weighting function  $w$  for all the  $m$  equations is introduced and used in what follows. Notwithstanding, it is important to remark that a different weighting function can be used for each equation. Multiplying Equation (3.1) by such a weighting function  $w$ , and integrating over the whole spatial domain, the following weighted residuals form is obtained

$$\int_{\Omega} w \rho_{pq} \frac{\partial u_q}{\partial t} d\Omega + \int_{\Omega} w \frac{\partial}{\partial x} (F_p) d\Omega + \int_{\Omega} w \gamma_{pq} u_q d\Omega = \int_{\Omega} w f_p d\Omega, \quad (3.6)$$

Integrating by parts the second term in the left hand side yields

$$\int_{\Omega} w \rho_{pq} \frac{\partial u_q}{\partial t} d\Omega - \int_{\Omega} \frac{\partial w}{\partial x} F_p d\Omega + [w F_p]_{\Gamma} + \int_{\Omega} w \gamma_{pq} u_q d\Omega = \int_{\Omega} w f_p d\Omega. \quad (3.7)$$

It is emphasized again that this way of applying integration by parts is not the standard in finite element based solutions in the fluids dynamics community. This choice, i.e. integration by part performed on the whole flux term, allows one to handle both essential and natural boundary conditions for convection-diffusion-reaction problems in a straightforward manner.

To discretize Equation (3.7), the weighting function  $w$  and the variable  $u_p$  are expressed as linear combinations of their corresponding nodal values using interpolation functions  $W_k$  and  $P_k$  associated with the  $n_e$  nodes within each finite element as follows

$$w = \sum_{k=1}^{n_e} W_k w_k \quad \text{and} \quad u_p = \sum_{k=1}^{n_e} P_k (u_p)_k. \quad (3.8)$$

Requiring the result to hold for all  $w_k$  leads to a global discretized system of the form

$$\mathbf{M}_{pq} \dot{\mathbf{u}}_q + (\mathbf{D}_{pq} + \mathbf{C}_{pq} + \mathbf{R}_{pq}) \mathbf{u}_q = \mathbf{f}_p, \quad (3.9)$$

where  $\mathbf{M}_{pq}$  are the global mass matrices,  $\mathbf{D}_{pq}$  the global diffusion matrices,  $\mathbf{C}_{pq}$  are the global convection matrices and  $\mathbf{R}_{pq}$  are the global reaction matrices. Again, it is emphasized that these matrices differ from those presented in Equation (3.5), and the same care should be taken with the unknowns and source term vectors. Nodal values of the transported quantities to be approximated are sorted in the  $m$  vectors  $\mathbf{u}_q = [u_q^{(1)}, u_q^{(2)}, \dots, u_q^{(n-1)}, u_q^{(n)}]^T$  (for  $q = 1, 2, \dots, m$ ), with  $n$  being the total number of nodes in the finite element discretization. Furthermore, these  $m$  numerical approximations can be sorted in a single degree-of-freedom vector as

$$\mathbf{u} = [u_1^{(1)}, u_1^{(2)}, \dots, u_1^{(n)}, u_2^{(1)}, u_2^{(2)}, \dots, u_2^{(n)}, \dots, u_m^{(1)}, u_m^{(2)}, \dots, u_m^{(n)}]^T, \quad (3.10)$$



which will be simply referred as the numerical approximation. Finally  $\mathbf{f}_p$  takes into account the  $m$  source terms  $f_p$  and boundary conditions.

The stability problem already highlighted in Chapter 2 when working with a single convection-diffusion-reaction equation is inherited to the multiple equations case when using a Bubnov-Galerkin approach for each of the  $m$  equations, i.e. with  $P_k = W_k$ .

### 3.3 Stabilization by coefficient perturbation

The stability problems first described in Section 2.3.1 for the single equation case are caused by the fact that the classical Bubnov-Galerkin method applied to the considered partial differential equation does not satisfy the discrete maximum principle. This principle is the discrete counterpart of the continuous maximum principle, to be satisfied by any feasible solution of the underlying differential equation [12, 43]. However, this maximum principle can be only rigorously established for the case of a single differential equation. When tackling systems of differential equations, barrier functions or compatibility conditions should be established and used instead [47, 48, 52, 54]. Irrespective of the problem considered, a stabilization technique is required in order to obtain physically meaningful approximations. In the present chapter, the above mentioned barrier functions or compatibility conditions will not be used since their derivation is beyond the scope of the present chapter. Therefore, the only guiding criterion for the stabilization technique development will be the removal of spurious oscillations. Thus, interior domain values of the approximated solutions will be allowed to be larger or smaller than the corresponding boundary values due to the fact that coupling terms between unknowns can be viewed as sources or sinks.

#### 3.3.1 Extension to systems of coupled equations

In this section, the proposed stabilization technique for a single convection-diffusion-reaction equation is heuristically extended to the case of multiple coupled equations. This extension is built, as for the single equation case, on the injection of the analytical solution of the linearised, homogeneous, and steady state version of the problem at hand into the numerical stencil obtained by the finite element discretization. This injection process yields a system of algebraic equations for each differential equation composing the coupled system. The determination of the coefficient perturbations is carried out by solving these systems of algebraic equations.

The development of the stabilization technique will make use of a simplified Dirichlet boundary value problem in steady state which reads as follows

$$\frac{d}{dx} \left( -\alpha_{pq} \frac{du_q}{dx} + \beta_{pq} u_q \right) + \gamma_{pq} u_q = f_p \quad \text{in} \quad \Omega = (0, 1), \quad (3.11)$$

$$u_p(x=0) = u_p^L \quad \text{and} \quad u_p(x=1) = u_p^R. \quad (3.12)$$

The discretization of the system of differential equations by the finite element method using a uniform mesh generates  $p = 1, 2, \dots, m$  numerical stencils, one for each of

the  $p$  differential equations contained in system (3.11). These stencils take the same general form

$$-\frac{\alpha_{pq}}{\ell} \left( u_q^{(i-1)} - 2u_q^{(i)} + u_q^{(i+1)} \right) - \frac{\beta_{pq}}{2} \left( u_q^{(i-1)} - u_q^{(i+1)} \right) + \frac{\gamma_{pq}\ell}{6} \left( u_q^{(i-1)} + 4u_q^{(i)} + u_q^{(i+1)} \right) = \ell f_p^{(i)}, \quad (3.13)$$

which correspond to the  $[i + (p-1)m]$ -th row of the system of algebraic equations produced by the finite element method after assembly.

To obtain the analytical solution of the system (3.11),  $m$  new variables are introduced in order to convert the system of  $m$  second-order differential equations into a system of  $2m$  first-order differential equations. These new variables are defined as

$$u_{j+m} = \frac{du_j}{dx} \quad \text{for } j = 1, 2, \dots, m. \quad (3.14)$$

After substituting Equation (3.14) in the system given by Equation (3.11) for the homogeneous case, i.e. with  $f_p = 0$  for  $p = 1, 2, \dots, m$ , the aforementioned system of  $2m$  first-order differential equations is obtained. It can be written in matrix form as

$$\frac{d\mathbf{u}}{dx} = \mathbf{K}\mathbf{u}, \quad (3.15)$$

with  $\mathbf{u} = [u_1, u_2, \dots, u_{2m}]^T$  and the  $2m \times 2m$  matrix  $\mathbf{K}$  defined as

$$\mathbf{K} = \begin{bmatrix} \mathbf{I} & \mathbf{0} \\ \mathbf{0} & \mathbf{A} \end{bmatrix}^{-1} \begin{bmatrix} \mathbf{0} & \mathbf{I} \\ \mathbf{G} & \mathbf{B} \end{bmatrix}, \quad (3.16)$$

where  $\mathbf{I}$  is the  $m \times m$  identity matrix and  $\mathbf{0}$  is the  $m \times m$  null matrix. The  $m \times m$  matrices  $\mathbf{A}$ ,  $\mathbf{B}$ , and  $\mathbf{G}$  are the diffusion, convection and reaction matrices defined in Equation (3.5).

With these conventions, the analytical solution of the system given by Equation (3.15) can be written as

$$\mathbf{u} = c_1 e^{\lambda_1 x} \mathbf{v}^{(1)} + c_2 e^{\lambda_2 x} \mathbf{v}^{(2)} + \dots + c_{2m} e^{\lambda_{2m} x} \mathbf{v}^{(2m)}, \quad (3.17)$$

where  $\lambda_k$  and  $\mathbf{v}^{(k)}$  are the  $2m$  eigenvalues and eigenvectors of the matrix  $\mathbf{K}$ , i.e. they satisfy  $\mathbf{K}\mathbf{v}^{(k)} = \lambda_k \mathbf{v}^{(k)}$  for  $k = 1, 2, \dots, 2m$ . The constants  $c_k$  only depend on the boundary conditions given by (3.12). Thus, the  $q$ -th solution of the system of equations (3.11) can be written as

$$u_q(x) = \sum_{k=1}^{2m} c_k v_q^{(k)} e^{\lambda_k x}, \quad (3.18)$$

where  $v_q^{(k)}$  is the  $q$ -th component of the eigenvector associated to the  $k$ -th eigenvalue.

The  $q$ -th component of the analytical solution can therefore be evaluated at the three nodes defining the finite element stencils (3.13), i.e. at  $x_{i-1}$ ,  $x_i$  and  $x_{i+1}$ :

$$u_q(x_i) = u_q^{(i)} = \sum_{k=1}^{2m} c_k v_q^{(k)} e^{\lambda_k x_i}, \quad \text{and} \quad u_q(x_{i\pm 1}) = u_q^{(i\pm 1)} = \sum_{k=1}^{2m} c_k v_q^{(k)} e^{\lambda_k x_i} e^{\pm \lambda_k \ell}. \quad (3.19)$$

These expressions for  $u_q^{(i-1)}$ ,  $u_q^{(i)}$ , and  $u_q^{(i+1)}$  are injected in the  $p$  perturbed finite element stencils resulting from the discretization of the system of differential equations (3.11). Such perturbed stencils have exactly the same form as the stencils given by (3.13) but using the perturbed coefficients  $\tilde{\alpha}_{pq}$ ,  $\tilde{\beta}_{pq}$ , and  $\tilde{\gamma}_{pq}$  instead of the corresponding original coefficients  $\alpha_{pq}$ ,  $\beta_{pq}$ , and  $\gamma_{pq}$ . After taking into account the coupling through the  $q$  index, each of the  $p$  perturbed stencils can be written as

$$\begin{aligned} & \frac{\tilde{\alpha}_{pq}}{\ell} \sum_{k=1}^{2m} c_k v_q^{(k)} e^{\lambda_k x_i} [1 - \cosh(\lambda_k \ell)] + \\ & \frac{\tilde{\beta}_{pq}}{2} \sum_{k=1}^{2m} c_k v_q^{(k)} e^{\lambda_k x_i} \sinh(\lambda_k \ell) + \\ & \frac{\tilde{\gamma}_{pq} \ell}{6} \sum_{k=1}^{2m} c_k v_q^{(k)} e^{\lambda_k x_i} [2 + \cosh(\lambda_k \ell)] = 0. \end{aligned} \quad (3.20)$$

Expression (3.20) represents  $m$  equations (for  $p = 1, 2, \dots, m$ ), each one corresponding to the  $p$ -th differential equation in the system (3.11). Expansion of the  $q = 1, 2, \dots, m$  index in each of these  $m$  equations makes clear that the unknowns of the equations included in Expression (3.20) are the  $m^2$  perturbed diffusion coefficients  $\tilde{\alpha}_{pq}$ , the  $m^2$  perturbed convection coefficients  $\tilde{\beta}_{pq}$ , and the  $m^2$  perturbed reaction coefficients  $\tilde{\gamma}_{pq}$ , each for  $p, q = 1, 2, \dots, m$ . Considering the  $m$  equations with  $3m^2$  unknowns in Equation (3.20), attention is now focused to the summation over  $k$ . The  $k = 1, 2, \dots, 2m$  index corresponds to the number of integration constants  $c_k$ , eigenvalues  $\lambda_k$ , and eigenvectors  $\mathbf{v}^{(k)}$ . The constants  $c_k$  depend only on the boundary conditions in (3.12). These boundary conditions are first chosen in such a way that  $c_1 \neq 0$  and  $c_2 = c_3 = \dots = c_{2m} = 0$ , generating  $m$  algebraic equations (for  $p = 1, 2, \dots, m$ ), for the particular value  $k = 1$ . Subsequently, the boundary conditions are modified in order to get  $c_1 = 0$ ,  $c_2 \neq 0$ , and  $c_3 = c_4 = \dots = c_{2m} = 0$ , generating this time another  $m$  algebraic equations for the value  $k = 2$ . This process is continued until  $k = 2m$ , generating  $m$  algebraic equations for each particular value of the  $k$  index. Note that after carrying out this process the product  $c_k e^{\lambda_k x_i}$  can be eliminated since it appears as a common factor once a particular  $k$  has been fixed. Thus, it is possible to write the resulting  $2m^2$  system of algebraic equations in a compact form as

$$\frac{\tilde{\alpha}_{pq}}{\ell} v_q^{(k)} [1 - \cosh(\lambda_k \ell)] + \frac{\tilde{\beta}_{pq}}{2} v_q^{(k)} \sinh(\lambda_k \ell) + \frac{\tilde{\gamma}_{pq} \ell}{6} v_q^{(k)} [2 + \cosh(\lambda_k \ell)] = 0, \quad (3.21)$$

where the eigenvalues  $\lambda_k$  and their corresponding eigenvectors  $\mathbf{v}^{(k)}$  of the  $\mathbf{K}$  matrix given by Equation (3.16) depend only on the transport coefficients and therefore can be easily determined through numerical computation. In order to solve this system of  $2m^2$

equations with  $3m^2$  unknowns,  $m^2$  transport coefficients should be kept unperturbed, allowing to solve (3.21) for the remaining  $2m^2$  perturbed coefficients.

Note that the system of two equations obtained in the previous chapter while developing the presented stabilization technique for the single equation case and given by (2.28-2.29) is indeed the special case of (3.21) with  $m = 1$ . The corresponding  $2 \times 2$  matrix  $\mathbf{K}$  is now given by

$$\mathbf{K} = \begin{bmatrix} 1 & 0 \\ 0 & \alpha \end{bmatrix}^{-1} \begin{bmatrix} 0 & 1 \\ \gamma & \beta \end{bmatrix}, \quad (3.22)$$

whose eigenvalues are exactly the same as the roots of the characteristic polynomial associated to the second-order convection-diffusion-reaction equation as given by Equation (2.25). This observation partially justifies the heuristic process adopted in order to extend the stabilization technique from the single equation case towards the case of systems containing  $m$  coupled equations. Additional arguments will be forwarded in the next section.

### 3.3.2 Particularization to uncoupled sets of equations

The goal of this section is to assess the validity of the extension of the presented stabilization technique to the multiple equations case. For this purpose, the special case when all coupling coefficients vanish, i.e. when  $\alpha_{pq} = \beta_{pq} = \gamma_{pq} = 0$  for  $p \neq q$ , is considered. In this case the eigenvalues of the  $\mathbf{K}$  matrix are given by

$$\lambda_{2p-1,2p} = \frac{\beta_{pp}}{2\alpha_{pp}} \pm \sqrt{\left(\frac{\beta_{pp}}{2\alpha_{pp}}\right)^2 + \frac{\gamma_{pp}}{\alpha_{pp}}}, \quad (3.23)$$

and their corresponding eigenvectors are in turn given by

$$\mathbf{v}^{(2p-1,2p)} = \left( \frac{\lambda_{2p-1,2p}\alpha_{pp} - \beta_{pp}}{\gamma_{pp}} \right) \hat{\mathbf{e}}^{(p)} + \hat{\mathbf{e}}^{(p+m)}, \quad (3.24)$$

where the vectors  $\hat{\mathbf{e}}^{(i)}$  for  $i = 1, 2, \dots, 2m$  have 1 in their  $i$ -th component and zeros otherwise.

Since  $\alpha_{pq} = \beta_{pq} = \gamma_{pq} = 0$  for  $p \neq q$ , their corresponding perturbations are, for simplicity, assumed to vanish, i.e.  $\alpha_{pq}^* = \beta_{pq}^* = \gamma_{pq}^* = 0$  for  $p \neq q$ . After substituting  $q = p$  in the expression (3.21) and factorizing the common factor  $v_p^{(k)}$ , the system of equations can be compactly written as

$$v_p^{(k)} \left\{ \frac{\tilde{\alpha}_{pp}}{\ell} [1 - \cosh(\lambda_k \ell)] + \frac{\tilde{\beta}_{pp}}{2} \sinh(\lambda_k \ell) + \frac{\tilde{\gamma}_{pp}\ell}{6} [2 + \cosh(\lambda_k \ell)] \right\} = 0. \quad (3.25)$$

Note that only the  $p$ -th and  $(p + m)$ -th entries of the  $(2p - 1)$ -th and the  $2p$ -th eigenvectors do not vanish, i.e.  $v_p^{(2p-1,2p)} \neq 0$  and  $v_{p+m}^{(2p-1,2p)} \neq 0$ . Thus, only the  $[2(p - 1)m + 2p - 1]$ -th and  $[2(p - 1)m + 2p]$ -th equations of the linear system are

non-trivial. All the other equations generated by (3.25) for  $k = 1, 2, \dots, 2m$  provide the trivial equality  $0 = 0$ . Therefore the linear system consisting originally of  $2m^2$  equations is reduced to only  $2m$  equations with  $3m$  unknowns, i.e. the perturbed coefficients  $\tilde{\alpha}_{pp}$ ,  $\tilde{\beta}_{pp}$ , and  $\tilde{\gamma}_{pp}$ . Furthermore, it is possible to write these equations by pairs after substituting  $k = 2p - 1$  and  $k = 2p$  and eliminating the common factor  $v_p^{(k)}$  as

$$\frac{\tilde{\alpha}_{pp}}{\ell} [1 - \cosh(\lambda_{2p-1}\ell)] + \frac{\tilde{\beta}_{pp}}{2} \sinh(\lambda_{2p-1}\ell) + \frac{\tilde{\gamma}_{pp}\ell}{6} [2 + \cosh(\lambda_{2p-1}\ell)] = 0, \quad (3.26)$$

$$\frac{\tilde{\alpha}_{pp}}{\ell} [1 - \cosh(\lambda_{2p}\ell)] + \frac{\tilde{\beta}_{pp}}{2} \sinh(\lambda_{2p}\ell) + \frac{\tilde{\gamma}_{pp}\ell}{6} [2 + \cosh(\lambda_{2p}\ell)] = 0. \quad (3.27)$$

Note that these two equations well resemble the two Equations (2.28-2.29) obtained when treating the single differential equation case, i.e. when  $m = 1$ . This allows to conclude that when applied to an uncoupled system of convection-diffusion-reaction equations, the extended stabilization technique simplifies to  $m$  independent problems, and stabilizes them as done in the previous chapter.

### 3.4 Applications and computational assessment

This section presents three numerical examples to illustrate and assess the efficiency and consistency of the developed stabilization technique. Its main goal is to demonstrate the ability of the presented stabilization technique to successfully accommodate and handle different types of problems, independently of the underlying physics for which the system of differential equations has been established.

This goal is pursued by presenting a thorough and detailed analysis of the numerical results obtained for three examples taken from different references. In all cases the convection and reaction coefficients have been taken exactly the same as those presented in the original reference. Except in the last example, all boundary conditions have also been taken of the same type as in the original references. The modification made in the last problem is for the sake of uniformity in the assessments presented here, and more importantly because the boundary conditions chosen here more easily trigger the development of sharp boundary layers, making the problem more challenging for the stabilization technique. Thus the problems elaborated in the present assessment are all of the Dirichlet type. The domain considered always has a unit length.

Only the parameter  $\epsilon$  controlling the amount of diffusion and the discretization size  $\ell$  are modified during this study. Once these are set for a particular problem they are not changed, i.e. for a particular simulation the diffusion parameter is constant over the whole domain discretized with a uniform mesh. The parameter  $\epsilon$  is always chosen as  $\epsilon = 10^{-j}$  with  $j = 0, 1, 2, \dots$  thus, as  $j$  increases the problem becomes less dominated by diffusion, and therefore its numerical approximation becomes more prone to numerical instabilities.

Regardless of the use of the presented stabilization technique, once the system of  $m$  differential equations has been discretized, a system of  $mn \times mn$  linear algebraic

equations has to be solved. For this purpose the iterative *BiCGStab* method has been used, considering future multidimensional extensions of the framework leading to large and sparse systems [77]. In all cases, the maximum number of allowed iterations is set equal to the number of nodes in the finite element mesh, although the iteration process is stopped as soon as  $\|\mathbf{r}^{(k)}\|/\|\mathbf{b}\| < \epsilon_s = 10^{-6}$  is reached, with  $\mathbf{r}^{(k)}$  the  $k$ -th residual vector and  $\mathbf{b}$  the right hand side vector. No preconditioning is used.

### 3.4.1 Convection-diffusion system

In this section, attention is focused on a problem having no reaction terms but a full convection matrix, i.e. containing cross convection terms. It has been chosen here to perturb only the diagonal entries of the diffusion matrix in order to capture the effect of the stabilization technique in a single coefficient perturbation easy to scrutinize. Since an analytical solution is available for this problem, an error analysis can be carried out to elucidate the effectiveness of the stabilization scheme.

This problem is taken from [55], where it was treated using upwind finite differences on a Shishkin mesh. It is the simplest case among all examples solved in the present chapter, where all the diffusion coefficients are equal and the convection coefficients and source terms all taken as constants.

The system consisting of  $m = 3$  differential equations reads as follows

$$-\epsilon \begin{bmatrix} 1 & 0 & 0 \\ 0 & 1 & 0 \\ 0 & 0 & 1 \end{bmatrix} \begin{bmatrix} u_1 \\ u_2 \\ u_3 \end{bmatrix}_{xx} - \begin{bmatrix} 3 & -1 & -1 \\ -1 & 4 & -2 \\ -1 & -2 & 4 \end{bmatrix} \begin{bmatrix} u_1 \\ u_2 \\ u_3 \end{bmatrix}_x = \begin{bmatrix} -4 \\ 11 \\ -7 \end{bmatrix}, \quad (3.28)$$

with boundary condition at the left  $\mathbf{u}(x=0) = [-1, 4, -1]^T$ , and at the right

$$\mathbf{u}(x=1) = e^{-1/\epsilon} \begin{bmatrix} 1 \\ 1 \\ 1 \end{bmatrix} + e^{-4/\epsilon} \begin{bmatrix} -2 \\ 1 \\ 1 \end{bmatrix} + e^{-6/\epsilon} \begin{bmatrix} 0 \\ 2 \\ -2 \end{bmatrix} + \begin{bmatrix} 1 \\ -2 \\ 0 \end{bmatrix}. \quad (3.29)$$

Note that the latter boundary condition depends on the diffusion parameter.

The previously mentioned analytical solution is available from [55] and reads

$$\mathbf{u}(x) = e^{-x/\epsilon} \begin{bmatrix} 1 \\ 1 \\ 1 \end{bmatrix} + e^{-4x/\epsilon} \begin{bmatrix} -2 \\ 1 \\ 1 \end{bmatrix} + e^{-6x/\epsilon} \begin{bmatrix} 0 \\ 2 \\ -2 \end{bmatrix} + \begin{bmatrix} x \\ -2x \\ x-1 \end{bmatrix}. \quad (3.30)$$

Figure 3.1 shows the numerical approximations in terms of  $u_1$ ,  $u_2$ , and  $u_3$ . The results obtained with the classical Bubnov-Galerkin method are depicted in the left column, while the right column shows the results obtained with the stabilization technique. These numerical schemes are respectively referred to as *classical* and *stabilized*.

Note in the first row of Figure 3.1; for  $\epsilon = 1$ , that, having diffusion coefficients  $\alpha_{pp} = 1$  for  $p = 1, 2, 3$ , the solutions of the classical and stabilized schemes are practically identical. Moreover, the solutions obtained using different meshes are practically indistinguishable from each other. Such smooth behaviour was expected since that even for the coarsest discretization, the Péclet numbers are all smaller than one  $\mathbf{Pe} = [0.15, 0.2, 0.2]^T$ .

The situation is slightly changed when moving to the next row; for  $\epsilon = 0.1$ , in which oscillations start to appear in the approximation obtained by the coarsest discretization with the classical scheme. This time the Péclet numbers are  $\mathbf{Pe} = [1.5, 2, 2]^T$ ; and therefore such an oscillatory behaviour could have been expected. It disappears for the next finer mesh with corresponding Péclet numbers  $\mathbf{Pe} = [0.4687, 0.625, 0.625]^T$ . In the right column the effectiveness of the proposed stabilization scheme in removing the spurious oscillations, even for the coarsest mesh, is illustrated. The main features in the boundary layers are also captured, although the approximations obtained using the coarsest meshes differ from the finest meshes approximations due to the limited resolution (lack of nodes) in the boundary layer region.

Moving to the last row in the left column, it is obvious that the amplitude of the oscillations increases as the problem gets more dominated by convection. They now even plague approximations on the finest mesh. On the other hand, the approximations obtained by the stabilized scheme, in the right column, are all free of spurious oscillations. They adequately capture the boundary layers and abrupt changes in the solutions even for the coarsest mesh for the whole range of diffusion coefficients tested.

The analytical solution of the problem can be used to assess the numerical approximation error. This analysis is done using the maximum norm, which is usually considered the most adequate for singularly perturbed problems such as convection-diffusion-reaction equations with weak diffusion [25, 53]. The analytical solution  $\mathbf{u}_a$  is evaluated at the same points for which the numerical approximation on a mesh having  $n$  nodes, denoted by  $\mathbf{u}_n$ , is available. Thus the numerical approximation error is given by

$$E_n = \|\mathbf{u}_a - \mathbf{u}_n\|_{\infty}. \quad (3.31)$$

This numerical approximation error  $E_n$  is shown in Figure 3.2 as a function of the number of nodes in the finite element mesh. This is done for all values of the diffusion parameters tested for the current problem. Dashed lines are used for the results obtained with the classical scheme, while continuous lines are used for the stabilized scheme.

Note that the darkest line in Figure 3.2, corresponding to the largest diffusion parameter  $\epsilon = 1$ , exhibits second order convergence in the coarsest meshes range. As soon as the discretization is sufficiently refined,  $n = 100$ , mesh invariance is established, where round-off errors start to dominate. Note also that the error of the stabilized scheme is always lower than its classical counterpart, precisely in the second order convergence range. It can be argued that this fact is caused by the (even weak) presence of convective terms, for which the classical scheme entails instabilities. Note the increase of the

approximation error for  $\epsilon = 1$  when going from the penultimate to the last discretization refinement level and exclusively observed for the stabilized scheme. It is presumed that such increase of the approximation error is due to the ill-conditioning introduced in Equation (3.21) by the evaluation of the hyperbolic functions. For instance, in this convection-diffusion problem, with  $\gamma_{pq} = 0$  and thus  $\tilde{\gamma}_{pq} = 0$  for  $p, q = 1, 2, 3$ , Equation (3.21) is reduced to

$$\frac{\tilde{\alpha}_{pq}}{\ell} v_q^{(k)} [1 - \cosh(\lambda_k \ell)] + \frac{\tilde{\beta}_{pq}}{2} v_q^{(k)} \sinh(\lambda_k \ell) = 0, \quad (3.32)$$

which, for any  $\lambda_k \neq 0$ , becomes trivial in the limit when  $\ell \rightarrow 0$  since  $\cosh(\lambda_k \ell) \rightarrow 1$  and  $\sinh(\lambda_k \ell) \rightarrow 0$ , yielding an indetermination. A practical strategy to prevent such a drawback is still under development.

While decreasing the diffusion parameter, going towards brighter lines, one can notice that the second order convergence and mesh invariance ranges are shifted to the right, implying that as the problem becomes more dominated by convection coarse meshes do not have the ability to resolve the solution features any more. The stabilized scheme properly captures these features, like boundary layers, supported by the fact that the associated error is lower than the error obtained with the classical scheme.

The last case,  $\epsilon = 10^{-4}$ , deserves special attention. For this problem, mesh refinement does not help in reducing the error while using either the classical or the stabilized scheme, until very fine meshes are used. Further refinement is not feasible in terms of computational cost, and more importantly does not improve accuracy. In order to elucidate the latter issue, let's evaluate the most conservative spectral condition number estimate, obtained for a single pure diffusive equation, i.e.  $\kappa_2 = \mathcal{O}(h^{-2})$  [63]. In the present case  $h^{-2} \approx 10^9$  for the finest mesh. This leads to a linear system with a huge condition number, the solution of which can be severely polluted by rounding errors [67, 78]. Obviously, this problem is of a different nature and also affects any stabilization method.

Finally, Figure 3.3 shows the diffusion perturbations for the first equation, i.e. for  $u_1$ , as a function of the discretization size for several values of the diffusion coefficient. As expected, the perturbations automatically increase as the problem becomes more dominated by convection. This is reflected by the fact that the brighter lines, which represent problems more dominated by advection, are always above the darker lines, which in turn represent diffusion dominated problems. More importantly, this plot reveals that the perturbations decrease quadratically as the mesh is refined, demonstrating the consistency of the proposed stabilization technique. The unexpected change in the slope for the line corresponding to the case with  $\epsilon = 1$  when going from the penultimate to the last discretization refinement level is attributed to the same ill-conditioning introduced by the evaluation of the hyperbolic functions discussed above.

### 3.4.2 Diffusion-reaction system

Next, a diffusion-reaction type problem is considered. This problem, originally presented in [52], introduces two new characteristics: the reaction and source coefficients



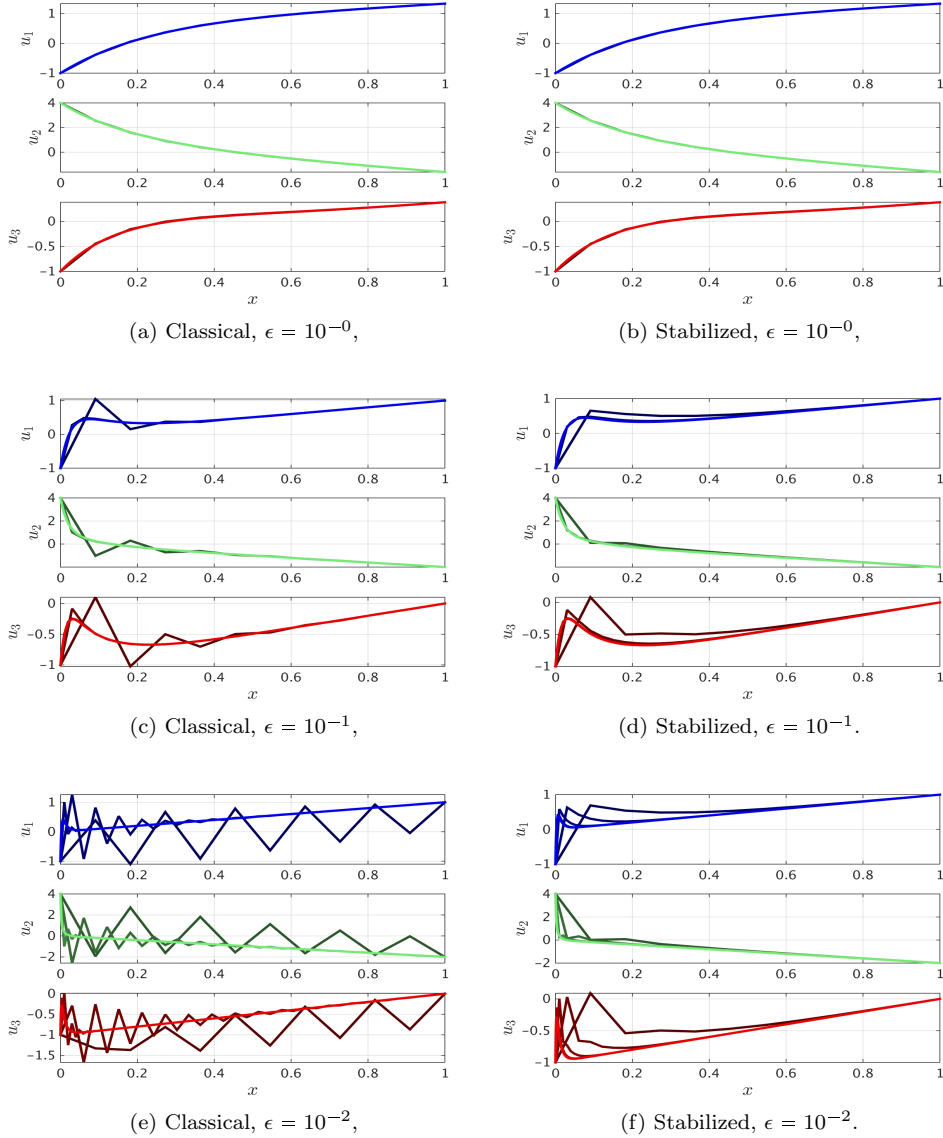


Figure 3.1: Numerical approximations obtained using different discretizations, darkest for the coarsest mesh consisting of  $n = 10$  nodes towards brightest for the finest mesh consisting of  $n = 10000$  nodes, with decreasing diffusion from top to bottom, for the classical (left) and stabilized (right) schemes.

are dependent on the spatial coordinate and the diffusion coefficients differ. Even if the spatial variability of the coefficient is mild, it allows to assess the proposed stabilization technique in handling common difficulties faced by traditional stabilization

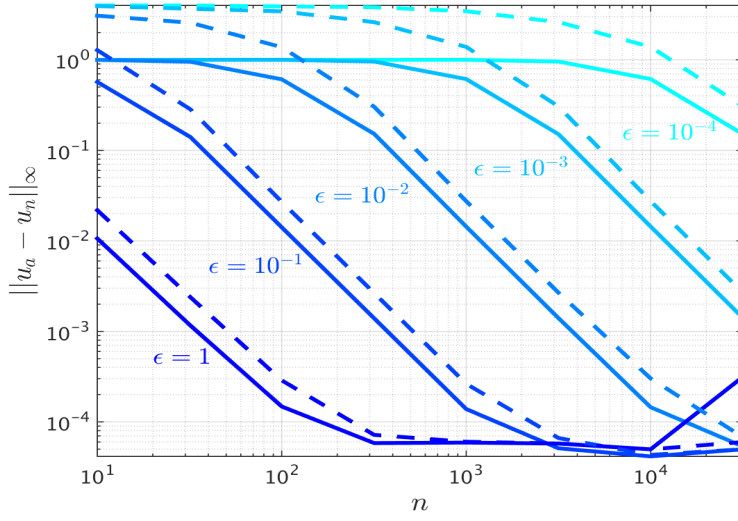


Figure 3.2: Numerical approximation error for various diffusion coefficients and mesh sizes. Dashed lines for the classical scheme and continuous lines for the stabilized scheme for  $\epsilon = 10^{-j}$  with  $j = 0, 1, 2, 3, 4$ , as a function of the number of nodes in the mesh.

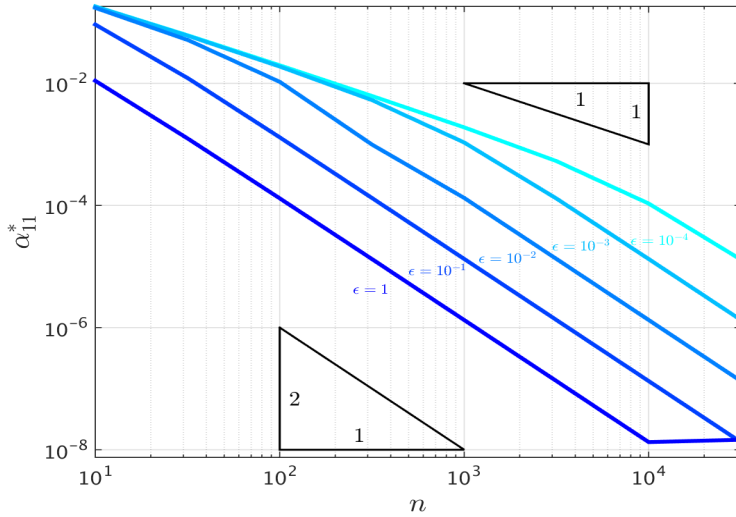


Figure 3.3: Diffusion perturbation required to achieve stability for various diffusion coefficients with  $\epsilon = 10^{-j}$  with  $j = 0, 1, 2, 3, 4$ , as a function of the number of nodes in the mesh.

techniques [1]. Strictly speaking, this characteristic is not a serious difficulty since, before discretization, the differential equations can be scaled in such a way that the previous case, (diffusion matrix equalling a scalar multiplied with the identity matrix) is recovered. However, this scaling may not be desired if the original physical model is to be preserved. Again, the choice was made to compute only the direct diffusion perturbations.

The system consisting of two differential equations is given by

$$-\begin{bmatrix} \epsilon & 0 \\ 0 & 1 \end{bmatrix} \begin{bmatrix} u_1 \\ u_2 \end{bmatrix}_{xx} + \begin{bmatrix} 2(x+1)^2 & -(1+x^3) \\ -2\cos(\pi x/4) & 2.2e^{1-x} \end{bmatrix} \begin{bmatrix} u_1 \\ u_2 \end{bmatrix} = \begin{bmatrix} 2e^x \\ 10x+1 \end{bmatrix}, \quad (3.33)$$

with homogeneous Dirichlet boundary conditions at both ends.

Figure 3.4 shows in each plot the numerical approximations obtained using different discretizations, varying the diffusion parameter row by row. The classical results are depicted in the left column and the stabilized results in the right column.

As expected, the classical and stabilized results are practically identical on the first row, corresponding to the diffusion dominated case. When reducing the diffusion parameter by two orders of magnitude, oscillations start to appear in the numerical approximations in the classical scheme with the coarsest mesh. The stabilized scheme (right column) effectively removes the oscillations. Moreover it recovers the same numerical approximation irrespective of the mesh used.

By moving to the third row, more oscillations appear in the classical scheme since the problem is more dominated by reaction. Even some of the finest meshes show irregularities near the boundary layers. The corresponding numerical approximations obtained with the stabilized scheme are free of spurious oscillations and adequately capture the sharp changes at the boundary layers. It is important to emphasize that mesh invariance is confirmed despite the high reactive character of the problem at hand.

Note that, since the perturbations of the coefficients are computed in each element, the proposed stabilization scheme is able to handle spatially heterogeneous transport coefficients. This is particularly important when dealing with time dependent coefficients or even with non-linear transport equations. This same feature allows handling variable mesh size, making the stabilization technique highly versatile and flexible.

### 3.4.3 Convection-diffusion-reaction system

In the final example, a general system involving all transport mechanisms is included. Approaching such a challenging problem involving convection, diffusion and reaction is precisely the main goal in developing the presented stabilization technique.

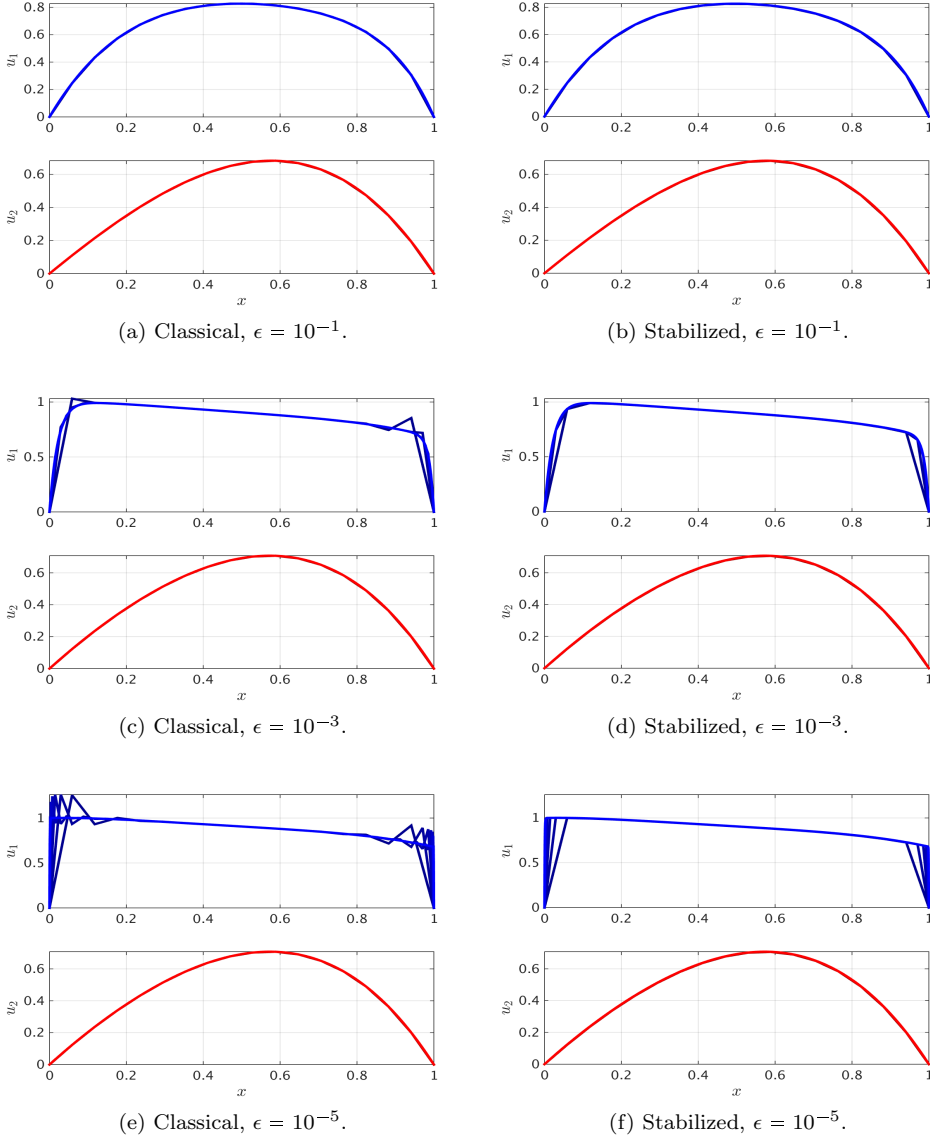


Figure 3.4: Numerical approximations obtained using different discretizations, darkest for the coarsest mesh consisting of  $n = 16$  nodes towards brightest for the finest mesh consisting of  $n = 4096$  nodes, with decreasing diffusion from top to bottom, for the classical (left) and stabilized (right) schemes.

The problem considered was originally defined and solved using an upwind finite difference scheme in [10]. It considers a case in which the diffusion matrix is isotropic,

and reads

$$\begin{aligned}
 -\frac{\epsilon}{2} \begin{bmatrix} 1 & 0 & 0 \\ 0 & 1 & 0 \\ 0 & 0 & 1 \end{bmatrix} \begin{bmatrix} u_1 \\ u_2 \\ u_3 \end{bmatrix}_{xx} + \begin{bmatrix} r_1 & 0 & 0 \\ 0 & r_2 & 0 \\ 0 & 0 & r_3 \end{bmatrix} \begin{bmatrix} u_1 \\ u_2 \\ u_3 \end{bmatrix}_x + \cdots \\
 \cdots + \begin{bmatrix} 2\mu_1 & -2\mu_1 & 0 \\ -\mu_2 & \mu_1 + \mu_2 & -\mu_1 \\ 0 & -2\mu_2 & 2\mu_2 \end{bmatrix} \begin{bmatrix} u_1 \\ u_2 \\ u_3 \end{bmatrix} = \begin{bmatrix} 0 \\ 0 \\ 0 \end{bmatrix}. \quad (3.34)
 \end{aligned}$$

This time, the convection coefficients are piece-wise constant and given by

$$r_k = \begin{cases} (k-1)(\lambda_1 + \lambda_2) - c & \text{if } 0 \leq x \leq b \\ (k-1)\lambda_1 - c & \text{if } b < x \leq 1 \end{cases}. \quad (3.35)$$

The original boundary conditions have been modified for consistency with the previous problems and to generate boundary layers challenging the stabilization scheme. They have been taken as  $\mathbf{u}(x=0) = [0.25, 0, 0.1]^T$  and  $\mathbf{u}(x=1) = [0, 0, 0]^T$ . All diffusion and discretization parameters are the same as in the previous problem. The parameters in the convection and reaction matrices are taken  $\mu_1 = 1$ ,  $\mu_2 = 0.5$ ,  $\lambda_1 = 1$ ,  $\lambda_2 = 0.4$ ,  $c = 1.2$ , and  $b = 0.3$ . Evaluation of the convection coefficients on the two different spatial regions yields:  $\mathbf{r}(0 \leq x \leq 0.3) = [-1.2, 0.3, 1.8]^T$  for the left region and  $\mathbf{r}(0.3 < x \leq 1.0) = [-1.2, -0.2, 0.8]^T$  for the right region. Note that the abrupt change in the last component relates to its magnitude, while the convection direction remains unchanged. In fact, the variation is more drastic in the second component, which changes its sign. Therefore, in addition to boundary layers, internal layers are also expected.

Figure 3.5 shows the numerical approximations in the same format as previously. In the diffusion dominated case, in the first row, the classical and stabilized results are practically identical. Note that  $u_1$  is convected towards the left since its corresponding convection coefficient is negative on the whole spatial domain while  $u_3$  is convected to the opposite direction because its convection coefficient is positive on the whole domain. Thus  $u_1$  and  $u_3$  exhibit boundary layers at the left and right boundaries respectively. The situation is drastically different for  $u_2$  since its boundary values are the same and its convection coefficients have opposite signs in the two different spatial regions, pointing towards the interior of the domain. Therefore, any quantity of  $u_2$  present in the spatial domain, and generated through the reaction terms, will be transported to the point  $x = b$  in which the convection coefficient changes sign. This generates a double internal layer for  $u_2$  itself, but additionally could generate internal layers for  $u_1$  and  $u_3$  through the reaction coupling.

The above mentioned phenomena are more pronounced when moving to the next row, in which the diffusion has been weakened by two orders of magnitude. From these diffusion values, the approximations obtained with the classical scheme are plagued by instabilities for the coarsest meshes. The stabilized scheme solutions are free of spurious oscillations and adequately capture the boundary and internal layers. Moving to the third row, the oscillations in the classical results are so violent that at first sight all numerical approximations are useless, regardless of the mesh used. This is not the

case for the stabilized scheme, since all of them still well approximate the solution of the problem at hand.

### 3.5 Comparison with other techniques

The main objective of this section is to compare the performance of the presented stabilization technique based on coefficient perturbation to other well-known stabilization techniques already available in the literature. This comparison is carried out with respect to the *Streamline Upwind Petrov-Galerkin* [7], *Galerkin Least-Squares* [40], and *Sub-Grid Scales* [39] techniques, which will be referred in what follows by their respective acronyms *SUPG*, *GLS*, and *SGS*. These stabilization techniques have been proposed independently, although they have all been presented in a comprehensive manner in [13, 14, 23]. For details see these references.

The comparison will be carried out using the vector form of the general convection-diffusion-reaction equation (3.4) in steady state. The following transport operators are introduced

$$\mathcal{L}_D(\mathbf{u}) = -\frac{d}{dx} \left( \mathbf{A} \frac{d\mathbf{u}}{dx} \right), \quad \mathcal{L}_C(\mathbf{u}) = \mathbf{B} \frac{d\mathbf{u}}{dx}, \quad \text{and} \quad \mathcal{L}_R(\mathbf{u}) = \mathbf{G}\mathbf{u}, \quad (3.36)$$

where the sub-indices  $D$ ,  $C$ , and  $R$  refer to diffusion, convection, and reaction respectively. It is possible to gather these three transport operators in a single operator  $\mathcal{L}$ . By doing so, it is possible to express Equation (3.4) in steady state as

$$\mathcal{L}(\mathbf{u}) \stackrel{\text{def}}{=} \mathcal{L}_D(\mathbf{u}) + \mathcal{L}_C(\mathbf{u}) + \mathcal{L}_R(\mathbf{u}) = \mathbf{f}, \quad (3.37)$$

and define its associated *residual* as

$$\mathcal{R}(\mathbf{u}) \stackrel{\text{def}}{=} \mathcal{L}(\mathbf{u}) - \mathbf{f}. \quad (3.38)$$

In order to discretize Equation (3.37) by finite elements via the weighted residual statement,  $m$  weighting functions, one for each of the  $m$  coupled convection-diffusion-reaction equations, are introduced and stored in a single vector as  $\mathbf{w} = [w_1, w_2, \dots, w_m]^T$ . After multiplying Equation (3.37) by  $\mathbf{w}^T$  and integrating over the whole domain one obtains the classical Bubnov-Galerkin scheme, known to be unstable when either convection, reaction or a combination of both dominate over diffusion. Therefore, a stabilizing term is introduced in order to remedy such instabilities. After the introduction of this stabilizing term the weighted form of the system of convection-diffusion-reaction equations can be written in all generality as

$$\int_{\Omega} \mathbf{w}^T \mathcal{L}(\mathbf{u}) \, d\Omega + \sum_{e=1}^{n_e} \int_{\Omega^{(e)}} \mathcal{P}^T(\mathbf{w}) \boldsymbol{\tau} \mathcal{R}(\mathbf{u}) \, d\Omega^{(e)} = \int_{\Omega} \mathbf{w}^T \mathbf{f} \, d\Omega. \quad (3.39)$$

where  $\mathcal{P}$  is a differential operator applied to the weighting functions whose particular definition depends on the stabilization technique used as discussed below. The  $m \times m$  matrix  $\boldsymbol{\tau}$  contains the stabilization parameters. Finally  $\mathcal{R}$  is the residual already

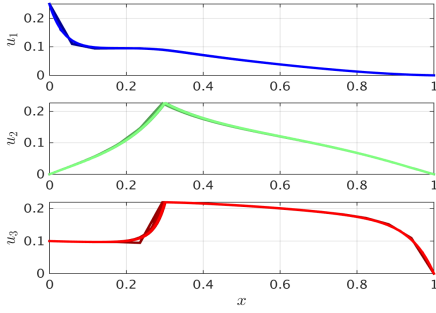
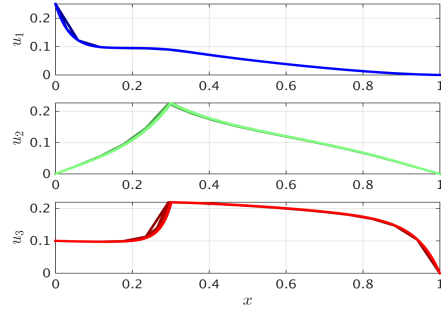
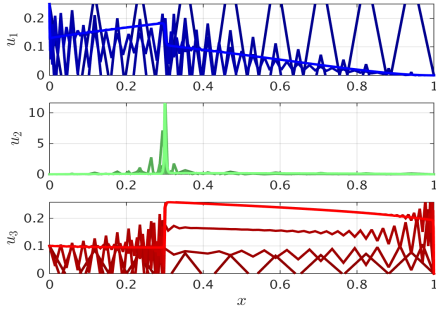
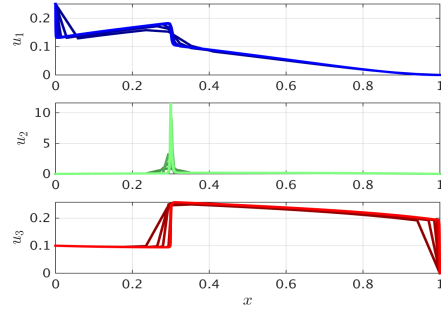
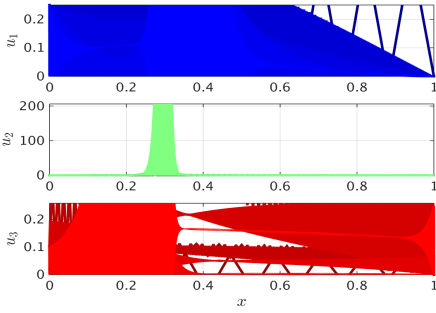
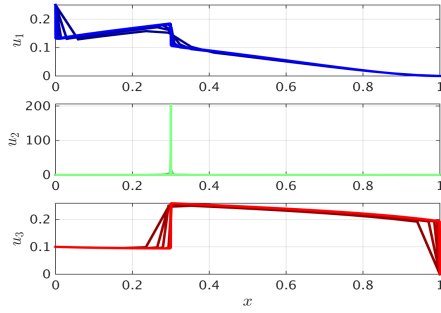
(a) Classical,  $\epsilon = 10^{-1}$ .(b) Stabilized,  $\epsilon = 10^{-1}$ .(c) Classical,  $\epsilon = 10^{-3}$ .(d) Stabilized,  $\epsilon = 10^{-3}$ .(e) Classical,  $\epsilon = 10^{-5}$ .(f) Stabilized,  $\epsilon = 10^{-5}$ .

Figure 3.5: Numerical approximations obtained using different discretizations, darkest for the coarsest mesh consisting of  $n = 16$  nodes towards brightest for the finest mesh consisting of  $n = 4096$  nodes, with decreasing diffusion from top to bottom, for the classical (left) and stabilized (right) schemes.

defined by Equation (3.38). Note that, for the sake of simplicity in the exposition, no integration by parts has been applied in Equation (3.39) and therefore fluxes on the boundary have not been incorporated. Moreover, the addition of the stabilization term as given here is not affected by the form (advective or divergence) of the transport equation to be discretized. Also note that such stabilization term is computed in an element-wise manner and subsequently incorporated in the global finite element system.

As mentioned above, the form of the differential operator  $\mathcal{P}$  defines the stabilization technique used [13, 14, 23]. The SUPG method has been specifically designed to cope with instabilities caused by convection dominance. This fact is reflected by the form of the corresponding differential operator  $\mathcal{P}_{\text{SUPG}}$ , which reads

$$\mathcal{P}_{\text{SUPG}}(\mathbf{w}) = \mathcal{L}_C^T(\mathbf{w}) = \mathbf{B}^T \frac{d\mathbf{w}}{dx}. \quad (3.40)$$

The GLS method attempts to minimize the residual associated to the differential equation via a least-squares process. Hence, the weighting functions enter in the same form of the original differential operator, i.e.  $\mathcal{P}_{\text{GLS}}$  is taken as

$$\mathcal{P}_{\text{GLS}}(\mathbf{w}) = \mathcal{L}^T(\mathbf{w}) = -\frac{d}{dx} \left( \mathbf{A}^T \frac{d\mathbf{w}}{dx} \right) + \mathbf{B}^T \frac{d\mathbf{w}}{dx} + \mathbf{G}^T \mathbf{w}. \quad (3.41)$$

Finally, the SGS method assumes that the solution can be additively decomposed into a coarse-scale component which can be determined by the finite element method and a fine-scale component which one tries to determine analytically. Furthermore, it is assumed that these two components live in mutually orthogonal function spaces. Thus the  $\mathcal{P}_{\text{SGS}}$  operator is defined as

$$\mathcal{P}_{\text{SGS}}(\mathbf{w}) = -\mathcal{L}^*(\mathbf{w}) = \frac{d}{dx} \left( \mathbf{A}^T \frac{d\mathbf{w}}{dx} \right) + \mathbf{B}^T \frac{d\mathbf{w}}{dx} - \mathbf{G}^T \mathbf{w}, \quad (3.42)$$

where  $\mathcal{L}^*$  is the adjoint operator of  $\mathcal{L}$ .

Finally, the matrix containing the stabilization parameters is defined as

$$\boldsymbol{\tau} = \left[ \frac{c_1}{\ell^2} \mathbf{A}_o + \frac{c_2}{\ell} \mathbf{B}_o + c_3 \mathbf{G}_o \right]^{-1}, \quad (3.43)$$

with

$$\mathbf{A}_o = (\mathbf{A}\mathbf{A})^{1/2}, \quad \mathbf{B}_o = (\mathbf{B}\mathbf{B})^{1/2}, \quad \text{and} \quad \mathbf{G}_o = (\mathbf{G}\mathbf{G})^{1/2}, \quad (3.44)$$

and  $c_1 = 4$ ,  $c_2 = 2$ , and  $c_3 = 1$ . This definition has been proposed by Codina [14] as a straightforward extension of the single equation case in the framework of the GLS method.



### 3.5.1 Convection-diffusion system

The comparison of stabilization techniques is first carried out using the convection-diffusion system (3.28) with boundary conditions (3.29). Figure 3.6 presents the numerical results obtained by the proposed stabilization technique, SUPG, GLS, and SGS using three different discretizations. The coarsest discretization consists of  $n = 16$  nodes, the medium of  $n = 64$  nodes and the finest of  $n = 256$  nodes. The mesh density is reflected in the figures by the colour brightness, i.e. the darkest lines correspond to the coarsest discretization while the brightest lines correspond to the finest discretization. All results shown in Figure 3.6 have been obtained using a diffusion parameter  $\epsilon = 10^{-2}$ . Thus, the results presented here are comparable with those depicted in the last row of Figure 3.1 which shows the classical approximation and the perturbation-stabilized solution.

It can be observed in Figure 3.6 that all numerical approximations are free of spurious oscillations. The results obtained with the SUPG, GLS and SGS methods are practically indistinguishable. The numerical approximations obtained with the perturbation-based stabilization technique differ from the other approximations. The SUPG, GLS and SGS methods are obtaining approximately the same nodal values irrespective of the discretization used. The perturbation-based stabilization technique shifts the boundary layers to the right, as can be seen most clearly for  $u_1$  and  $u_3$  respectively in Figure 3.6. This effect is at the cost of accuracy, i.e. the numerical approximations rendered by the proposed stabilization scheme are notably influenced by the discretization used.

### 3.5.2 Diffusion-reaction system

Now the comparison is carried out on the diffusion-reaction problem given by Equation (3.33) with homogeneous Dirichlet boundary conditions at both ends for the two equations.

The numerical results obtained are depicted in Figure 3.7 in the same manner as in the previous sub-section. The diffusion parameter has been taken as  $\epsilon = 10^{-3}$ . The results presented here correspond to those presented in the middle row of Figure 3.4; in fact, Figure 3.7(a) reproduces Figure 3.4(d).

For this diffusion-reaction problem not all results are free of spurious oscillations. Indeed, the failure of the SUPG method to obtain stable solutions in the present case is expected since the technique has not been designed to cope with reaction problems. From Equation (3.40) it is easy to see that  $\mathcal{P}_{\text{SUPG}}$  vanishes identically, providing no stabilization at all. This is not the case for the GLS method since  $\mathcal{P}_{\text{GLS}}$  does not vanish, although the scheme is unable to remove the spurious oscillations close to the boundary layers. For reaction dominated problems, this limitation has been reported for both one and two-dimensional domains even for the single equation case by Donea and Huerta [23]. It has also been reported by these authors that only the SGS method is able to render numerical approximations free of spurious oscillations. However, in this case it does not provide the same nodal values when different discretizations are used, while the proposed perturbation-based stabilization technique does so.

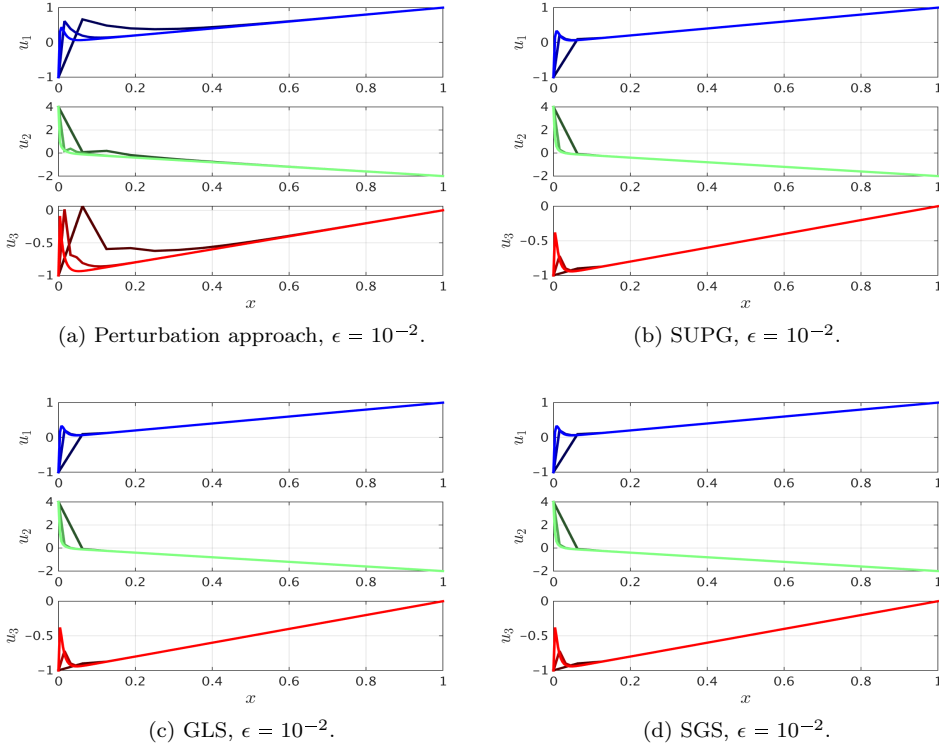


Figure 3.6: Numerical approximations obtained using three different discretizations consisting of  $n = 16$  nodes (darkest), of  $n = 64$  nodes (medium), and of  $n = 256$  nodes (brightest), for  $\epsilon = 10^{-2}$ , for the proposed stabilized scheme (top-left), the Streamline Upwind Petrov-Galerkin (top-right), Galerkin Least-Squares (bottom-left), and Sub-Grid Scale (bottom-right) methods. The corresponding classical results are depicted in Figure 3.1(e) and the perturbation approach results are repeated from Figure 3.1(f).

It is remarkable the ability of the presented stabilization technique, for the diffusion-reaction problem at hand, to render numerical approximations free of spurious oscillations with approximately the same nodal values when using different discretizations.

### 3.5.3 Convection-diffusion-reaction system

Finally, the comparison is made for the general convection-diffusion-reaction problem given by Equation (3.34). The results presented in Figure 3.8 have been obtained using a diffusion parameter  $\epsilon = 10^{-3}$  and correspond to those presented in the middle row of Figure 3.5.

It is worth noting that this time the SGS method fails in rendering acceptable numerical approximations. For the present problem, it is the SUPG method which performs better, in the sense that it is capable of rendering solutions which are free

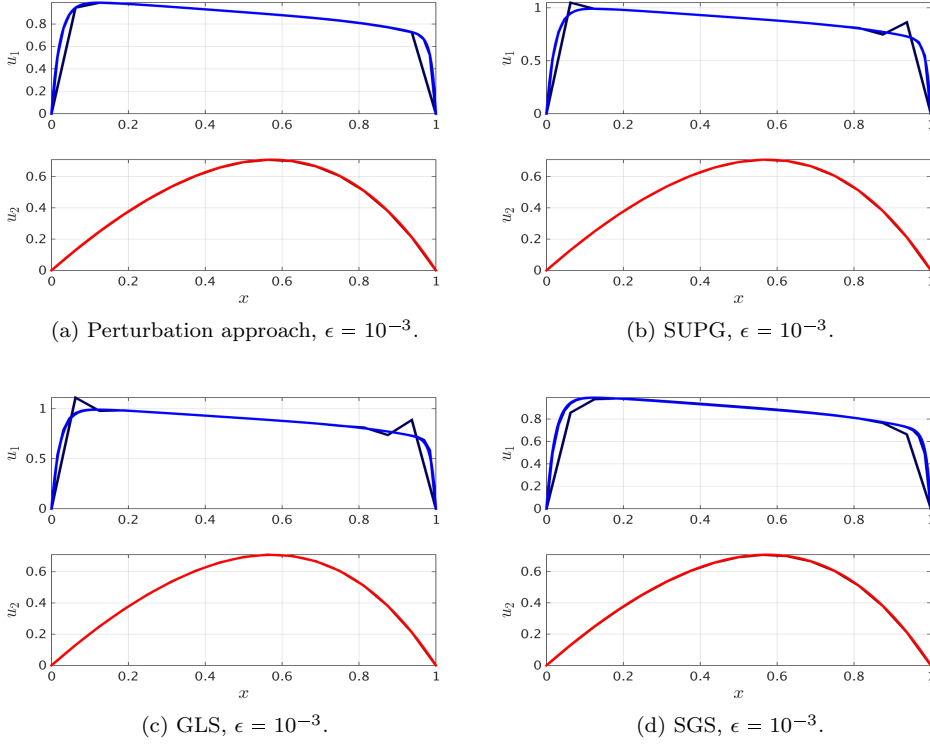


Figure 3.7: Numerical approximations obtained using three different discretizations consisting of  $n = 16$  nodes (darkest), of  $n = 64$  nodes (medium), and of  $n = 256$  nodes (brightest), for  $\epsilon = 10^{-3}$ , for the proposed stabilized scheme (top-left), the Streamline Upwind Petrov-Galerkin (top-right), Galerkin Least-Squares (bottom-left), and Sub-Grid Scale (bottom-right) methods. The corresponding classical results are depicted in Figure 3.4(c) and the perturbation approach results are repeated from Figure 3.4(d).

of spurious oscillations and with the coarse approximation that best resembles its corresponding fine approximation. The perturbation-based stabilization technique seems to over-diffuse the first solution, i.e.  $u_1$ , for the coarsest discretization. A similar but milder effect can be observed for the GLS method.

### Concluding remarks

The comparison has highlighted both the strengths and weaknesses of the presented stabilization technique with respect to well established stabilization methods. It is worth to mention that its ability to deal satisfactorily with all three different kinds of problems presented here is not shared by any of the other stabilization techniques. This shows its versatility and flexibility when dealing with general convection-diffusion-reaction problems and the convection-diffusion and diffusion-reaction sub-cases as well.

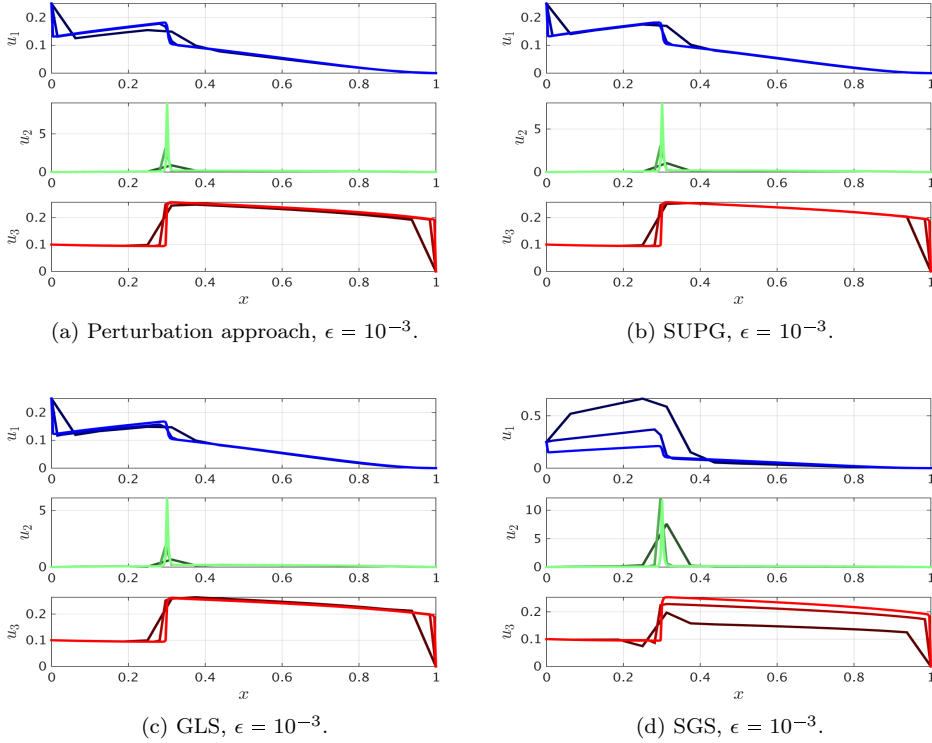


Figure 3.8: Numerical approximations obtained using three different discretizations consisting of  $n = 16$  nodes (darkest), of  $n = 64$  nodes (medium), and of  $n = 256$  nodes (brightest), for  $\epsilon = 10^{-3}$ , for the proposed stabilized scheme (top-left), the Streamline Upwind Petrov-Galerkin (top-right), Galerkin Least-Squares (bottom-left), and Sub-Grid Scale (bottom-right) methods. The corresponding classical results are depicted in Figure 3.5(c) and the perturbation approach results are repeated from Figure 3.5(d).

### 3.6 Conclusions and outlook

In this chapter a stabilization technique for general systems of coupled convection-diffusion-reaction equations with constant coefficients was developed. For the linear uncoupled case the proposed stabilization technique recovers the approach presented in [34]. That stabilization technique was developed for a single equation yielding unconditionally stable solutions based on the discrete maximum principle. The stabilization is achieved by effectively perturbing the transport coefficients of the equation to be discretized. Such perturbations are optimally determined to be the minimum ones required to obtain smooth and stable approximations. Additionally, it was shown that the numerical approximations obtained with the stabilized scheme converge to the classical Bubnov-Galerkin solution when the mesh Péclet number is small enough, a fact confirmed using a thorough and detailed numerical assessment. An illustrative

application demonstrates that the general convection-diffusion-reaction case also inherits these desirable properties. The stabilization technique is applicable regardless whether the advective or the divergence form of the partial differential equation is used for the spatial discretization, making it highly flexible and general, and allowing it to deal with different types of complex boundary conditions.

Although originally developed for coupled equations with constant coefficients, the stabilization technique has also been successfully applied to equations having spatially variable convection and reaction coefficients. This renders the method particularly versatile for problems with time dependent or even non-linear transport coefficients, including also the diffusion coefficients. Furthermore, since the perturbations required to render smooth numerical approximations are computed element by element this stabilization technique is locally adaptive, properly handling variable element sizes. Finally, there is no need to compute in advance, adapt, or change the mesh at any stage of the computation. This flexibility also removes the need for ordering or scaling of the system of differential equations prior to discretization.

For future work, the proposed stabilization technique can be extended to multidimensional configurations. Although the present chapter mainly focused on constant diffusion and space dependent convection and reaction coefficients in steady state with Dirichlet boundary conditions, variable diffusion coefficients, time dependency of the transport coefficients, non-linearity and other types of boundary conditions will be investigated in steady and transient states.

In this chapter, the effect the stabilization technique on the general properties of the system of algebraic equations after discretization has not been addressed. In particular, the spectral properties of this system may guide one to more effective strategies to solve it, especially when using iterative methods combined with preconditioning techniques. This will be the subject of forthcoming work.

## Chapter 4

# Applications to Coupled Continuum Dislocation Transport Equations

---

### Abstract

Plasticity of crystalline materials is physically described at the meso-scale by dislocations transport models, typically formulated in terms of dislocation densities. This leads to sets of coupled partial differential equations involving diffusion-like and convection-like processes combined with non-linearity. Since exact solutions for these systems are not available, numerical approximations are needed to efficiently solve them. However, the properties of these systems of equations cause most traditional numerical methods to fail, even for the case of a single equation. For systems of equations the problem is even more challenging due to the lack of fundamental principles guiding numerical discretization strategies. Therefore, dedicated strategies must be developed and carefully applied in order to obtain physically meaningful and numerically stable approximations. The objective of this chapter is to present a stabilization technique for systems of convection-diffusion-reaction equations and apply it to the equations modelling one-dimensional dislocation transport. This stabilization technique, based on coefficient perturbation, renders well-behaved and physically admissible numerical approximations. Several of its favourable characteristics are discussed, providing evidence of its versatility and effectiveness through a detailed numerical assessment.

**keywords.-** Convection-diffusion-reaction, Coupled systems, Finite element method, Crystal plasticity, Continuum dislocation transport.

---

---

This chapter is based on: [Hernández H.](#), Massart T.J., Peerlings R.H.J., and Geers M.G.D. 2016. *Stabilization of Coupled Convection-Diffusion-Reaction Equations for Continuum Dislocation Transport*. In preparation.

## 4.1 Introduction

In applied materials science the accurate description of the plastic behaviour of materials is of paramount importance since it highly influences the material's mechanical behaviour. For crystalline solids, inelastic effects have been taken into account at the level of single crystals by various crystal plasticity models [66]. At a higher spatial resolution, plasticity in a single crystal can be modelled in a physical setting using dislocation transport equations [21, 32, 36].

These frameworks are typically formulated in terms of dislocation densities, resulting in a continuum description at the meso-scale. The transport equations consist of a set of coupled, transient, and non-linear partial differential equations, involving derivatives in space of both first-order and second-order [31, 32]. The simultaneous presence of both order derivatives of transported densities complicates the numerical treatment of such systems of equations. This is particularly true if the first-order convection-like term dominates the second-order diffusion-like term.

Using classical numerical schemes, e.g. centred finite differences or Bubnov-Galerkin finite elements, to approximate the solution of these transport problems (combining convection and diffusion), spurious and non-physical oscillations appear, rendering the numerical approximation unstable. Hence, stabilization approaches must be used in order to retrieve physically meaningful and numerically stable approximations. In a general finite element context, several stabilization techniques have been proposed; e.g. the Streamline Upwind Petrov-Galerkin method [7, 41], the Galerkin Least-Squares method [27], the bubble multi-scale stabilization method [60], the sub-grid method [33], and the finite calculus-based approach [57]. The vast majority of these techniques mainly deals with convection dominated problems [23, 87]. The addition of a reaction term may cause numerical instabilities by itself, even in the absence of convection [60].

An stabilization technique based on coefficients perturbation was first developed in [34], relaying on system equations with signed dislocation densities. In that chapter it is shown, and confirmed numerically, that the stabilized finite element approximation obtained by coefficient perturbation converges to the classical Bubnov-Galerkin scheme if diffusion-like terms dominate over the convection-like terms on a sufficiently fine mesh. This has been achieved by enforcing the discrete maximum principle, which is the translation of the continuous maximum principle related to the physics of the problem [12, 80].

Unfortunately, the stabilization technique proposed in [34] has proven to be useless when straightforwardly applied to dislocation transport equations involving total and geometrically necessary dislocation densities as the field variables, rather than positive and negative dislocation densities. This is due to the fact that when signed dislocations are considered, it is possible to arrange the non-linear terms in such a way that the negative dislocation density acts as a transport coefficient in the positive dislocation density equation and vice-versa. Therefore, the system consisting of two partial differential equations can be handled numerically as two independent problems from a numerical stability viewpoint, although its numerical time integration is

done alternately. This uncoupling is not possible when total and geometrically necessary dislocation densities are the governing field variables, since terms containing only the geometrically necessary dislocation density appear in the total dislocation density equation and vice-versa. The problem cannot be decomposed into two problems, which would have allowed for the use of stable approximations of single convection-diffusion partial differential equations. Instead, a single problem consisting of two strongly coupled equations should be solved simultaneously and monotonically.

This change of perspective has profound conceptual and technical consequences. It suggests to treat the fully general case with  $m$  coupled convection-diffusion-reaction equations, where the particular case  $m = 1$  received most attention during the past decades among numerical methods practitioners. Such systems of coupled equations are met in several branches of science such as bio-mechanics [18], combustion [5], computer science [30], ecology [45], economy [6], epidemiology [84], finance [17], groundwater pollution [4], heat transfer [70], neuroscience [3], physiology [37], seepage flow [71], solid mechanics [14] or turbulence [15]. Since for this multiple equations case, analytical solutions are even harder to obtain than for the single equation case, numerical approximations constitute the only available option to solve such systems. Nevertheless, only limited attention has been given to the stabilization of systems of equations. The lack of reliable and robust numerical approximation techniques results from the lack of a maximum principle when passing from a single equation to systems of coupled equations in the most general form [62].

Numerical difficulties present in the single equation case; and observed when convection, reaction, or a combination of them dominates over diffusion or when the discretization is not fine enough; are inherited by the multiple equations case. Solving such instability problems for systems of equations has been tackled by extending and adapting techniques originally developed for the single equation case. The most representative approaches consist of upwind finite differences applied to the convective terms on layer adapted meshes according to the construction methodologies proposed by Shishkin and Bakhvalov [29, 48]. For finite volumes, the use of discontinuous and high order approximations, upwinding and adaptive meshes were the most successful techniques to deal with coupled equations [16, 58]. In the finite element method context; streamline upwind Petrov-Galerkin, Galerkin least-squares, algebraic sub-grid scale with high order elements together with shock capturing techniques are the most common techniques [4, 5, 14]. Notwithstanding all this progress, the straightforward application of these techniques is rendered useless due to the particular characteristics of the continuum dislocation transport equations, mainly the non-standard boundary conditions with which they are supplemented.

Taking the single equation case as the departure point, a stabilization technique based on coefficients perturbations was proposed and proven to be effective for systems of linear one-dimensional convection-diffusion-reaction equations in steady state [35]. The main objective of the present chapter is to exploit and to apply this stabilization technique for dislocation transport problems expressed in terms of the total and geometrically necessary dislocation densities, including its non-linearity in the



transient regime. The stabilization technique is expected to be versatile despite these two additional complexities associated with dislocation transport.

The chapter is organized as follows. In Section 4.2, the physical model problem, consisting of the shearing of an infinite crystal, is described. Section 4.3 assesses the effectiveness of the stabilization technique presented in the previous chapter for the system of equations through two numerical examples comparing stabilized results with those obtained with the classical Bubnov-Galerkin scheme. This is followed by two additional numerical examples, allowing to thoroughly assess the efficiency and consistency of the stabilization technique. To close this section, several numerical simulations obtained for different dislocation transport modelling assumptions are presented. Due to the non-linearity of the continuum dislocation transport equations, the definition of the diffusion and convection matrices is non-unique. Section 4.4 has been included in order to evaluate the influence of an alternative definition on the performance of the stabilization technique. Finally, Section 4.5 presents the main conclusions of this chapter and discusses some future work.

## 4.2 Continuum model for dislocation transport

The main focus of this chapter is to apply an efficient stabilization technique for the simulation of dislocation transport in a single crystal, regardless of the field variables considered. The equations to be discretized are written in terms of dislocation densities on glide planes. For the sake of simplicity, a single glide system with infinite parallel edge dislocations is considered. In chapter 2, positive and negative dislocations densities, denoted respectively by  $\rho^+$  and  $\rho^-$ , were used in the construction of the continuum model for dislocation transport. This choice was made since  $\rho^+$  and  $\rho^-$  have a clear intuitive physical interpretation. However, it is possible to use different types of dislocation densities as the field to be approximated numerically, as more commonly done in the literature. This change of variables can introduce coupling coefficients for which the proposed stabilization technique (extended to systems of differential equations) is particularly well suited.

### 4.2.1 Governing equations

It is a common practice in literature to use the *total dislocation density*  $\rho$  and the *geometrically necessary dislocation density*  $\kappa$  rather than the previously used positive and negative dislocations densities, since these total dislocations and geometrically necessary dislocations densities are directly related to macroscopic properties such as incompatibility and hardening. They are related to the positive and negative dislocation densities by

$$\rho = \rho^+ + \rho^-, \quad \text{and} \quad \kappa = \rho^+ - \rho^-. \quad (4.1)$$

Using these relations it is possible to rewrite the transport equations, first for  $\rho$  by adding Equations (2.2) and (2.3) and then for  $\kappa$  by subtracting Equation (2.3) from Equation (2.2), yielding

$$\frac{\partial \rho}{\partial t} + \frac{\partial}{\partial x} (\Phi_\rho) = s_\rho, \quad (4.2)$$

$$\frac{\partial \kappa}{\partial t} + \frac{\partial}{\partial x} (\Phi_\kappa) = s_\kappa, \quad (4.3)$$

where the fluxes are obtained similarly as  $\Phi_\rho = \Phi^+ + \Phi^-$  and  $\Phi_\kappa = \Phi^+ - \Phi^-$  which can again be expressed in terms of  $\rho$  and  $\kappa$ . By introducing the following two constants

$$C_4 = b'_1 C_1 \mathcal{L}, \quad \text{and} \quad C_5 = b'_2 C_1 \mathcal{L}, \quad (4.4)$$

the corresponding fluxes are expressed in a compact form as

$$\Phi_\rho = C_0 \kappa - C_4 \rho \frac{\partial \rho}{\partial x} - C_5 \kappa \frac{\partial \kappa}{\partial x}, \quad (4.5)$$

$$\Phi_\kappa = C_0 \rho - C_5 \rho \frac{\partial \kappa}{\partial x} - C_4 \kappa \frac{\partial \rho}{\partial x}. \quad (4.6)$$

The substitution of these fluxes (4.5-4.6) in the conservation Equations (4.2-4.3) leads to a system of two coupled transient and non-linear partial differential equations for which analytical solutions are not available. Therefore, a numerical approximation is required for which the finite element method will be used in the next section.

The two more representative types of boundary conditions are not altered by the change of variables. The first one consists of a free surface where dislocations can escape, causing their corresponding density to vanish, i.e.  $\rho(\Gamma_D) = \kappa(\Gamma_D) = 0$ , where  $\Gamma_D$  is the part of the boundary of the domain on which the above mentioned condition applies. This corresponds to Dirichlet boundary conditions for the conservation Equations (4.2-4.3). In the other extreme the boundary presents an impenetrable barrier for the dislocations, e.g. a hard grain or phase boundary. This situation can be stated as  $\Phi_\rho(\Gamma_R) = \Phi_\kappa(\Gamma_R) = 0$ .

Initial conditions, but this time for the total and geometrically necessary dislocation densities, i.e.  $\rho_0(\Omega) = \rho(\Omega, t = 0)$  and  $\kappa_0(\Omega) = \kappa(\Omega, t = 0)$  should be added in order to properly define the continuum dislocation transport problem.

## 4.3 Computational assessment of the stabilization technique

This section presents the application of the extension to systems of coupled equations of the stabilization technique to the dislocation transport system given by Equations (4.2-4.3) with their corresponding fluxes given by Equations (4.5-4.6). Of particular interest is the illustration of the efficiency and consistency of the stabilization scheme presented in Chapter 3.

In order to apply the stabilization technique to the non-linear dislocation transport problem, the fluxes of dislocations given by Equations (4.5-4.6) are directly substituted in the dislocation density conservation Equations (4.2-4.3), giving

$$\frac{\partial \rho}{\partial t} + \frac{\partial}{\partial x} \left[ -C_4 \rho \frac{\partial \rho}{\partial x} + \left( C_0 - C_5 \frac{\partial \kappa}{\partial x} \right) \kappa \right] = s_\rho, \quad (4.7)$$

$$\frac{\partial \kappa}{\partial t} + \frac{\partial}{\partial x} \left[ -C_5 \rho \frac{\partial \kappa}{\partial x} + C_0 \rho - C_4 \frac{\partial \rho}{\partial x} \kappa \right] = s_\kappa, \quad (4.8)$$

where the terms composing the fluxes have been re-written in a slightly different format than in Equations (4.5-4.6). This change has been done in order to clearly identify the convection-like coefficients or diffusion-like coefficients, either direct or crossed, and finally to be able to cast this system of coupled partial differential equations in the generic matrix form given by Equation (3.5). In such a generic form, the unknown vector is taken as  $\mathbf{u} = [\rho, \kappa]^T$ ; it follows naturally that the source vector is  $\mathbf{f} = [s_\rho, s_\kappa]^T$ . Thus, the diffusion matrix  $\mathbf{A}$  and the advection matrix  $\mathbf{B}$  can be expressed as:

$$\mathbf{A} = \rho \begin{bmatrix} C_4 & 0 \\ 0 & C_5 \end{bmatrix}, \quad \text{and} \quad \mathbf{B} = \begin{bmatrix} 0 & C_0 - C_5 \frac{\partial \kappa}{\partial x} \\ C_0 & -C_4 \frac{\partial \rho}{\partial x} \end{bmatrix}. \quad (4.9)$$

Note that this form can be established irrespective of: (i) the dislocation transport model type used (e.g. [21] for Dogge model or [32] for Groma model), (ii) the length scale adopted (constant or variable), (iii) the presence of interactions between dislocations of different sign.

It is useful to analyse in some depth the properties of these diffusion and advection matrices. First note that the effectiveness of the stabilization technique will be determined by the positive definiteness of the diffusion matrix which can be seen as the vector equivalent of having a positive diffusion coefficient in the scalar case, i.e. diffusion always takes place in the negative gradient's direction. This property can be easily verified through the diffusion matrix determinant which is given by  $|\mathbf{A}| = C_4 C_5 \rho^2$ ; which apart of the square of the  $\rho$  value, it is determined by the  $C_4$  and  $C_5$  constants. These are given by Equation (4.4). After continued substitution, the diffusion matrix determinant can be finally be written as

$$|\mathbf{A}| = b'_1 b'_2 (\rho C_1 \mathcal{L})^2. \quad (4.10)$$

It is clear that the positiveness of the diffusion matrix is not affected by the length scale  $\mathcal{L}$ , nor by the material properties since  $C_1 \neq 0$ . This property is only affected by the model used and if the interactions between dislocations of different signs are taken into account or not. This can be observed by identifying the  $b'_1$  and  $b'_2$  values for the two considered models, shown in tabular form as

	Crossed interaction			Crossed interaction	
	$b'_1$	With    Without		$b'_2$	With    Without
Dogge		3            1	Dogge		1            1
Groma		0            0	Groma		4            12

Note that the Groma model poses a serious difficulty to the stabilization technique presented here since the conservation equation for the total dislocation density  $\rho$  becomes a purely hyperbolic partial differential equation. Such equations have been successfully handled by the finite difference and finite volume communities by means of several techniques that have shown to be effective throughout the years, the up-wind differences being the oldest and simplest one. In general terms all these techniques,

and up-winding in particular, rely on the addition of artificial diffusion. Therefore all of them can be interpreted as perturbation techniques that introduce ellipticity into the original hyperbolic partial differential equation. This is the main reason to consider the introduction of a threshold diffusion when dealing with the Groma type models. Such threshold will be taken as  $\alpha_{min} = 10^{-12}$  in all subsequent computations.

To incorporate the transient character of the problem, the fully implicit backward Euler method has been used for time integration. This scheme is unconditionally stable with respect to the time step size  $\Delta t$  and to the spectral properties of the matrices resulting from the space-time discretization, despite having only first order accuracy [2, 19, 38, 49, 63].

For all simulations, the Picard iterative method is used to deal with the non-linear system of equations obtained after discretization of the dislocation transport equations at each time step [63, 64]. The difference among two successive approximations is measured as

$$d^{(j)} = \sqrt{\|\boldsymbol{\rho}_t^{(j)} - \boldsymbol{\rho}_t^{(j-1)}\|_2^2 + \|\boldsymbol{\kappa}_t^{(j)} - \boldsymbol{\kappa}_t^{(j-1)}\|_2^2}, \quad (4.11)$$

where the vectors  $\boldsymbol{\rho} = [\rho_1, \rho_2, \dots, \rho_{n-1}, \rho_n]^T$  and  $\boldsymbol{\kappa} = [\kappa_1, \kappa_2, \dots, \kappa_{n-1}, \kappa_n]^T$ , with  $n$  being the total number of nodes composing the finite element mesh, are the nodal values of the total dislocation and the geometrically necessary dislocation densities, respectively. In Equation (4.11) the sub-index  $t$  is the current time instance, not to be confused with the nodal labels used for the individual components of such vectors. The iteration is stopped as soon as the tolerance  $\epsilon_n = 10^{-6}$  is reached, i.e.  $d^{(j)} < \epsilon_n$ . The initial guess is always taken as the final solution at the previous time step, i.e.  $\boldsymbol{\rho}_{t+\Delta t}^{(0)} = \boldsymbol{\rho}_t^{(j)}$  and  $\boldsymbol{\kappa}_{t+\Delta t}^{(0)} = \boldsymbol{\kappa}_t^{(j)}$ .

At each non-linear iteration, a linear system of equations has to be solved. For this purpose the *BiCGStab* method has been used, having in mind a future multidimensional extension of the framework involving very large and sparse systems [67, 77]. In all cases, the maximum number of allowed iterations is set equal to the size of the linear system, although the iterative process is stopped as soon as  $\|\mathbf{r}^{(k)}\|/\|\mathbf{b}\| < \epsilon_s = 10^{-6}$  is reached, with  $\mathbf{r}^{(k)}$  the  $k$ -th residual vector and  $\mathbf{b}$  the right hand side vector. The final approximation of the previous iteration is always taken as the initial guess for the linear solver. No preconditioning is used.

The physical parameters have been taken constant for the ease of comparison. The values used correspond to those presented by [50] and are comparable to those used in [21]. The domain considered has unit length  $L = 1 \mu m$ , and a single phase has been used on the whole domain. Its properties are as follows;  $h = 0.1 \mu m$ ,  $b = 0.3 nm$ ,  $B = 10^{-4} Pa s$ ,  $\nu = 1/3$ ,  $G = 25 GPa$ . The initial condition for all problems was given by  $\rho_0 = 400 \mu m^{-2}$  and  $\kappa_0 = 0 \mu m^{-2}$ . Finally, the time step is the same for all simulations, with  $\Delta t = 10^{-1} \mu s$ .

For all subsequent numerical examples, except those presented in the last Section 4.3.4 in which a comparison between models is carried out, the Dogge model with

a constant length scale and considering interactions between dislocations of different sign, i.e.  $\mathcal{L} = h$ ,  $a = 1$  and  $b_1 = b_2 = 1$ .

Only the applied stress  $\tau$  and the mesh size  $\ell$  are modified during this study. Once they are chosen for a particular problem they remain unchanged, i.e. for a particular simulation the applied stress is constant over the whole domain which is discretized with a uniform mesh.

The precise definition of a mesh Péclet number in its most traditional way is, for the coupled equations at hand, an intricate matter. Indeed, it is only possible for the second equation to compute it according to Equation (2.30). After simplifying, it can be expressed as

$$\text{Pe}_\kappa = \frac{\ell}{2} \frac{b'_1}{b'_2} \left( \frac{1}{\rho} \frac{\partial \rho}{\partial x} \right). \quad (4.12)$$

First notice that for the Groma model, such number is zero since  $b'_1 = 0$ . Moreover, due to the non-linear nature of the dislocation transport problem, this Péclet number depends on the total dislocation density and its gradient, which change over time. However, if a uniform distribution of the total dislocation density is reached, or if a uniform initial condition is used, the Péclet number vanishes here as well. The situation is even more complicated for the first equation, since in this case the direct advection coefficient  $\beta_{\rho\rho}$  is always zero, thus  $\text{Pe}_\rho = 0$ , irrespective of the model, irrespective of the length scale used and irrespective of the account for interactions between different types of dislocations.

As dislocation transport starts, this situation becomes even more intricate because dislocations are expected to pile up at the impenetrable boundaries, forming *boundary layers*. Since the applied stress  $\tau$  will be taken constant through the whole spatial domain, a *V*-shape profile for the total dislocation density is expected. As transport continues, dislocations are expected to pile up in a smaller region reducing the boundary layers width. At this moment three different regions can be roughly identified. The first one is close to the boundaries where the total dislocation density and its gradient attain their largest values through the spatial domain. These two facts reduce and increase, respectively, the local Péclet number. The second region is the central one in which the total dislocation density and its gradient attain both their lowest values causing an increase and reduction, respectively, of the local Péclet number. The third and more critical region is the transitional one in which a low total dislocation density and a high value of its gradient both involve an increase of the Péclet number. Thus, as the simulations advance in time, and the uniform distribution of the total dislocations density changes to the mentioned *V*-shape profile, it is expected that the adaptive nature of the stabilization technique will play a more prominent role.

### 4.3.1 Influence of the applied stress

In this first example, the main focus is put on the ability of the stabilization technique to remove spurious oscillations and to yield only non-negative total dislocation densities. To this aim, three different cases are presented, all using the same uniform coarse mesh of  $2^4 = 16$  linear elements. Only the applied stress is increased in each of

the cases, taking the values  $\tau = 0.01, 0.1$ , and  $1.0$  GPa. All the presented results are obtained at time  $t = 10^6 \mu\text{s}$ .

Figure 4.1 shows the results in terms of total dislocation and geometrically necessary dislocation densities in blue and red respectively. The results obtained with the classical (non-stabilized) Bubnov-Galerkin method are depicted in the left column, while the right column shows the results obtained with the stabilization technique. These numerical schemes are referred to as *classical* and *stabilized* respectively.

Note that in the first case depicted in the top row of Figure 4.1, for a small applied stress ( $\tau = 0.01$  GPa), no noticeable difference can be observed between the classical and stabilized approximations for both dislocation densities. The applied stress is not large enough to generate tight and sharp boundary layers and therefore the middle of the spatial domain remains sufficiently occupied by dislocations, avoiding a large reduction of the diffusion coefficients given by  $\alpha_{\rho\rho} = C_4 \rho$  and  $\alpha_{\kappa\kappa} = C_5 \rho$ .

The results for the second case with  $\tau = 0.1$  GPa are shown in the middle row of Figure 4.1. For the classical scheme, saw-tooth-like wiggles start appearing in the central region of the spatial domain where the total dislocation density is close to zero, which causes a decrease of the diffusion coefficients. This effect pollutes the numerical approximation, with the nodal values of the total dislocation density at some nodes being negative, which is physically meaningless. The numerical approximation obtained with the stabilization scheme, as shown on the right, is smooth, non-negative for the total dislocation density, and free of any oscillation. It is important to note that the maximum and minimum values attained by both total dislocation and geometrically necessary dislocations differ between the classical and stabilized approximations. Larger values are obtained by the classical scheme, but this classical numerical approximation is meaningless since it reveals spurious oscillations and negative values for a strictly non-negative quantity.

The results for the third case with  $\tau = 1.0$  GPa are shown in the last row of Figure 4.1, a stress level that matches practical applications. On the left, corresponding to the classical scheme, the oscillations are much larger than in the previous case, making the numerical approximation completely useless for any application. This effect is partially due to the fact that the convective character of the problem, has increased by one order of magnitude through the applied stress increment. The second important reason is the decrease of the effective local diffusion coefficients due to the starvation of dislocations in the central part of the spatial domain. The corresponding stabilized result is shown on the right in the last row. It does not exhibit any wiggles or oscillations and the total dislocation density is non-negative in the entire spatial domain. As expected, the width of the boundary layer is decreased and dislocation densities reach higher values compared to the case with a lower applied stress.

These results confirm that the stabilization technique is effective when required. If spurious oscillations are not present because the problem is not dominated by convection, the effect of the stabilization is negligible, as confirmed by the plots depicted in the first row of Figure 4.1. On the other hand, the beneficial effect of the stabilization

technique becomes apparent as soon the convective character of the system of partial differential equations starts polluting the numerical approximation obtained by the classical scheme, distorting it with wiggles and non-physical negative density values.

In terms of computing time, for the same discretization, the use of the stabilization technique practically doubles the elapsed time with respect to the classical scheme for cases in which the latter still furnishes physically meaningful results. One nevertheless expects a significant gain in computational efficiency, because using the stabilization technique allows coarsening the mesh drastically compared to a classical formulation for convection dominated problems.

### 4.3.2 Influence of the discretization

The aim of this example is to analyse the behaviour of the stabilization technique under mesh refinement and the non-linearity influence as time advances. Therefore, the element size  $\ell$  is progressively reduced and the applied stress is kept constant and equal to  $\tau = 10^{-0.5}$  GPa for all current examples.

In each plot in Figure 4.2, the total dislocation density profiles obtained at equally spaced time instances between  $t_o = 0$   $\mu\text{s}$  and  $t_f = 10^6$   $\mu\text{s}$  are shown, the brightest one corresponding to the initial time and the darkest one to the last time instance. As in the previous example, classical approximations are depicted on the left and stabilized ones on the right. The results obtained using increasingly refined meshes of 16, 32, 64, and 128 elements with linear shape functions are depicted.

Note that for the coarsest mesh, depicted in the first row of Figure 4.2, the approximations obtained with the classical scheme start to show an oscillatory behaviour from early time instances onwards, precisely in the above mentioned transitional region. Such spurious oscillations start to scatter and become more pronounced as time advances due to the reduction of the diffusion coefficients as the total dislocation density  $\rho$  approaches zero. In contrast, the approximations obtained with the stabilized scheme are, for all time instances, strictly non-negative and free of spurious oscillations even in the central region, where the total dislocation density reaches almost vanishing values. This is also true for the transitional regions, where the high value reached by the geometrically necessary dislocation density gradient increases the crossed advection coefficient  $\beta_{\rho\kappa}$ , making the numerical approximation more prone to oscillatory behaviour. From the discrepancy of the vertical axis scale in these two plots it can be noticed that the maximum values of the numerical approximations attained for the classical and stabilized schemes differ considerably. The surplus obtained by the classical scheme is presumably due to the lack of stability of that scheme, the solution of which is not reliable due to the presence of wiggles and negative values.

Moving to the second row of Figure 4.2, the number of elements composing the finite element mesh is doubled while all other parameters remain identical. Again, from the left plot corresponding to the classical scheme, it is noticeable that wiggles appear in the transitional region, and propagate to the central region at increasing times due to the decrease of the total dislocation density in this region. For this case

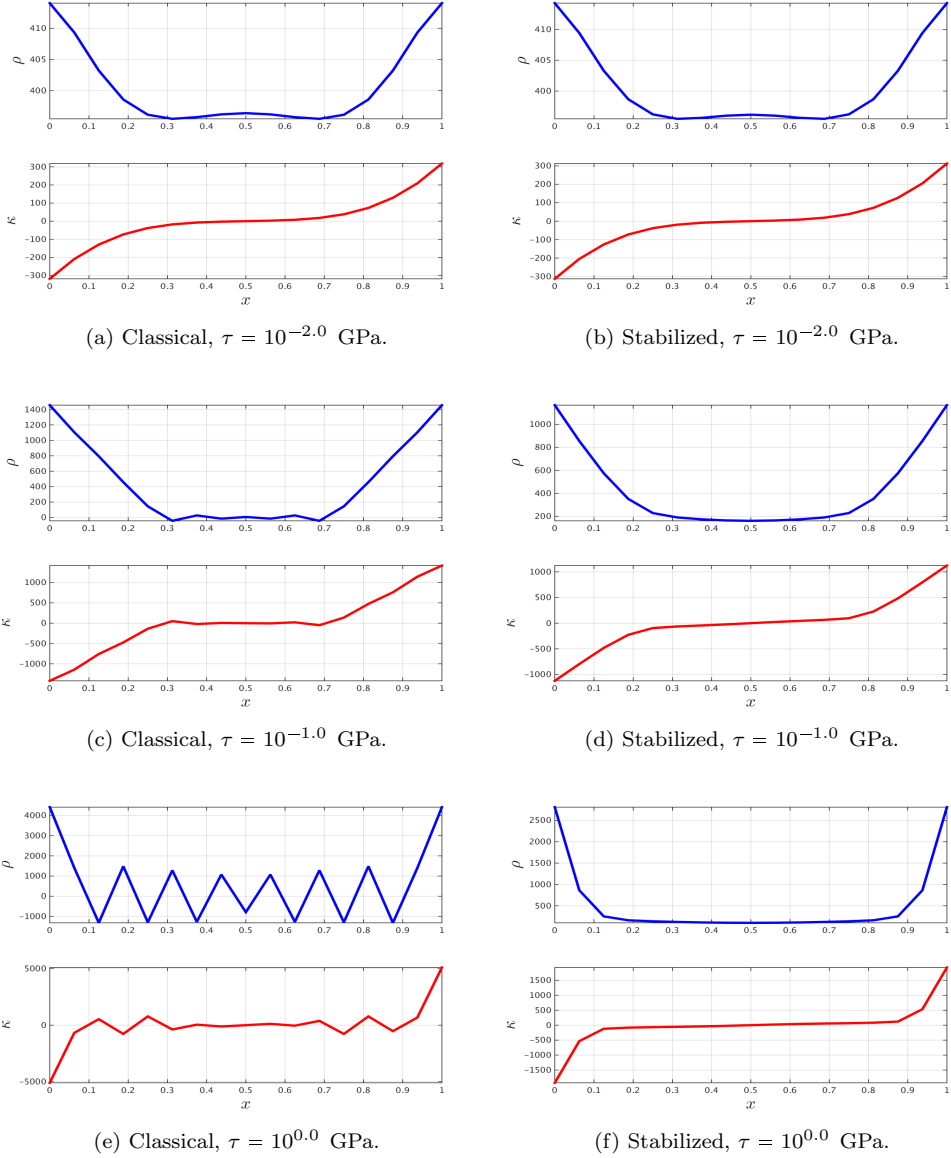


Figure 4.1: Comparison of the total dislocation density  $\rho$  in blue and the geometrically necessary dislocation density in red, both in  $\mu m^{-2}$  obtained with the classical (left) and stabilized (right) scheme using a discretization with 16 elements, increasing the stress  $\tau$  from top to bottom.



the oscillations do not grow as severely compared to the previous case because the mesh has been refined. Like before, the classical scheme still overestimates maximum values. For the stabilized scheme, at all time instances, the approximations are strictly positive and free of spurious oscillations. Note that the maximum values attained are higher with respect the stabilized results using a coarser mesh. This discrepancy will be further analysed in what follows.

By doubling again the number of elements used in the mesh, the numerical approximations shown on the third row of Figure 4.2 are obtained. The classical scheme approximation is now also free of oscillations at all time instances, except at the final time instance at which tiny but still noticeable wiggles can be observed in the transitional region. This is consistent with the explanation of the results obtained with the two previous meshes. Again, the stabilized scheme results are strictly non-negative and free of any wiggle through the whole spatial domain for all time instances. Furthermore, it is emphasized that the difference between the maximum values attained by the classical or stabilized schemes is now progressively reduced as time advances, to become insignificant at the last time instance.

Finally, the fourth and last row of Figure 4.2 shows the results obtained using the finest mesh for the present example, consisting of 128 elements. The first important feature to observe is that for this refinement level, the classical scheme now recovers a stable approximation, which does not exhibit spurious oscillations. For this level of refinement, the classical scheme approximation can be regarded as reliable for comparative purposes with respect to the approximation obtained with the stabilized scheme. Both approximations are very similar at the last time instance, not only for the maximum values attained in the boundary layers, but also for the profile shape in the whole spatial domain, while this is less the case at intermediate time instances. The stabilized approximation seems to be blunter than the classical approximation in those regions where a high gradient change occurs. For the stabilized scheme more intermediate time step solutions can be discerned, contrary to the classical scheme in which only two intermediate approximations can be recognized apart from the initial condition and the steady state solution. Hence, the steady state solution corresponding to the last time instance is somewhat delayed in the stabilized scheme, even if the stabilization effect on this last approximation is negligible.

To close this analysis, two important observations remain to be discussed, namely the maximum values discrepancies when using a series of refined meshes with stabilization, and the steady state solution delay observed when analysing the finest mesh results. Both effects can be associated with the artificial diffusion introduced by the stabilization scheme in order to render stable numerical approximations. When using the stabilization scheme, the original problem is not solved but rather another problem with slightly modified coefficients. This in turn is the conceptual basis of the stabilization technique since it is based on perturbing the original problem, and instead solve a problem with coefficients selected to resemble as close as possible the original one, but with which the approximation remains free of wiggles and spurious oscillations when discretized using a given mesh. The classical and stabilized results obtained with an even more refined mesh containing 256 elements (not shown here) are almost identical

at all time instances, a fact that confirms the artificial diffusion addition argument. This confirms the fact that the present stabilization technique intervenes only when it is strictly needed, whereas it is inactive if the mesh is fine enough to get numerically stable approximations.

### 4.3.3 Non-linear and time evolution adaptivity

In this section a detailed analysis of the stabilization technique behaviour is carried out in order to provide evidence of its flexibility and adaptive nature. This analysis is performed by modifying the applied stress and mesh refinement. Henceforth, only results obtained with the stabilization scheme will be considered.

#### Stress variation

In the first situation, the mesh is fixed and consists of 256 elements. The stress level is modified in order to observe its influence on the evolution of the direct diffusion and advection coefficients for the geometrically necessary dislocation densities  $\kappa$  given by Equation (4.8). These coefficients are in turn used by the stabilization technique to determine the direct advection perturbation  $\beta_{\kappa\kappa}^*$ . In order to simplify the current analysis, the crossed advection perturbation is set to zero, i.e.  $\beta_{\kappa\rho}^* = 0$ , even though its corresponding coefficient does not vanish, being indeed a time invariant constant through the whole spatial domain, i.e.  $\beta_{\kappa\rho} = C_0$ . Thus the effects of both, direct and crossed, advection coefficients will be active on the direct advection perturbation only.

Figure 4.3 shows on the first row the direct diffusion coefficient  $\alpha_{\kappa\kappa} = \rho C_5$ , while on the second row the direct advection coefficient  $\beta_{\kappa\kappa} = -C_4 \partial\rho/\partial x$  is depicted. Similar plots for the crossed advection coefficient are not shown since, even if it influences the perturbation evolution to analyse, since it remains constant. The third row of Figure 4.3 shows the direct advection perturbation  $\beta_{\kappa\kappa}^*$ , which is the main quantity of interest in the present analysis. The stress level is increased column by column by one order of magnitude.

The first important observation is that the direct diffusion coefficient decreases in the central region and increases close to the impenetrable boundaries exhibiting a boundary layer behaviour. This is of course due to the fact that the direct diffusion coefficient is simply a scalar multiplied by the total dislocation density. As expected, the boundary layer width decreases and the maximum values attained are larger as the stress is increased, see first column of Figure 4.3. An almost perfect linear relationship exists between the magnitude of the maximum values attained by  $\alpha_{\kappa\kappa}$  and of the applied stress.

A second important observation can be made in the second row of Figure 4.3, where the time evolution of the direct advection coefficient for three different stress levels is shown. Since the plotted quantity is a scalar times the total dislocation density gradient, these plots keep a close relationship with those presented in the first row. The boundary layer pattern is not as apparent as in the previous row but, mainly from the third column, it is clear that the same behaviour is also exhibited by the direct

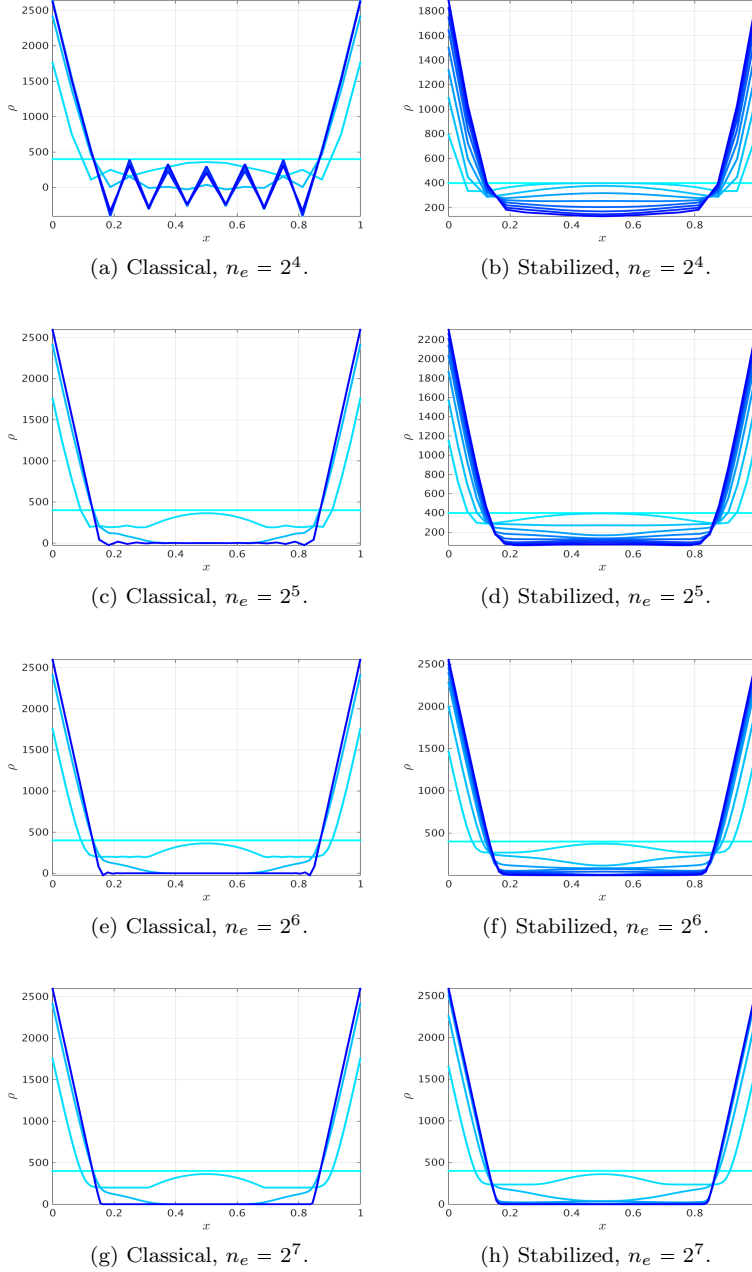


Figure 4.2: Comparison of the time evolution of the total dislocation density  $\rho$  in  $\mu\text{m}^{-2}$  obtained with the classical (left) and stabilized (right) scheme for an applied stress  $\tau = 10^{-0.5}$  GPa, doubling the number of elements composing the finite element mesh from top to bottom. The cyan line corresponds to the initial condition and the blue one to the last computed time instance ( $t = 10^6 \mu\text{s}$ ), intermediate approximations are at equidistant time intervals.

advection coefficient  $\beta_{\kappa\kappa}$ . Note again that the order of magnitude of the maximum values attained for  $\beta_{\kappa\kappa}$  is approximately linearly related to the order of magnitude of the applied stress as observed in the vertical axis scale.

Once the behaviour of  $\alpha_{\kappa\kappa}$  and  $\beta_{\kappa\kappa}$  have been analysed, the perturbation  $\beta_{\kappa\kappa}^*$  can be scrutinized based on the third row of the Figure 4.3. As expected, a localized behaviour can also be recognized, but in this case these are not due to boundary layers, instead they are now *internal layers*. Such internal layers in which  $\beta_{\kappa\kappa}^*$  strongly evolves appear precisely in the transitional region where a low total dislocation density is combined with a large value of its spatial gradient. The development of such regions for  $\beta_{\kappa\kappa}^*$  starts to be evident even in the left-most plot corresponding to the weakest applied stress, where one would expect high values in the central region based on the direct diffusion decrease there. For the central plot with an incremental applied stress, the width of the internal layer reduces from outside the spatial domain towards its centre, since the total dislocation density gradient becomes, though high in magnitude, constant close the boundaries where the total dislocation density itself attains its maximum values. This combined effect becomes more prominent by increasing the applied stress. The right-most column, reveals an internal layer of  $\beta_{\kappa\kappa}^*$  that is much thinner with respect to the previous ones.

### Mesh variation

The manner in which the stabilization technique affects the stability issues when the mesh is refined for a fixed applied stress is investigated next. This is carried out by scrutinizing the crossed advection perturbation for the total dislocation density equation  $\beta_{\rho\kappa}^*$ , in relation with the two physical coefficients controlling it, i.e. the direct diffusion coefficient  $\alpha_{\rho\rho} = \rho C_4$  and the crossed advection coefficient  $\beta_{\rho\kappa} = C_0 - C_5 \partial\kappa/\partial x$ . The direct advection perturbation will be set as zero, i.e.  $\beta_{\rho\rho}^* = 0$ , and therefore the effect of the direct diffusion and crossed advection coefficients will be active only on the crossed advection perturbation, in a similar way as done in the previous example.

Figure 4.4 shows on the first row the direct diffusion coefficient through the spatial domain for equally spaced time instances for three different meshes with 16, 64, and 256 elements; while the second row shows the crossed advection coefficient. These two physical coefficients are the ones affecting in the computation of the crossed advection perturbation, which in turns is the main quantity of interest in this analysis. This perturbation is shown in the third row of Figure 4.4.

The analysis is much simpler than in the previous example since now both, the direct diffusion and crossed advection coefficients show exactly the same boundary layer pattern. Here, their effects are mutually reinforced, and not counteracted as in the previous example. For instance, the central region where the direct diffusion coefficient tends to vanish is the same region where the crossed advection remains high as the simulation evolves in time. On the other hand, the pile up of dislocations close to the boundaries increases the direct diffusion coefficient, an effect reinforced by the local reduction of the crossed advection coefficient due to the positive geometrically necessary dislocation gradient  $\partial\kappa/\partial x$  caused by the pile up of dislocations.

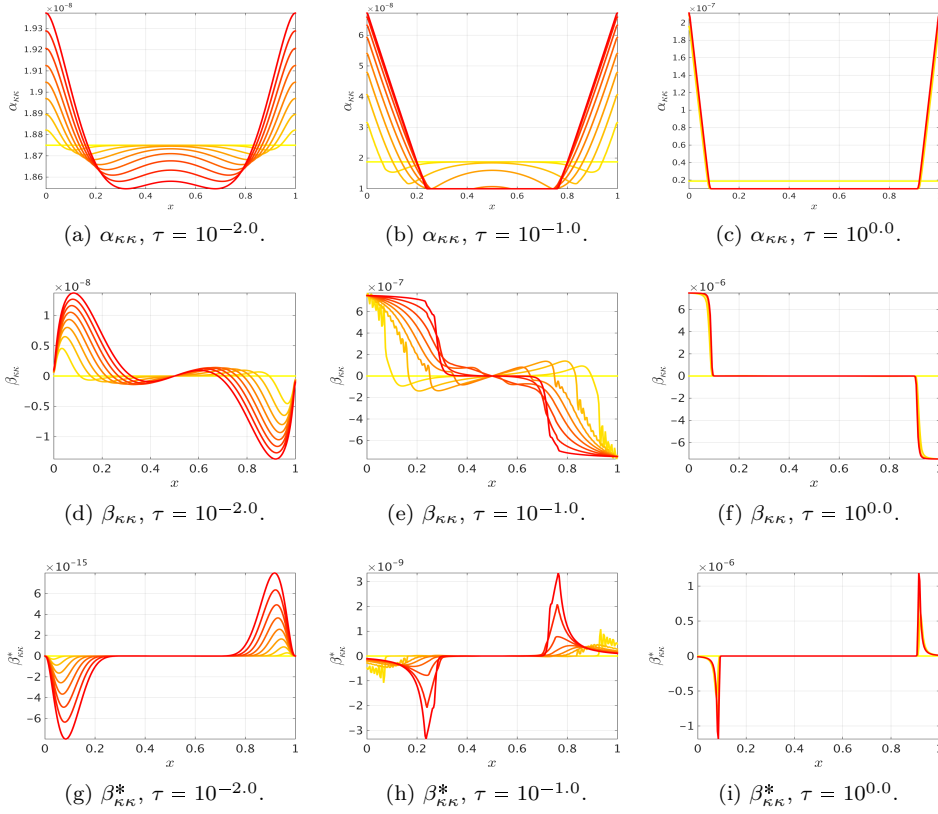


Figure 4.3: Comparison of the time evolution of the direct diffusion coefficient  $\alpha_{\kappa\kappa}$ , in  $\mu\text{m}^2/\text{s}$ , and the direct advection coefficient  $\beta_{\kappa\kappa}$  and its perturbation  $\beta_{\kappa\kappa}^*$ , both in  $\mu\text{m}/\text{s}$ , obtained using a discretization consisting of  $n_e = 2^8$  elements, increasing the stress from left to right. The yellow line corresponds to the initial condition and the red one to the last time instance computed ( $t = 10^6 \mu\text{s}$ ), intermediate approximations are at equidistant time intervals.

A final observation relates to the magnitude of the maximum values of the required crossed advection perturbation given in the third row of Figure 4.4. The maximum values of this perturbation decrease as the mesh is refined. Its convergence towards zero can be shown to be super-linear using more refined meshes for a fixed stress, and considering the same mesh refinement procedure for different applied stresses.

The presented examples demonstrate that the presented stabilization technique successfully renders stable numerical approximations irrespective of the local values of the diffusion and advection coefficients being direct or crossed. This proves its flexibility and adaptivity. More specifically, the second example reveals that the stabilization technique is consistent, i.e. the perturbations magnitudes vanish as the mesh is refined.

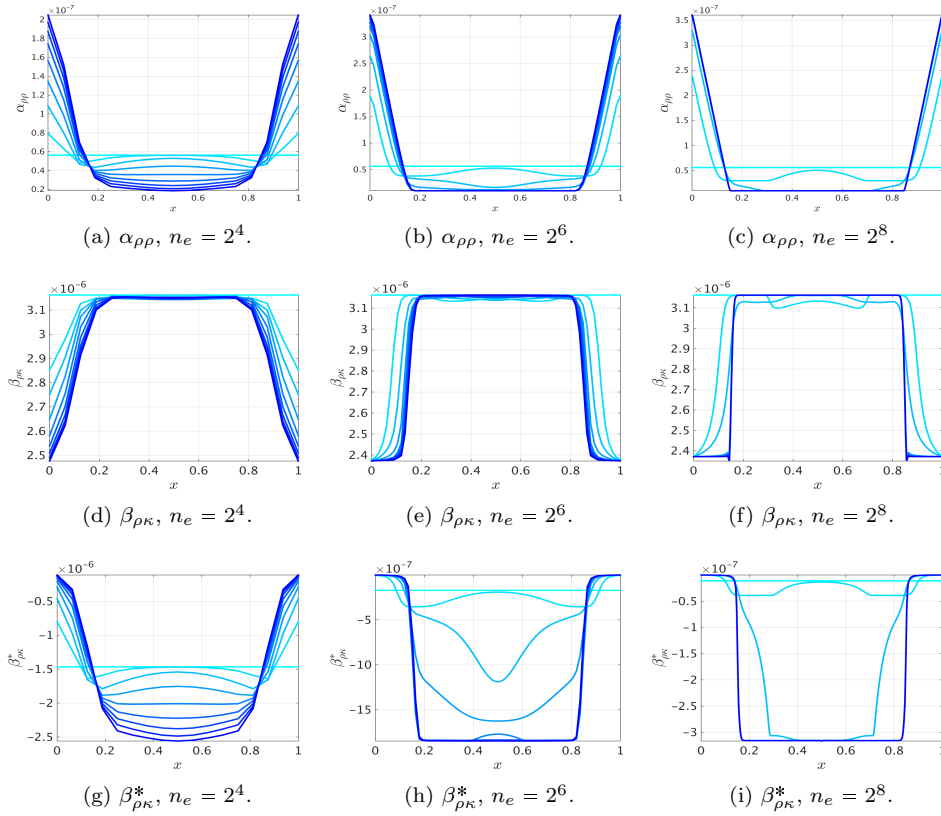


Figure 4.4: Comparison of the time evolution of the direct diffusion coefficient  $\alpha_{\rho\rho}$ , in  $\mu m^2/s$ , the crossed advection coefficient  $\beta_{\rho\kappa}$  and its perturbation  $\beta_{\rho\kappa}^*$ , both in  $\mu m/s$ , obtained when applying a stress of  $\tau = 10^{-0.5}$  GPa quadrupling the number of elements composing the finite element mesh from left to right (16, 64 and 256 elements). The cyan line corresponds to the initial condition and the blue one to the last time instance computed ( $t = 10^6 \mu s$ ), intermediate approximations are at equidistant time intervals.

#### 4.3.4 Models and length scale comparison

This last section has the aim to show that the presented stabilization technique renders numerical approximations free of spurious oscillations, irrespective of the model used: (i) Dogge or Gomma, (ii) with either a constant or variable length scale. As in the previous section, only stabilized results are shown here.

Figure 4.5 depicts the numerical approximation of the geometrically necessary dislocation density obtained using a mesh with 256 elements with a moderate applied stress  $\tau = 10^{-0.5}$  GPa for the four possible combinations obtained by changing the model type (Dogge or Groma) and the length scale (constant or variable). In all four

results shown, interactions between dislocations of different signs have been taken into account.

The first row of Figure 4.5 shows the results obtained when using the Dogge model while the second row corresponds to the Groma model. The left column depicts the results obtained using a constant length scale while the right column contains the results obtained with a variable length scale.

Although all the profiles are rather similar, some differences provide valuable information for a comparative analysis. The first important observation is related to the boundary layer width. When a constant length scale is used, this width tends to widen significantly compared to results with a variable length scale, irrespective of the model used (Dogge or Groma). As an obvious and immediate consequence of the smaller boundary layers width for a variable length scale, the maximum values reached by the dislocation density are an order of magnitude larger than those obtained with a constant length scale.

A second important observation is the fact that individual numerical approximations for the Groma model at different time instances can be well discerned. This is not the case for the results obtained with the Dogge model. Only a few individual numerical approximations at different time instances can be recognized with a constant length scale, while such distinction is even more difficult when using a variable length scale. This suggest that the Dogge model tends to *accelerate* the dislocation transport process with respect to the Groma model; i.e. both models have different kinetics. At first glance it could be argued that the slower kinetics in the Groma model may be caused by the adopted diffusion threshold for the total dislocation density equation. However, this difference in dislocation transport velocities was also observed when using positive and negative dislocation densities as the main variables.

## 4.4 Rearrangement of convection and diffusion matrices

The purpose of this section is to assess the performance of the presented stabilization technique when the diffusion and convection matrices are defined in a way different from the one used previously in Section 4.3. In order to carry out this assessment note that, due to the non-linearity of the Equations (4.7-4.8), the definition of the diffusion and convection matrices is not unique. It is also possible to define these matrices differently from (4.9) as follows

$$\mathbf{A} = \begin{bmatrix} \rho C_4 & \kappa C_5 \\ \kappa C_4 & \rho C_5 \end{bmatrix}, \quad \text{and} \quad \mathbf{B} = \begin{bmatrix} 0 & C_0 \\ C_0 & 0 \end{bmatrix}. \quad (4.13)$$

The numerical assessment is now repeated for this alternative definition and the corresponding results are presented below in a compact form.

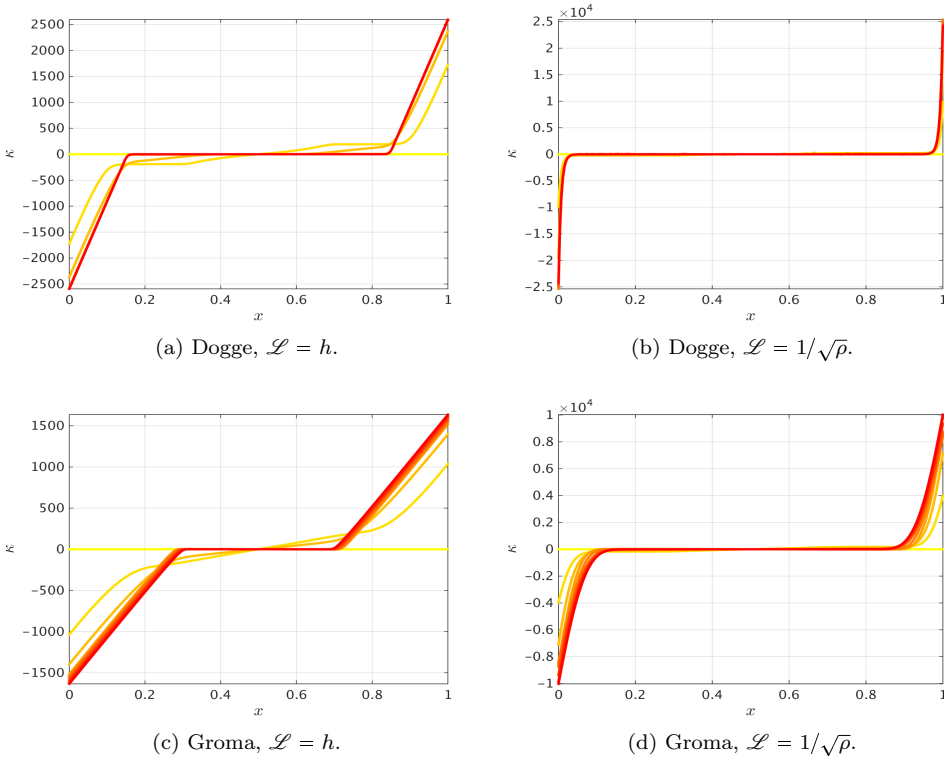


Figure 4.5: Dogge (top) and Groma (bottom) models with constant (left) and variable (right) length scales: time evolution of the geometrically necessary dislocation density  $\kappa$  in  $\mu\text{m}^{-2}$  for an applied stress  $\tau = 10^{-0.5}$  GPa on a mesh composed of  $n_e = 2^8$  elements. The yellow line corresponds to the initial condition while the red one to the last time instance computed ( $t = 10^6 \mu\text{s}$ ), intermediate approximations are at equidistant time intervals.

Figure 4.6 should be compared with Figure 4.1. The classical scheme results have been re-computed as well. This has been done in order to assess the effect of the rearrangement of the transport coefficients even when no stabilization technique is used. The classical scheme results are shown in the left column and the stabilized scheme results in the right column. The results in the first row, corresponding to the smallest applied stress, are practically identical, for both classical and stabilized schemes. For the next two rows, corresponding to  $\tau = 0.1$  GPa and  $\tau = 1.0$  GPa respectively, the classical scheme results show the same oscillatory behaviour as their counterparts depicted in Figure 4.1. The stabilized scheme results presented in Figure 4.6, like those depicted in Figure 4.1, are numerically well-behaved and free of any spurious oscillation. However, it is possible to recognize that the current definition of the diffusion and convection matrices leads to slightly smoother solutions. It is suspected that this effect is caused by the fact that formerly convective terms are now taken as diffusive terms.



Figure 4.7 corresponds to Figure 4.2. It confirms that irrespective of the two tested arrangements of the convection and diffusion matrices the results obtained with both, the classical and stabilized, schemes are qualitatively the same. It confirms that stabilization is necessary to obtain numerically well-behaved approximations and, more importantly, that the proposed stabilization technique is able to render strictly positive numerical approximations free of spurious oscillations. The stabilized scheme results, depicted in the right column, also confirm that the current arrangement of the convection and diffusion matrices slightly increases the smoothness of the numerical approximations obtained.

The comparison of Figure 4.8 with Figure 4.3 is not so straightforward and needs further explanation. Since the direct convection coefficient  $\beta_{\kappa\kappa}$  formerly plotted in the second row of Figure 4.3 is zero under the new arrangement of the transport matrices, it is not shown here. Note from (4.13) that, while using the new arrangement, only the crossed convection coefficient for the  $\kappa$  equation, i.e.  $\beta_{\kappa\rho}$ , is non-zero. Since it is constant, it is not shown here. The next row depicts the corresponding perturbation  $\beta_{\kappa\rho}^*$ . Note that its spatial distribution is directly correlated with the direct diffusion coefficient  $\alpha_{\kappa\kappa}$  and that it is proportional to the applied stress.

Finally, Figure 4.9 corresponds to Figure 4.4. Under the new arrangement the crossed convection coefficient for the  $\rho$  equation, i.e.  $\beta_{\rho\kappa}$ , is constant. Therefore, the second row of Figure 4.4, has been dropped in Figure 4.9. Its actual value is  $\beta_{\rho\kappa} = 1.162 \times 10^{-6}$  for an applied stress of  $\tau = 10^{-0.5}$  GPa. Note that the perturbations of the crossed convection coefficient, i.e.  $\beta_{\rho\kappa}^*$ , are practically the same as in the former arrangement. It is argued that this is the case because it is the direct diffusion coefficient that mostly influences the behaviour of this crossed convection perturbation.

The results presented in this section allow concluding that irrespective of the two tested arrangements of the convection and diffusion matrices the numerical approximation of the problem at hand requires the use of a stabilization technique able to deal with its convection dominated character. Furthermore, they also allow to conclude that the ability of presented stabilization technique to render numerical approximations free of spurious oscillations is not affected by this rearrangement of the convection and diffusion matrices.

## 4.5 Conclusions and outlook

In this chapter a stabilization technique for general systems of coupled convection-diffusion-reaction equations with constant coefficients has been proposed and demonstrated to be effective for solving dislocation transport problems. Stabilization is achieved irrespective of the set of field variables chosen in the numerical approximation. The stabilization technique was first used to handle the case of a single equation, yielding unconditionally stable solutions through the enforcement of the discrete maximum principle. Additionally, it was shown that the numerical approximations obtained with the stabilized scheme converges to the classical Bubnov-Galerkin solution when

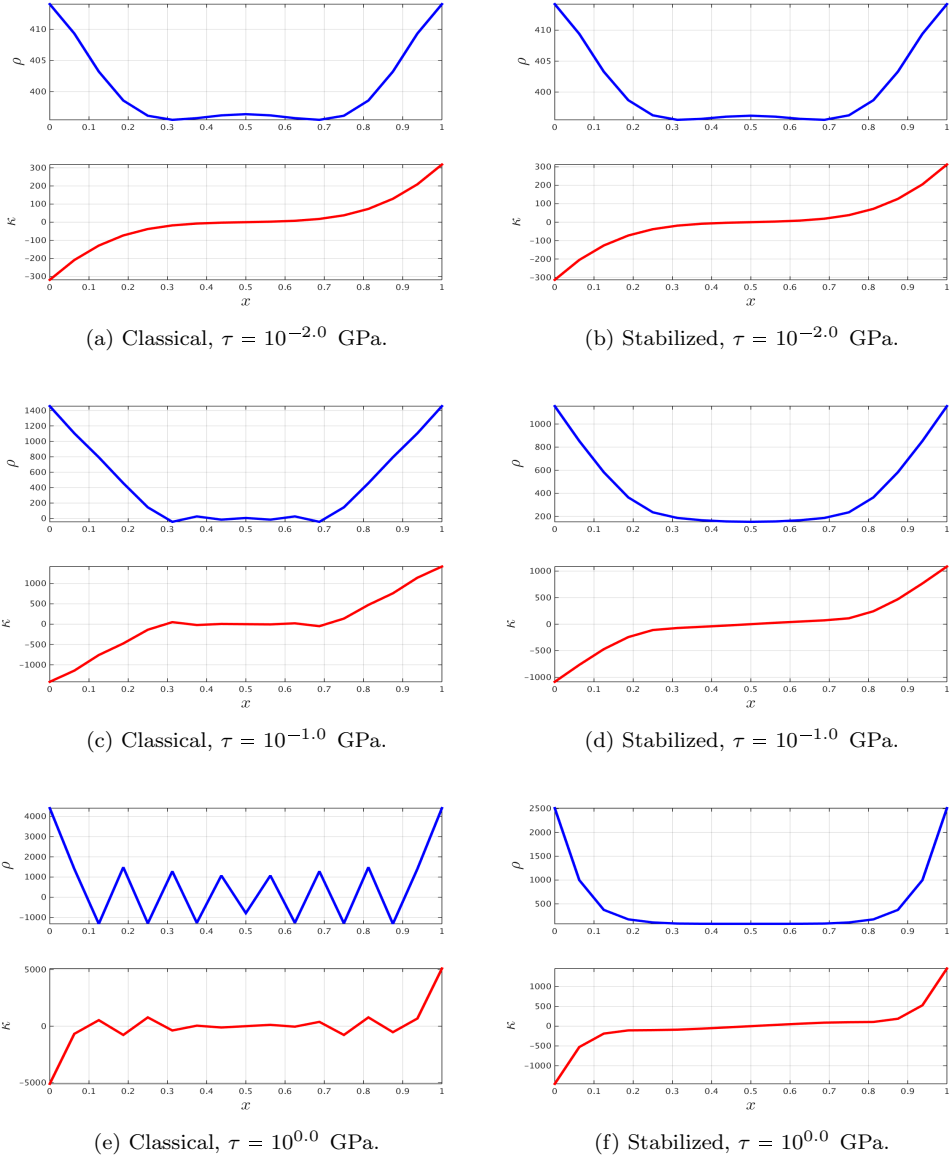


Figure 4.6: Comparison of the total dislocation density  $\rho$  in blue and the geometrically necessary dislocation density in red, both in  $\mu\text{m}^{-2}$  obtained with the classical (left) and stabilized (right) scheme using a discretization with 16 elements, increasing the stress  $\tau$  from top to bottom.

the mesh Péclet number is small enough, a fact confirmed using two thorough and detailed numerical assessments. Furthermore, this stabilization technique is applicable

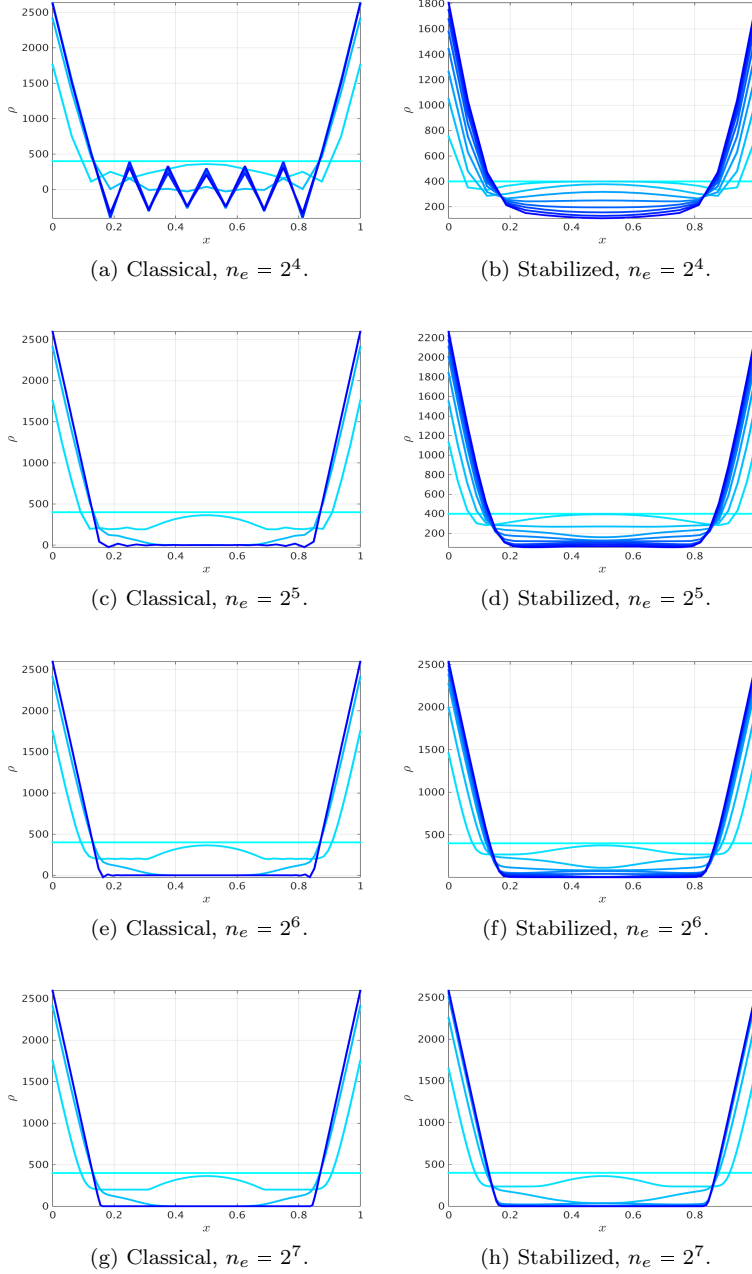


Figure 4.7: Comparison of the time evolution of the total dislocation density  $\rho$  in  $\mu\text{m}^{-2}$  obtained with the classical (left) and stabilized (right) scheme for an applied stress  $\tau = 10^{-0.5}$  GPa, doubling the number of elements composing the finite element mesh from top to bottom. The cyan line corresponds to the initial condition and the blue one to the last computed time instance ( $t = 10^6 \mu\text{s}$ ), intermediate approximations are at equidistant time intervals.

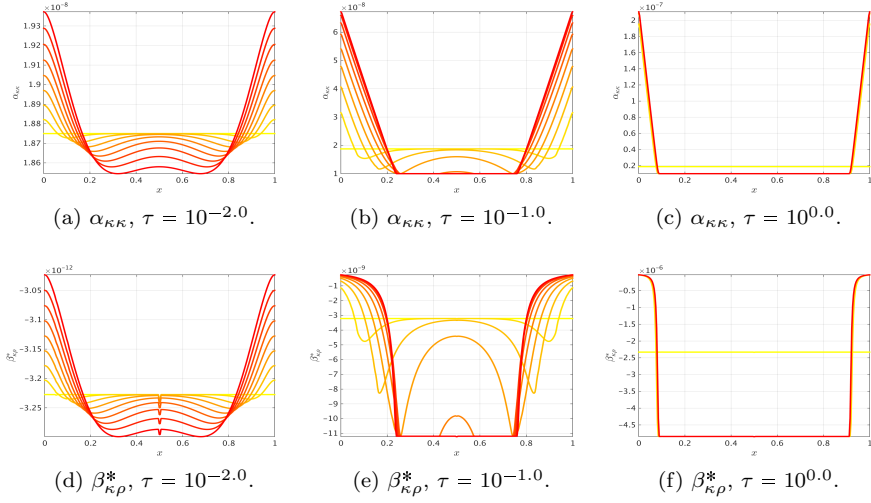


Figure 4.8: Time evolution of the direct diffusion coefficient  $\alpha_{\kappa\kappa}$ , in  $\mu m^2/s$ , and the crossed convection perturbation  $\beta_{\kappa\rho}^*$ , in  $\mu m/s$ , obtained using a discretization consisting of  $n_e = 2^8$  elements, increasing the stress from left to right. The yellow line corresponds to the initial condition and the red one to the last time instance computed ( $t = 10^6 \mu s$ ), intermediate approximations are at equidistant time intervals.

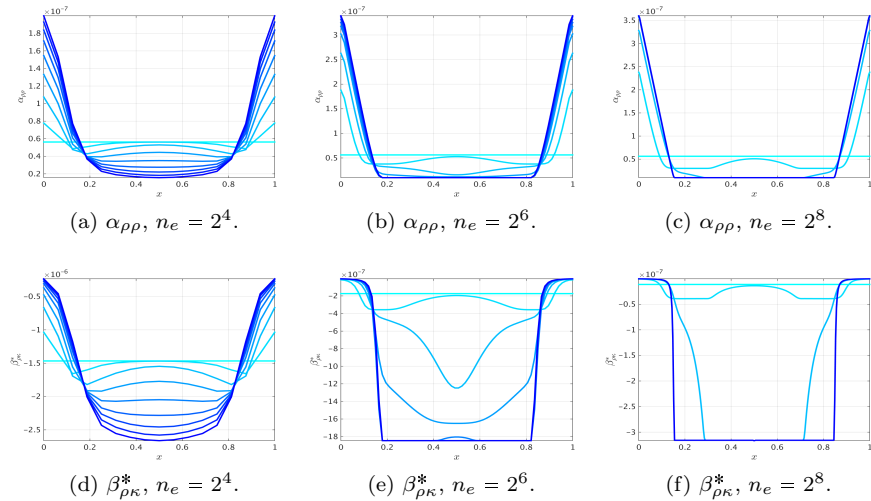


Figure 4.9: Time evolution of the direct and crossed diffusion coefficients  $\alpha_{\rho\rho}$  and  $\alpha_{\rho\kappa}$ , in  $\mu m^2/s$ , the crossed convection perturbation  $\beta_{\rho\kappa}^*$ , in  $\mu m/s$ , obtained when applying a stress of  $\tau = 10^{-0.5}$  GPa quadrupling the number of elements composing the finite element mesh from left to right (16, 64 and 256 elements). The cyan line corresponds to the initial condition and the blue one to the last time instance computed ( $t = 10^6 \mu s$ ).

when either the advective or the divergence form is used for the spatial discretization, making it highly flexible and general, and allowing to deal with different types of complex boundary conditions.

It is emphasized that although the dislocation density transport equations of interest in this chapter are transient, non-linear, and with variable coefficients, the stabilization scheme properly deals with these challenges due to its element by element operative mechanism. Its effectiveness in stabilizing the classical Bubnov-Galerkin scheme and its consistency have both been demonstrated in the numerical simulations performed. The effectiveness of the stabilization technique remains unaffected by the choice of the dislocation transport model used (Dogge or Groma) or by the choice of a constant or variable length scale. In this manner, it is expected this effectiveness remains unaltered when accounting or not for interactions between dislocations of different signs.

As future work, it is planned to extend this stabilization technique to multidimensional configurations and apply it to more general and complex dislocation transport problems. For instance, the present chapter mainly focused on parallel edge dislocations. More complex dislocation density transport models, such as those modelling screw and mixed dislocations and other phenomena as annihilation could be investigated as well. From the numerical perspective, an in depth mathematical analysis of this stabilization technique may be valuable to provide additional insights and routes for further improvements.

## Chapter 5

# Multidimensional Extension

---

### Abstract

Partial differential equations involving diffusive, convective and reactive terms appear in several branches of science. Often, several species or components interact with each other, leading to strongly coupled systems of convection-diffusion-reaction equations. The majority of such systems have to be solved on spatial domains with complex geometries. These difficulties prohibit analytical solutions for problems of practical interest. Approximated numerical solutions remain therefore the best strategy for solving these problems. For many problems, the lack of sufficient physical diffusion causes most traditional numerical methods to exhibit instability, with the appearance of violent and non-physical node to node oscillations in the solutions, even for the case of a single one-dimensional equation. When going to systems of equations, the situation becomes even harder due to the lack of fundamental principles guiding numerical discretization strategies. Then, strategies must be developed in order to obtain physically meaningful and numerically stable approximations. Such stabilization techniques have been extensively developed for the single equation case. By contrast, the multiple equations case has received little attention. The objective of this chapter is to present such a stabilization technique and to apply it to systems of multidimensional coupled convection-diffusion-reaction equations. Several of its attractive characteristics are discussed, providing evidence of its versatility, effectiveness, and efficiency through a computational assessment.

**keywords.-** Numerical instability, Stabilized finite element method, Convection-diffusion-reaction equations, Coupled systems.

---

---

This chapter is based on: [Hernández H.](#), Massart T.J., Peerlings R.H.J., and Geers M.G.D. 2017. *A Stabilization Technique for Multidimensional Coupled Convection-Diffusion-Reaction Equations*. In preparation.

## 5.1 Introduction

Partial differential equations including convection, diffusion, and reaction terms arise naturally in many branches of engineering and science. Analytical solutions are only available for very few simple cases that generally lack practical interest, even if they provide valuable mathematical, physical, or computational insights. In real problems, non-linearity, intricate boundary conditions, irregular geometries, heterogeneity in the space and time dependence of the transport coefficients complicate the situation, rendering them intractable by analytical tools. For this reason, numerical approximation methods remain the best strategy for solving such problems.

In recent decades, finite differences, finite volumes, finite elements, spectral or meshless methods, to name a few, have been applied to solve such convection-diffusion-reaction equations with different degrees of success. Some of them have excelled for specific problems, while not obtaining satisfactory results, or even completely failing, for other problems. A general purpose numerical methodology therefore does not seem to be available yet. The vast majority of the available numerical methods is successful when dealing with a *purely diffusive* process. Their performance is drastically reduced when either convection, reaction, or a combination of both overwhelms diffusion, causing numerical instabilities. The numerical approximations are then usually plagued by spurious oscillations near boundary and internal layers, and solutions can exhibit negative values even if the underlying partial differential equation only accepts non-negative solutions.

This stability problem is inherent to the numerical discretization scheme, and not to the underlying partial differential equation. The magnitude of the oscillations can decrease or even completely disappear when the discretization is refined, tending towards a smooth numerical approximation. This suggests that the lack of numerical stability and the subsequent oscillations appear when the discretization is too coarse to adequately capture the physics of the governing transport mechanisms. This can also be interpreted as a lack of richness of the approximation space to fully capture the behaviour of the continuous model. In many cases, however, the refinement required to get acceptable numerical approximations is so excessive that it becomes prohibitive in computational terms, especially when multidimensional problems are considered.

Over the years, ad hoc discretization strategies or stabilization techniques have been developed to overcome such difficulties. Finite difference method practitioners defined several techniques such as upwinding schemes, the use of high order schemes, or the use of fitted meshes [9, 25, 29, 52, 54]. Flux reconstruction, total variation diminishing techniques, high order schemes, essentially non-oscillatory schemes, and their weighted versions are now well established techniques in the finite volume method community [68, 72, 76]. Streamline upwind Petrov-Galerkin, Galerkin least-squares, discontinuous Galerkin schemes; bubble enrichment, algebraic sub-grid scale approaches, among others, have been devised over the years in the finite element method community [7, 13, 44, 56, 60].

In view of the significant number of contributions dealing with instabilities, one may get the incorrect impression that the issue has been fully solved. Yet, less attention has been paid to *systems* of convection-diffusion-reaction equations, although they arise naturally in branches of science as diverse as bio-mechanics [18], combustion [5], computer science [30], ecology [45], economy [6], epidemiology [84], finance [17], groundwater pollution [4], heat transfer [70], neuroscience [3], physiology [37], seepage flow [71], solid mechanics [14] or turbulence [15]. The reason for this immaturity is the lack of a maximum principle to guide the construction of the numerical approximation, when going from a single transport equation towards systems of coupled equations in the most general form [62].

In a contribution by Abrahamson, Keller, and Kreiss [1], a stabilization technique has been proposed and successfully applied for systems of one dimensional convection-diffusion-reaction equations in steady state, i.e. systems of ordinary differential equations. This technique is a direct extension of a previously developed upwinding scheme for first order derivative terms [65, 69, 74, 83]. Additional progress in the approximations for systems of convection-diffusion-reaction equations until the late 1990's was mainly driven by finite difference method developments. The issue was addressed by extending techniques previously used for discretizing a single equation. The most representative approaches consist of the use of upwind finite differences for the convective terms on layer-adapted meshes [29, 48]. In these papers, theoretical developments have unravelled the conditions for a continuous maximum principle to be valid. In other cases, compatibility conditions are derived and used instead. For finite volumes, similar strategies were used. Discontinuous and high order approximations, upwinding and adaptive meshes were the most successful techniques to deal with coupled equations [16, 58]. In the finite element method context, streamline upwind Petrov-Galerkin, Galerkin least-squares, algebraic sub-grid scale with high order elements together with shock capturing techniques have been the most promising techniques [4, 5, 14]. In general, and within all these methodologies, the case of coupled systems of equations has been traditionally addressed using techniques previously successfully applied in the case of a single equation. The same guiding strategy will be followed in the present chapter.

The main objective of this chapter is to extend the present stabilization technique to a system of multidimensional coupled convection-diffusion-reaction equations, which is able to resolve the main shortcomings of the aforementioned stabilization techniques such as mesh fitting or adaptation, the use of high order or discontinuous approximations or the introduction of excessive diffusive up-winded differences. This methodology extends an approach proposed recently for a single one-dimensional equation [34], and for one-dimensional systems of equations [35], towards a multidimensional system of coupled convection-diffusion-reaction equations. The methodology is conceptually based on perturbing the original system of partial differential equations, the discretized form of which on a particular discretization is on beforehand known to yield an unstable approximation. This is achieved by modifying the system transport coefficients to obtain a well behaved numerical approximation, with a minimal alteration of the underlying physics [7, 43]. The required coefficient modifications are thus optimally determined to be the smallest perturbations that still guarantee stability.



These perturbations are chosen such that certain compatibility conditions analogous to a maximum principle are satisfied. Once the computed perturbations are injected in the classical Bubnov-Galerkin finite element method, they deliver smooth and stable numerical approximations.

The chapter is organized as follows. In Section 5.2, the basic terminology and notation are introduced. Subsequently, the classical Bubnov-Galerkin finite element discretization is introduced in the most traditional way and important issues on the treatment of the boundary conditions are discussed. Section 5.2.1 extends to multidimensional problems the stabilization technique originally developed for problems in one dimension. Section 5.3 assesses the multidimensional stabilization technique through three numerical examples with increasing generality. The first one is of the convection-diffusion type, while the second one involves diffusion and reaction transport mechanisms. Finally, the third problem is of the convection-diffusion-reaction type with boundary and internal layers. Throughout this computational assessment the reliability, robustness and flexibility of the stabilization technique are shown. Section 5.5 closes this chapter by drawing its main conclusions, and discusses some future perspectives.

## 5.2 Problem definition and finite element discretization

In all generality, consider a system of  $m$  conservation equations with reaction terms of the form

$$\rho_{pq} \frac{\partial u_q}{\partial t} + \frac{\partial}{\partial x_i} (F_{ip}) + \gamma_{pq} u_q = f_p, \quad (5.1)$$

where the use of repeated indices implies the traditional summation convention. The main field variables to be approximated are  $u_p$ , the physical quantities to be transported, with  $F_{ip}$  being their corresponding fluxes in the  $i$ -th direction with  $i = 1, 2, 3$ , and  $f_p \in \mathbb{R}$  are the source terms, all for  $p = 1, 2, \dots, m$ . The reaction coefficients  $\gamma_{pq} \in \mathbb{R}$ , for  $p, q = 1, 2, \dots, m$  will be referred to as *direct* when  $p = q$  and as *coupled* when  $p \neq q$ . Finally,  $\rho_{pq} \in \mathbb{R}^+$  are the mass coefficients, which are assumed to vanish when  $p \neq q$ .

The fluxes are composed of diffusive and convective contributions

$$F_{ip} = -\alpha_{ijpq} \frac{\partial u_q}{\partial x_j} + \beta_{ipq} u_q. \quad (5.2)$$

Here  $\alpha_{ijpq} \in \mathbb{R}^+$  are the diffusion coefficients and  $\beta_{ipq} \in \mathbb{R}$  are the convection coefficients. It is emphasized that the indices  $i, j = 1, 2, 3$  are associated with the spatial dimensions. The diffusion and convection coefficients will also be referred to as *direct* or *coupled* using the above mentioned convention. Throughout this section all coefficients will be regarded as constants.

The direct substitution of the flux given by Equation (5.2) in the general conservation Equation (5.1) leads to

$$\rho_{pq} \frac{\partial u_q}{\partial t} + \frac{\partial}{\partial x_i} \left( -\alpha_{ijpq} \frac{\partial u_q}{\partial x_j} + \beta_{ipq} u_q \right) + \gamma_{pq} u_q = f_p. \quad (5.3)$$

which will be referred to as the *divergence* form of the conservation equation due to the fact that integration over the whole domain involves, via the divergence theorem, the total flux across the boundary.

Expanding the spatial derivative on the terms composing the flux and taking into account that all physical coefficients are constants, one gets

$$\rho_{pq} \frac{\partial u_q}{\partial t} - \alpha_{ijpq} \frac{\partial^2 u_q}{\partial x_i \partial x_j} + \beta_{ipq} \frac{\partial u_q}{\partial x_i} + \gamma_{pq} u_q = f_p. \quad (5.4)$$

which will be referred to as the *advective* form because of the direct interpretation of the first order spatial derivative term as representing convection.

For the sake of clarity in the notation, a single weighting function  $w$  for all the  $m$  equations is used in what follows. Multiplying Equation (5.1) by the weighting function  $w$ , and integrating over the whole spatial domain, the following weighted residual form is obtained

$$\int_{\Omega} w \rho_{pq} \frac{\partial u_q}{\partial t} d\Omega + \int_{\Omega} w \frac{\partial}{\partial x_i} (F_{ip}) d\Omega + \int_{\Omega} w \gamma_{pq} u_q d\Omega = \int_{\Omega} w f_p d\Omega, \quad (5.5)$$

Integration by parts of the second term in the left hand side yields

$$\int_{\Omega} w \rho_{pq} \frac{\partial u_q}{\partial t} d\Omega - \int_{\Omega} \frac{\partial w}{\partial x_i} F_{ip} d\Omega + \int_{\Gamma} w F_{ip} n_i d\Gamma + \int_{\Omega} w \gamma_{pq} u_q d\Omega = \int_{\Omega} w f_p d\Omega, \quad (5.6)$$

with  $\mathbf{n}$  being the unit vector normal to the boundary  $\Gamma$ . Note again the non-standard form in which integration by parts has been performed taking into account terms differentiated to both the first and second order in space. The purpose of this procedure is to easily incorporate *natural* boundary conditions of the Neumann type in the absence of convective terms, i.e.  $\beta_{ipq} = 0$ , or of the Robin type in the more general case when at least one of the convection coefficients  $\beta_{ipq}$  does not vanish. The Robin boundary condition involves the total flux across the boundary, and not only its diffusive part, and is more easily treated using the divergence form (5.3) that will be used in the remainder of the chapter.

By expressing the weighting function  $w$  and the variable  $u_p$  as linear combinations of their corresponding nodal values with the use of the interpolation functions  $W_k$  and  $P_k$  associated with the  $n_e$  nodes within each finite element and requiring the weak form 5.6 to hold for any  $w_k$ , one obtains after assembly the following global system of algebraic equations

$$\mathbf{M}_{pq} \dot{\mathbf{u}}_q + (\mathbf{D}_{pq} + \mathbf{C}_{pq} + \mathbf{R}_{pq}) \mathbf{u}_q = \mathbf{f}_p, \quad (5.7)$$

where  $\mathbf{M}_{pq}$  are the global mass matrices,  $\mathbf{D}_{pq}$  the global diffusion matrices,  $\mathbf{C}_{pq}$  the global convection matrices and  $\mathbf{R}_{pq}$  the global reaction matrices. The nodal values of the discretized fields are collected in the  $m$  vectors  $\mathbf{u}_p = \left[ u_p^{(1)}, u_p^{(2)}, \dots, u_p^{(n-1)}, u_p^{(n)} \right]^T$  (for  $p = 1, 2, \dots, m$ ), with  $n$  being the total number of nodes in the finite element discretization. Furthermore, these  $m$  numerical approximations can be collected in a single unknown vector as

$$\mathbf{u} = \left[ u_1^{(1)}, u_1^{(2)}, \dots, u_1^{(n)}, u_2^{(1)}, u_2^{(2)}, \dots, u_2^{(n)}, \dots, u_m^{(1)}, u_m^{(2)}, \dots, u_m^{(n)} \right]^T, \quad (5.8)$$

which will be simply referred to as the numerical approximation. Finally  $\mathbf{f}_p$  takes into account the  $m$  source terms  $f_p$  and associated boundary conditions.

### 5.2.1 Multidimensional extension of the stabilization technique

In this section the main objective of this paper is pursued, namely the extension of the stabilization technique, originally devised for the one-dimensional case, to multi-dimensional configurations. This is done by addressing the two-dimensional case, the three-dimensional case being a straightforward extension.

Previous extensions to multidimensional configurations of stabilization techniques for convection-diffusion problems, which were initially developed in the context of one dimensional problems, have been proposed paying special attention to avoiding the addition of excessive artificial diffusion. For example, two-dimensional implementations of the SUPG method make use of an auxiliary coordinate system with one of its axes aligned with the direction in which the physical convection acts. This allows decoupling the original two-dimensional convection-diffusion problem into two problems, i.e. a one-dimensional convection-diffusion problem complemented by a second pure diffusive problem. The originally developed one-dimensional SUPG method is then applied to the former problem, using as the discretization size the maximum possible length inscribed inside the finite element in the direction of the convection velocity. Meanwhile, the second, purely diffusive problem does not need any stabilization [7].

The aforementioned strategy is applied when dealing with the multi-dimensional single equation case, i.e. when  $m = 1$ , together with the one-dimensional stabilization technique based on coefficient perturbation proposed in [34]. Moreover, when the convection and reaction coupling coefficients vanish, the same strategy can also be successfully applied to the stabilization technique presented in [35] since in this case the equations are in fact decoupled. Unfortunately this does not hold when coupling convection and reaction coefficients are introduced, since it is then impossible to define a single convection velocity and its acting direction. In this situation it is also impossible to fix a single auxiliary coordinate system with one of its axes aligned with the convection velocity.

Therefore, even if this carries the risk of adding more than the strictly needed artificial diffusion to obtain a stable numerical approximation, the stabilization technique

developed for the one-dimensional case is applied in a similar manner as the vast majority of the up-winded finite difference schemes to multidimensional configurations. When using such up-winding, it is applied in each mutually orthogonal direction,  $x$  and  $y$ , using their corresponding physical advection velocities,  $\beta_x$  and  $\beta_y$ , not considering each other in the stabilization process. Thus, this procedure treats a multi-dimensional problem as a set of mutually independent one-dimensional convection-diffusion problems, each one aligned with the Cartesian coordinate axis. It is common practice in the finite difference context to have structured discretizations aligned with the coordinate axis, thus facilitating the use of this strategy. In the finite element context this restriction is loosened allowing the treatment of problems having irregular and complicated geometries as spatial domains. Thus the approach used here should allow accommodating irregular and unstructured meshes.

The implementation thus considers a one-dimensional convection-diffusion-reaction problem, with a discretization size  $\ell_x$ , diffusion coefficients  $\alpha_{xppq}$ , convection coefficients  $\beta_{xppq}$  and reaction coefficients  $\gamma_{pq}$ , for  $p, q = 1, 2, \dots, m$ . Then, the stabilization technique for systems of coupled convection-diffusion-reaction equations is applied as explained in Section 3.3.1 through the computation of the coefficient perturbations for the  $x$  direction physical coefficients of the original problem. Then, a second convection-diffusion problem is considered, with a discretization size  $\ell_y$ , diffusion coefficients  $\alpha_{yypq}$  and convection coefficients  $\beta_{yypq}$ , for  $p, q = 1, 2, \dots, m$ , this time the stabilization technique is used to determine the coefficient perturbations for the  $y$  direction physical coefficients. These discretization sizes,  $\ell_x$  and  $\ell_y$ , are taken as the maximum possible length inscribed inside the finite element along the corresponding coordinate axes, as sketched in an arbitrary quadrilateral finite element in Figure 5.1. This definition of the discretization sizes,  $\ell_x$  and  $\ell_y$ , has been adopted after carrying out a thorough numerical assessment specifically conducted to such a task.

## 5.3 Applications and computational assessment

This section presents three numerical examples to illustrate and assess the efficiency and consistency of the developed stabilization technique. Its main goal is to demonstrate the ability of the presented stabilization technique to successfully handle different types of problems, independently of the physics underlying the considered system of differential equations.

This goal is pursued by presenting a thorough and detailed analysis of the numerical results obtained for three problems taken from different references and adapted to suit the purpose of evaluation. In all cases the convection and reaction coefficients and the boundary conditions have been taken as close as possible to those presented in the original references. Modifications have been made only for the sake of uniformity in the assessments, and more importantly because the boundary conditions chosen here trigger more easily the development of sharp boundary layers, making the problems more challenging for the stabilization technique. The domain considered is always the unit square.

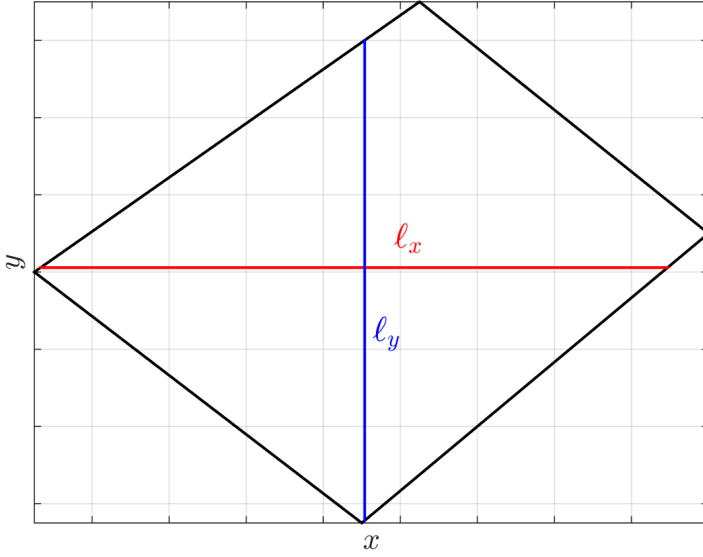


Figure 5.1: Discretization sizes in the  $x$  and  $y$  directions in an arbitrary quadrilateral finite element.

The assessment is conducted by modifying only the parameter  $\epsilon$  controlling the amount of diffusion and the discretization size  $\ell$ . Once these parameters are set for a particular problem, they are not changed, i.e. for a particular simulation the diffusion parameter is constant over the whole domain discretized with a uniform mesh. The parameter  $\epsilon$  is always chosen as  $\epsilon = 10^{-j}$  with  $j = 0, 1, 2, \dots$ . Thus, as  $j$  increases the problem becomes less dominated by diffusion, and its numerical approximation becomes more prone to numerical instabilities. In the present study, without loss of generality in the assessment of the stabilization technique, no transverse diffusion is considered, i.e.  $\alpha_{ijpq} = 0 \ \forall \ p, q = 1, 2, \dots, m$  when  $i \neq j$ . The mesh is always uniform and made of square, four-noded quadrilaterals having linear Lagrange interpolation functions. Since all the discretizations used in the present study have the same number of elements in each direction, a single parameter suffices to characterize each mesh, i.e.  $\ell_x = \ell_y = \ell = n^{-1}$ .

Regardless of the use of the presented stabilization technique, once the system of  $m$  differential equations has been discretized, a system of  $m \times n$  linear algebraic equations has to be solved. For this purpose the iterative *BiCGStab* method has been used because of its efficiency when dealing with large and sparse systems [77]. In all cases, the maximum number of allowed iterations is set equal to the number of nodes in the finite element mesh, although the iteration process is stopped as soon as  $\|\mathbf{r}^{(k)}\|/\|\mathbf{b}\| < \epsilon_s = 10^{-6}$  is reached, with  $\mathbf{r}^{(k)}$  the  $k$ -th residual vector and  $\mathbf{b}$  the right hand side vector. No preconditioning is used.

### 5.3.1 Convection-diffusion system

In this section, the attention is focused on a problem without reaction terms, but with a full convection matrix in the  $x$  direction, i.e. containing cross convection terms. The convection matrix in the  $y$  direction is diagonal. It has been chosen here to perturb only the diagonal entries of the diffusion matrices when  $p = q$  for each dimension  $i = x, y$ , in order to capture the effect of the stabilization technique in a single coefficient perturbation, thus rendering its effect easy to scrutinize.

The example treated here is based on an originally one-dimensional problem taken from [55], where it was treated using upwind finite differences on a Shishkin mesh. It is the simplest case among all examples solved in the present chapter, where all the diffusion coefficients are equal and the convection coefficients and source terms are all taken as constants.

The system, consisting of  $m = 3$  differential equations, extended to two dimensions by adding diffusive and convective terms in the  $y$  direction, reads as follows

$$\begin{aligned}
 & -\epsilon \begin{bmatrix} 1 & 0 & 0 \\ 0 & 1 & 0 \\ 0 & 0 & 1 \end{bmatrix} \begin{bmatrix} u_1 \\ u_2 \\ u_3 \end{bmatrix}_{xx} - \epsilon \begin{bmatrix} 1 & 0 & 0 \\ 0 & 1 & 0 \\ 0 & 0 & 1 \end{bmatrix} \begin{bmatrix} u_1 \\ u_2 \\ u_3 \end{bmatrix}_{yy} \cdots \\
 & \cdots - \begin{bmatrix} 3 & -1 & -1 \\ -1 & 4 & -2 \\ -1 & -2 & 4 \end{bmatrix} \begin{bmatrix} u_1 \\ u_2 \\ u_3 \end{bmatrix}_x + \begin{bmatrix} 1 & 0 & 0 \\ 0 & 2 & 0 \\ 0 & 0 & 3 \end{bmatrix} \begin{bmatrix} u_1 \\ u_2 \\ u_3 \end{bmatrix}_y = \begin{bmatrix} -4 \\ 11 \\ -7 \end{bmatrix}, \quad (5.9)
 \end{aligned}$$

with boundary conditions at the left and top edges as  $\mathbf{u}(x = 0, 0 < y < 1) = \mathbf{u}(0 \leq x \leq 1, y = 1) = [-1, 4, -1]^T$ , and at the right and top edges as  $\mathbf{u}(x = 1, 0 < y < 1) = \mathbf{u}(0 \leq x \leq 1, y = 0) = [1, 1, 1]^T$ .

Figure 5.2 shows the numerical approximations obtained for  $u_1$ ,  $u_2$ , and  $u_3$  using a mesh consisting of  $n = 16$  elements in each direction. The results obtained with the classical Bubnov-Galerkin method are depicted in the left column, while the right column shows the results obtained with the stabilization technique. These numerical schemes are respectively referred to as *classical* and *stabilized*.

In the first row of Figure 5.2; for  $\epsilon = 1$ , i.e. having diffusion coefficients  $\alpha_{pii} = 1$  for  $p = 1, 2, 3$  and  $i = x, y$ , the solutions of the classical and stabilized schemes are practically identical. This observed smooth behaviour was expected since the direct Péclet numbers, defined in this case for each direction as  $\mathbf{Pe}_x = (\ell_x/2\epsilon) [\beta_{x11}, \beta_{x22}, \beta_{x33}]^T$  and  $\mathbf{Pe}_y = (\ell_y/2\epsilon) [\beta_{y11}, \beta_{y22}, \beta_{y33}]^T$ , are smaller than one:  $\mathbf{Pe}_x = [0.0935, 0.125, 0.125]^T$  and  $\mathbf{Pe}_y = [0.25, 0.0625, 0.0935]^T$ .

The situation is radically changed when moving to the next row; for  $\epsilon = 10^{-3}$ , in which spurious oscillations appear in the approximation obtained with the classical scheme. This time the direct Péclet numbers are multiplied by  $10^3$  with respect to the values mentioned above; and therefore such an oscillatory behaviour of the classical

solution should be expected. In the right column the effectiveness of the proposed stabilization scheme in removing the spurious oscillations is clearly illustrated. The main features in the boundary layers are properly captured.

Moving to the last row in the left column, it can be seen that the amplitude of the oscillations increases as the problem gets more dominated by convection. On the other hand, the approximations obtained by the stabilized scheme, in the right column, remain free of spurious oscillations. They adequately capture the boundary layers and abrupt changes in the solutions for the whole range of diffusion coefficients tested.

As no analytical solution is available for this problem, the accuracy of the stabilization scheme is evaluated by computing for each mesh having  $n$  elements in each direction the Euclidean norm of the *two-mesh difference* defined as

$$D_n = \|\bar{\mathbf{u}}^{(2n)} - \mathbf{u}^{(n)}\|_2, \quad (5.10)$$

where the bar means that the numerical approximation on a mesh containing  $2n$  elements in each direction is restricted to the same positions as the nodes of the mesh made of  $n$  elements in each direction.

Figure 5.3 depicts  $D_n$  for the classical scheme using dashed lines and the stabilized scheme in solid lines for different values of the diffusion parameter  $\epsilon = 10^{-j}$  for  $j = 0, 1, 2, 3$ , as a function of the number of elements in each direction  $n$ . First note that when the problem is dominated by diffusion, i.e.  $\epsilon = 1$ , corresponding to the darkest lines at the bottom, the classical and stabilized schemes provide practically the same results. The fact that these lines are almost identical demonstrates that, for diffusion dominated problems not showing spurious oscillations in the numerical approximations, the proposed stabilization technique does not introduce any noticeable perturbation; it becomes active only when the problem becomes dominated by convection.

In the same plot, it is observed that the magnitude of the two-mesh differences corresponding to the classical scheme (dashed lines) keeps growing when decreasing the diffusion parameter. This indicates that as the problem becomes more dominated by convection, the classical scheme is unable to yield accurate numerical approximations. By considering the solid lines in the same plot it can be seen that the stabilized scheme renders numerical approximations with two-mesh differences that are always bounded, irrespective of the magnitude of the diffusion parameter, as suggested by the coincident lines corresponding to  $\epsilon = 10^{-j}$  for  $j = 2, 3$  for coarse discretizations (low values of  $n$ ). The superiority of the stabilized scheme in capturing the main features of the solution introduced by convective effects, such as boundary layers, is evidenced by the fact that all dashed lines, for the classical scheme, are above the corresponding solid lines.

In this plot it is also easy to perceive how the convergence rate of the stabilized scheme is affected when decreasing the diffusion parameter. The curve corresponding to the diffusion dominated case, i.e  $\epsilon = 1$ , exhibits a second order convergence rate. On the other hand, the curve corresponding to the more convection dominated case, i.e

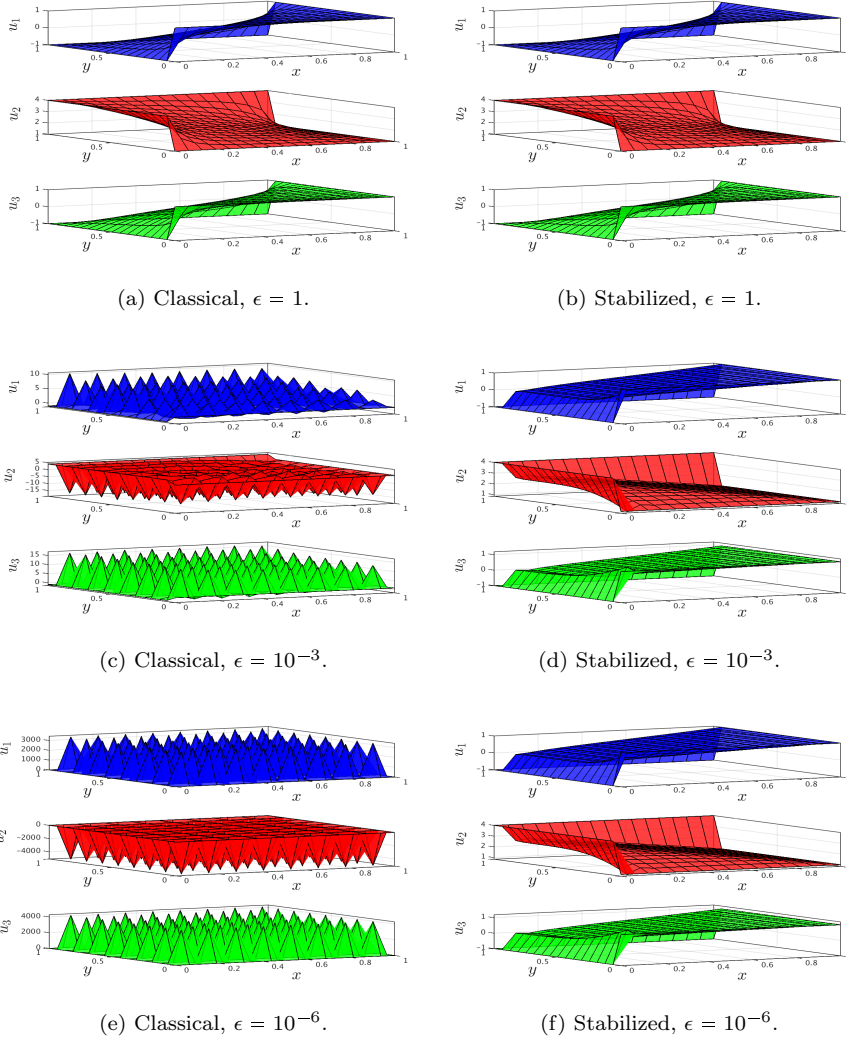


Figure 5.2: Numerical approximations for the boundary value problem associated with Equation (5.9) obtained using a mesh consisting of  $n = 16$  elements in each spatial dimension, with decreasing diffusion from top to bottom, for the classical (left) and stabilized (right) schemes.

$\epsilon = 10^{-3}$ , exhibit only first order convergence rate. Moreover, note that when  $n \approx 10$  the curve corresponding to the diffusion parameter  $\epsilon = 10^{-1}$  starts to switch from a first order convergence rate towards to a second order convergence rate. Additionally, note that the curve corresponding to  $\epsilon = 10^{-2}$  switches from first to second order convergence rate when the discretization reaches  $n \approx 100$  elements in each direction.



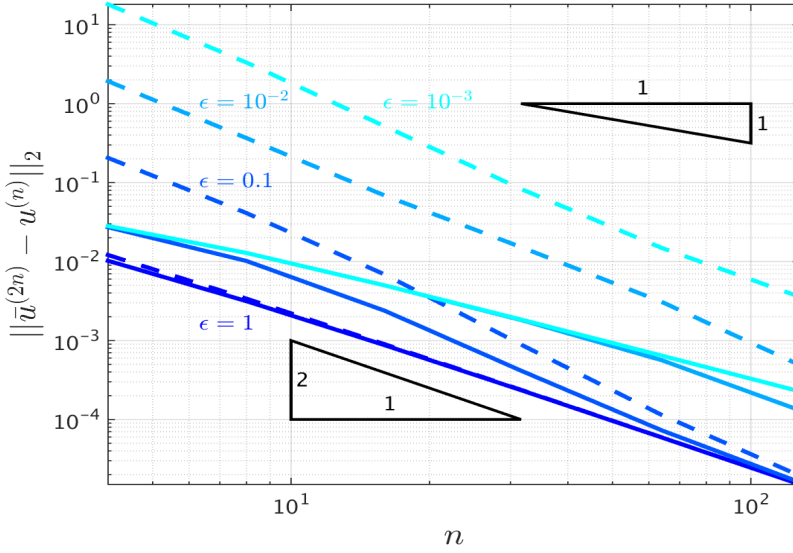


Figure 5.3: Euclidean norm of the two-mesh difference for the problem of Equation (5.9). The classical scheme results are shown with dashed lines and stabilized scheme results with solid lines. Each curve corresponds to the diffusion parameters  $\epsilon = 10^{-j}$  with  $j = 0, 1, 2, 3$ , as a function of the number of elements in each direction  $n$ .

These observations allow concluding that when the discretization is not fine enough to capture the sharp changes in the solution due to boundary or internal layers, the stabilized scheme, despite having a first order convergence rate, is able to render adequate numerical approximations. This is not the case for the classical scheme approximations which exhibit higher two-mesh differences  $D_n$  than those obtained by the perturbation-based stabilization technique. Once the discretization is able to capture these sharp changes, the stabilized scheme will exhibit a second order convergence rate.

Finally, Figure 5.4 depicts the diffusion perturbations for the first equation in the  $y$  direction, i.e. for  $\alpha_{yy11}^*$ , as a function of the number of elements in each direction  $n$  for several values of the diffusion coefficient. As expected, the perturbations automatically increase as the problem becomes more dominated by convection. This is reflected by the fact that the brighter lines, which represent problems more dominated by convection, are always above the darker lines, which represent diffusion dominated problems. More importantly, this plot reveals that, when  $\epsilon = 10^{-2} - 10^0$  the perturbations decrease quadratically as the mesh is refined, demonstrating the consistency of the proposed stabilization technique in this range of values of the diffusion parameter. For lower diffusion parameters, in the range  $\epsilon = 10^{-3} - 10^{-8}$  this decrease is only linear. The same conclusions can be obtained irrespective of the equation,  $p = 1, 2, 3$ , or direction,  $i = x, y$ , considered.

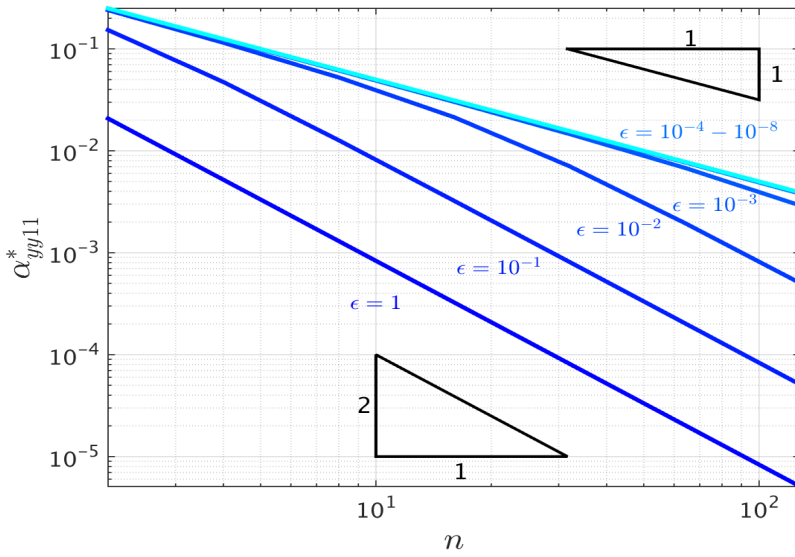


Figure 5.4: Diffusion perturbations needed to deal with the convective term in the  $y$  direction in Equation (5.9) for  $\epsilon = 10^{-j}$  with  $j = 0, 2, \dots, 8$  as a function of the number of elements in each direction  $n$ .

### 5.3.2 Diffusion-reaction system

Next, a diffusion-reaction type problem is considered. This problem, originally presented in [52] for a one-dimensional domain, introduces two new features: the reaction and source coefficients are dependent on the spatial coordinate and the direct diffusion coefficients differ. Even if the spatial variability of the reaction coefficients is mild, this allows assessing the proposed stabilization technique in handling common difficulties faced by traditional stabilization techniques [1]. Strictly speaking, the difference in the diffusion coefficients is not a serious difficulty since, before discretization, the differential equations can be scaled in such a way that the previous case (diffusion matrices equaling a scalar multiplied with the identity matrix) is recovered. However, this scaling may not be desired if the original physical model is to be preserved. As for the first example, the choice was made to stabilize the problem using direct diffusion perturbations only.

The system consisting of two differential equations is extended with respect to [52] towards two dimensions by simply adding a diffusive term in the  $y$  direction. It is given by

$$\begin{aligned}
 & - \begin{bmatrix} \epsilon & 0 \\ 0 & 1 \end{bmatrix} \begin{bmatrix} u_1 \\ u_2 \end{bmatrix}_{xx} - \begin{bmatrix} \epsilon & 0 \\ 0 & 1 \end{bmatrix} \begin{bmatrix} u_1 \\ u_2 \end{bmatrix}_{yy} + \dots \\
 & \dots + \begin{bmatrix} 2(x+1)^2 & -(1+x^3) \\ -2\cos(\pi x/4) & 2.2e^{1-x} \end{bmatrix} \begin{bmatrix} u_1 \\ u_2 \end{bmatrix} = \begin{bmatrix} 2e^x \\ 10x+1 \end{bmatrix}, \quad (5.11)
 \end{aligned}$$

with homogeneous Dirichlet boundary conditions on the entire boundary.

Figure 5.5 shows in each plot the numerical approximations obtained using a mesh with  $n = 16$  elements in each direction, varying the diffusion parameter row by row. The classical results are depicted in the left column and the stabilized results in the right column.

As expected, the classical and stabilized results are practically identical in the first row, corresponding to the diffusion dominated case. When reducing the diffusion parameter by three orders of magnitude, oscillations start to appear in the numerical approximations for  $u_1$ , obtained by the classical scheme. Such oscillations appear close to the boundaries. Moreover, where these boundary layer oscillations meet in the corners they generate easily recognisable peaks. The stabilized scheme (right column) effectively removes the edge oscillations and the corner peaks generated by their interaction.

By moving to the third row, the amplitude of the above mentioned spikes increases for the classical scheme because the problem is more dominated by reaction. The corresponding numerical approximations obtained with the stabilized scheme are free of spurious oscillations, adequately capture the sharp changes at the boundary layers, and do not exhibit any peaks in the corners.

Note that since the perturbations of the coefficients are computed in each element, the proposed stabilization scheme is able to handle spatially heterogeneous transport coefficients. This is particularly important when dealing with time dependent coefficients or even with non-linear transport equations. This same feature allows handling variable mesh sizes, making the stabilization technique highly versatile and flexible.

### 5.3.3 Convection-diffusion-reaction system

In the final example, a general system involving all transport mechanisms is considered. Being able to treat such a challenging problem involving convection, diffusion and reaction is the main goal in developing the presented stabilization technique.

The original one-dimensional problem considered in [10] is defined and solved there using an upwind finite difference scheme. It considers a case in which the diffusion matrices are isotropic. Again the two-dimensional extension is achieved by adding the diffusive and convective terms in the  $y$  direction. The resulting equation reads

$$\begin{aligned}
 -\frac{\epsilon}{2} \begin{bmatrix} 1 & 0 & 0 \\ 0 & 1 & 0 \\ 0 & 0 & 1 \end{bmatrix} \begin{bmatrix} u_1 \\ u_2 \\ u_3 \end{bmatrix}_{xx} - \frac{\epsilon}{2} \begin{bmatrix} 1 & 0 & 0 \\ 0 & 1 & 0 \\ 0 & 0 & 1 \end{bmatrix} \begin{bmatrix} u_1 \\ u_2 \\ u_3 \end{bmatrix}_{yy} + \begin{bmatrix} r_1 & 0 & 0 \\ 0 & r_2 & 0 \\ 0 & 0 & r_3 \end{bmatrix} \begin{bmatrix} u_1 \\ u_2 \\ u_3 \end{bmatrix}_x + \dots \\
 \dots + \frac{\eta}{4} \begin{bmatrix} 4 & 2 & 1 \\ 2 & 4 & 2 \\ 1 & 2 & 4 \end{bmatrix} \begin{bmatrix} u_1 \\ u_2 \\ u_3 \end{bmatrix}_y + \begin{bmatrix} 2\mu_1 & -2\mu_1 & 0 \\ -\mu_2 & \mu_1 + \mu_2 & -\mu_1 \\ 0 & -2\mu_2 & 2\mu_2 \end{bmatrix} \begin{bmatrix} u_1 \\ u_2 \\ u_3 \end{bmatrix} = \begin{bmatrix} 0 \\ 0 \\ 0 \end{bmatrix}.
 \end{aligned} \tag{5.12}$$

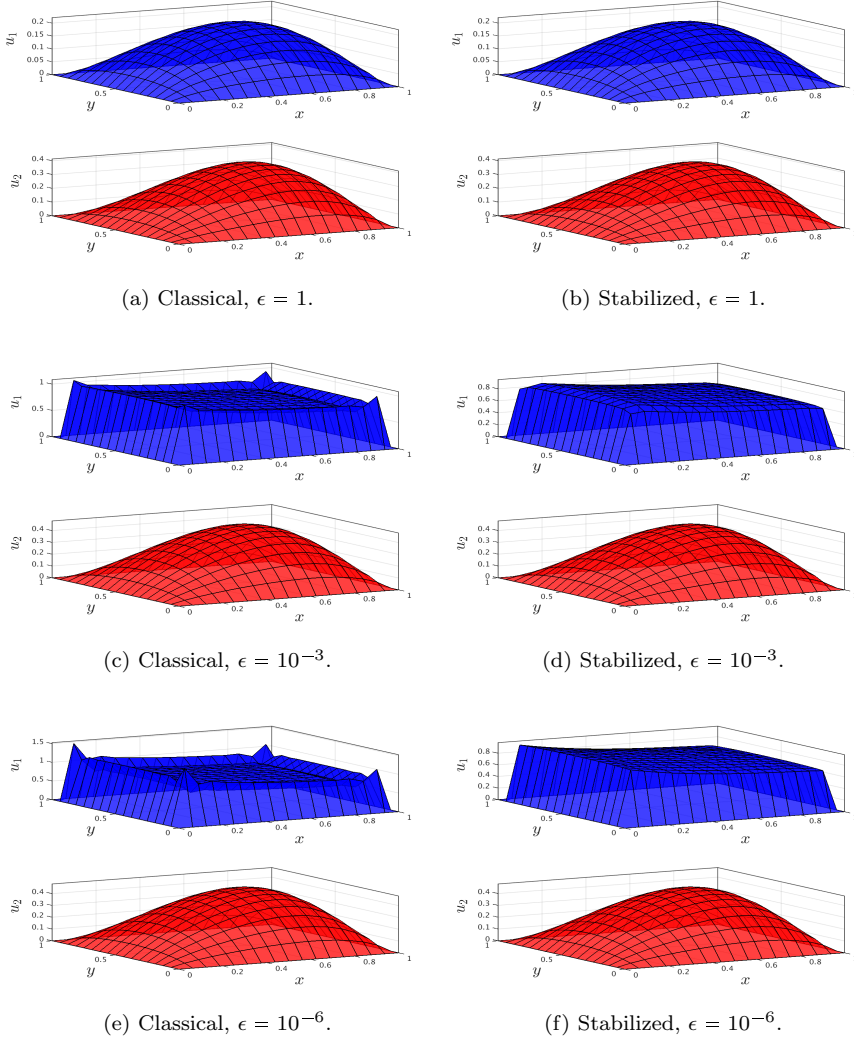


Figure 5.5: Numerical approximations for the boundary value problem associated with Equation (5.11) obtained using a mesh consisting of  $n = 16$  elements in each spatial dimension, with decreasing diffusion from top to bottom, for the classical (left) and stabilized (right) schemes.

The convection coefficients are piece-wise constant and given by

$$r_k = \begin{cases} (k-1)(\lambda_1 + \lambda_2) - c & \text{if } 0 \leq x \leq b \\ (k-1)\lambda_1 - c & \text{if } b < x \leq 1 \end{cases}. \quad (5.13)$$

The original boundary conditions have been modified for consistency with the previous problems and to generate boundary layers challenging the stabilization scheme. They have been taken as  $\mathbf{u}(x = 0, 0 \leq y \leq 1) = [0.25, 0, 0.1]^T$  and  $\mathbf{u}(x = 1, 0 \leq y \leq 1) = [0, 0, 0]^T$ . Homogeneous Robin boundary conditions are imposed on the bottom and top edges, i.e.  $F_{ip}n_i = 0$ , for  $i = 1, 2$ , and  $p = 1, 2, 3$ , on  $\Gamma_R = \{0 < x < 1, y = 0\} \cup \{0 < x < 1, y = 1\}$ . All diffusion and discretization parameters are the same as in the previous problem. The parameters in the convection and reaction matrices are taken as  $\mu_1 = 1$ ,  $\mu_2 = 0.5$ ,  $\lambda_1 = 1$ ,  $\lambda_2 = 0.4$ ,  $c = 1.2$ ,  $b = 0.3$ , and  $\eta = 1.0$ . The evaluation of the convection coefficients on the two different spatial regions yields:  $\mathbf{r}(0 \leq x \leq 0.3) = [-1.2, 0.3, 1.8]^T$  for the left region and  $\mathbf{r}(0.3 < x \leq 1.0) = [-1.2, -0.2, 0.8]^T$  for the right region. Note that the abrupt change in the last component only affects its magnitude, while the convection direction remains unchanged. In fact, the variation is more drastic in the second component, which changes its sign. Therefore, in addition to boundary layers, internal layers are expected.

Figure 5.6 shows the numerical approximations in the same format as previously. In the diffusion dominated case, in the first row, the classical and stabilized results are practically identical. Note that  $u_1$  is convected towards the left since its corresponding convection coefficient in the  $x$  direction is negative on the whole spatial domain and at the same time it is also convected towards the top because the convection coefficients in the  $y$  direction are positive. Note too that  $u_3$  is convected to the right because its convection coefficient in the  $x$  direction is positive on the whole domain. Thus  $u_1$  and  $u_3$  exhibit boundary layers at the left and right boundaries respectively. The situation is different for  $u_2$  since its boundary values on the lateral edges are the same and its convection coefficients in the  $x$  direction have opposite signs in the two regions separated by a vertical line at  $x = b$ , pointing towards the interior of the domain. Therefore, any quantity of  $u_2$  present in the spatial domain, and generated through the reaction terms, will be transported towards the line  $x = b$  in which the convection coefficient changes sign, and towards the top edge due to the positive convection coefficients in the  $y$  direction. This generates a double internal layer for  $u_2$  itself, but additionally could also generate internal layers for  $u_1$  and  $u_3$  through the reaction coupling.

The above mentioned phenomena are more pronounced when moving to the next row, in which the diffusion has been weakened by three orders of magnitude. From these diffusion values, the approximations obtained with the classical scheme are plagued by spurious oscillations. The stabilized scheme solutions are free of such instabilities and adequately capture the boundary and internal layers. Moving to the third row, the classical results also show such oscillatory behaviour. This is not the case for the stabilized scheme which still renders smooth numerical approximations.

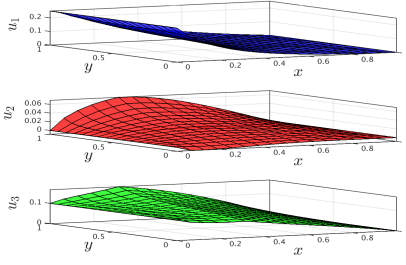
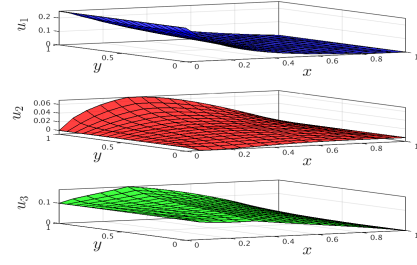
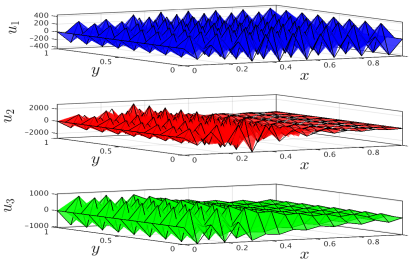
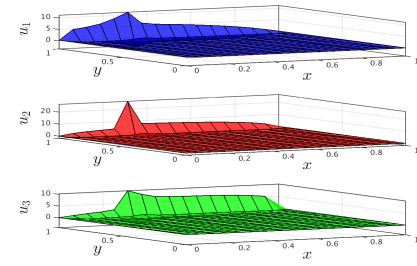
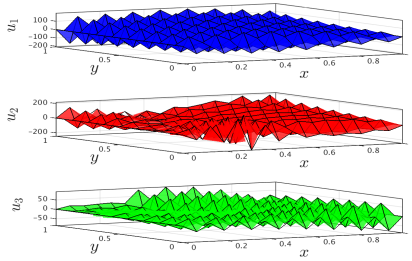
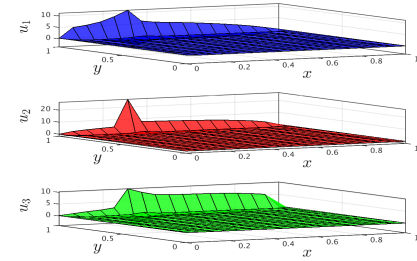
(a) Classical,  $\epsilon = 1$ .(b) Stabilized,  $\epsilon = 1$ .(c) Classical,  $\epsilon = 10^{-3}$ .(d) Stabilized,  $\epsilon = 10^{-3}$ .(e) Classical,  $\epsilon = 10^{-6}$ .(f) Stabilized,  $\epsilon = 10^{-6}$ .

Figure 5.6: Numerical approximations for the boundary value problem associated with Equation (5.12) obtained using a mesh consisting of  $n = 16$  elements in each spatial dimension, with decreasing diffusion from top to bottom, for the classical (left) and stabilized (right) schemes.

## 5.4 Comparison with other techniques

The purpose of this section is, as done in Section 3.5 for one-dimensional problems, to perform a comparative study of the presented stabilization technique with other well-known and established methods, but this time for two-dimensional configurations.

In order to extend the general framework for the application of the SUPG, GLS and SGS methods to multiple dimensional configurations, the diffusion, convection and reaction operators originally defined for one-dimensional problems in (3.36) are re-written for multiple dimensions as

$$\mathcal{L}_D(\mathbf{u}) = -\frac{\partial}{\partial x_i} \left( \mathbf{A}_{ij} \frac{\partial \mathbf{u}}{\partial x_j} \right), \quad \mathcal{L}_C(\mathbf{u}) = \mathbf{B}_i \frac{\partial \mathbf{u}}{\partial x_i}, \quad \text{and} \quad \mathcal{L}_R(\mathbf{u}) = \mathbf{G}\mathbf{u}, \quad (5.14)$$

where repeated indices imply the traditional summation convention.

It is possible to write Equation (5.4) in steady state by using the general transport operator  $\mathcal{L}$  defined in the same way as done for one-dimensional problems in Equation (3.37). It then follows that the associated residual is defined as already done in Equation (3.38). Moreover, after application of the weighted residuals statement and the addition of the stabilization term, an expression identical to (3.39) is obtained.

Therefore, it remains to extend the differential operators  $\mathcal{P}$  used for the different methods when dealing with multi-dimensional configurations [14]. For the SUPG method it can be written as

$$\mathcal{P}_{\text{SUPG}}(\mathbf{w}) = \mathcal{L}_C^T(\mathbf{w}) = \mathbf{B}_i^T \frac{\partial \mathbf{w}}{\partial x_i}. \quad (5.15)$$

The operators for the GLS and SGS methods are in turn written as

$$\mathcal{P}_{\text{GLS}}(\mathbf{w}) = \mathcal{L}^T(\mathbf{w}) = -\frac{\partial}{\partial x_i} \left( \mathbf{A}_{ij}^T \frac{\partial \mathbf{w}}{\partial x_j} \right) + \mathbf{B}_i^T \frac{\partial \mathbf{w}}{\partial x_i} + \mathbf{G}^T \mathbf{w}. \quad (5.16)$$

and

$$\mathcal{P}_{\text{SGS}}(\mathbf{w}) = -\mathcal{L}^*(\mathbf{w}) = \frac{\partial}{\partial x_i} \left( \mathbf{A}_{ij}^T \frac{\partial \mathbf{w}}{\partial x_j} \right) + \mathbf{B}_i^T \frac{\partial \mathbf{w}}{\partial x_i} - \mathbf{G}^T \mathbf{w}. \quad (5.17)$$

The definition of the matrix of stabilization parameters given by Equation (3.44) is left unchanged, only the  $\mathbf{A}_o$  and  $\mathbf{B}_o$  matrices are re-defined as

$$\mathbf{A}_o = (\mathbf{A}_{ij} \mathbf{A}_{ij})^{1/2}, \quad \mathbf{B}_o = (\mathbf{B}_i \mathbf{B}_i)^{1/2}, \quad \text{and} \quad \mathbf{G}_o = (\mathbf{G} \mathbf{G})^{1/2}. \quad (5.18)$$

### 5.4.1 Convection-diffusion system

The comparison of stabilization techniques is done in the same way as in Section 3.5, although this time only the numerical approximations obtained using a discretization consisting of  $n = 16$  elements in each spatial direction are depicted.

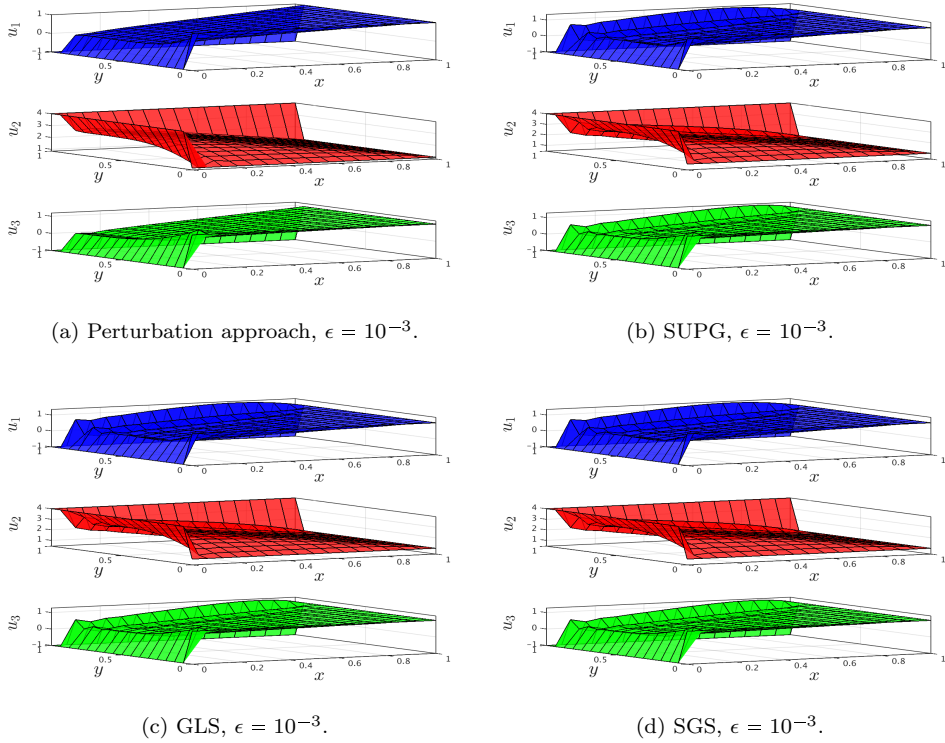


Figure 5.7: Numerical approximations for the boundary value problem associated with Equation (5.9) obtained using a mesh consisting of  $n = 16$  elements in each spatial dimension and a diffusion parameter of  $\epsilon = 10^{-3}$ , for the proposed stabilized scheme (top-left), the Streamline Upwind Petrov-Galerkin (top-right), Galerkin Least-Squares (bottom-left), and Sub-Grid Scale (bottom-right) methods. The corresponding classical results are depicted in Figure 5.2(c) and the perturbation approach results are repeated from Figure 5.2(d).

Figure 5.7 shows the results obtained for the convection-diffusion problem given by Equation (5.9) with a diffusion parameter  $\epsilon = 10^{-3}$ . All the methods, except the coefficient perturbation scheme, render solutions with ridges along the boundary layers. This effect can be easily observed along the edge ( $0 \leq x \leq 1, y = 1$ ) for  $u_1$  and  $u_3$ . Such an effect has been reported previously by Donea and Huerta [23] for the single equation case and by Codina [14] in the multiple equations case.

The presented perturbation-based stabilization technique is able to provide numerical approximations that better capture the sudden change of the solution close to the boundary layers exhibiting neither ridges nor spurious oscillations.



### 5.4.2 Diffusion-reaction system

Now, the attention is turned to the diffusion-reaction problem with a source term given by Equation (5.11). The results for the two-dimensional case presented here confirm the conclusions obtained in Section 3.5.2 for the one-dimensional configuration. These results are depicted in Figure 5.8.

The SUPG and GLS approximations clearly exhibit spurious oscillations. Indeed, the SUPG solution of this diffusion-reaction problem is identical to the classical solution since all the convection matrices  $\mathbf{B}_i$  vanish identically and thus the differential operator  $\mathcal{P}_{\text{SUPG}}$  vanishes as well. Only the proposed perturbation-based stabilization technique and the SGS method are able to provide numerical approximations free of spurious oscillations. Note that this time the over-diffusivity introduced by the SGS method in comparison with the presented stabilization technique is not as evident as in the one-dimensional case.

### 5.4.3 Convection-diffusion-reaction system

The results of the most challenging problem addressed in this chapter, involving convection, diffusion and reaction, are depicted in Figure 5.9. Both the SUPG and GLS methods deliver numerical approximations which exhibit ridges of the same kind as observed for the convection-diffusion case. This effect is most notable in the numerical approximation of  $u_1$ . Moreover, spurious oscillations appear close to the internal layers present in  $u_2$ . The SGS method, as in the one-dimensional case, completely fails to render acceptable numerical approximations.

### Concluding remarks

The results obtained in this comparative study for two-dimensional configurations confirm those obtained for the one-dimensional case presented in Section 3.5: the presented perturbation-based stabilization technique, unlike any of the existing methods tested, is able to render numerical approximations free of spurious oscillations for the three different problems tested.

## 5.5 Conclusions and outlook

In this chapter, a stabilization technique for general systems of coupled convection-diffusion-reaction equations with constant coefficients has been formulated and successfully applied to two-dimensional configurations. For the uncoupled linear convection-diffusion case the proposed stabilization technique recovers the approach presented in [34]. The stabilization technique was initially developed in [34] for a single equation, yielding unconditionally stable solutions based on the discrete maximum principle. The scheme achieves stability by effectively perturbing the transport coefficients of the equation to be discretized. Such perturbations are optimally determined to be the smallest ones required to obtain smooth and stable approximations. Furthermore, it was shown that the numerical approximations obtained with the stabilized scheme converge to the classical Bubnov-Galerkin solution when the mesh Péclet number is small enough, a fact confirmed using a thorough and detailed numerical assessment.

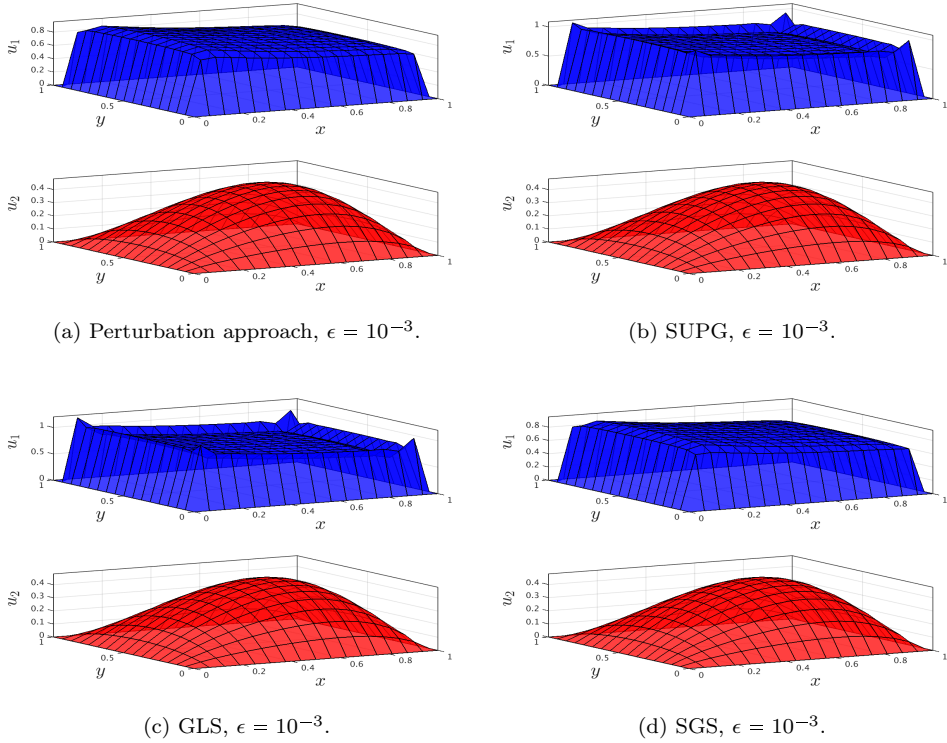


Figure 5.8: Numerical approximations for the boundary value problem associated with Equation (5.11) obtained using a mesh consisting of  $n = 16$  elements in each spatial dimension and a diffusion parameter of  $\epsilon = 10^{-3}$ , for the proposed stabilized scheme (top-left), the Streamline Upwind Petrov-Galerkin (top-right), Galerkin Least-Squares (bottom-left), and Sub-Grid Scale (bottom-right) methods. The corresponding classical results are depicted in Figure 5.5(c) and the perturbation approach results are repeated from Figure 5.5(d).

An illustrative application demonstrates that the general convection-diffusion-reaction case also inherits these desirable properties. The stabilization technique is applicable regardless whether the advective or the divergence form of the partial differential equation is used for the spatial discretization, making it highly flexible and general and able to accommodate different types of complex boundary conditions.

Although originally developed for one-dimensional coupled equations with constant coefficients in [35], the stabilization technique has here been successfully applied to equations with spatially variable convection and reaction coefficients in two-dimensional domains. This makes the method particularly versatile for problems with time dependent or even non-linear transport coefficients, including also the diffusion coefficients. Furthermore, since the perturbations required to render smooth numerical approximations are computed element by element, this stabilization technique is

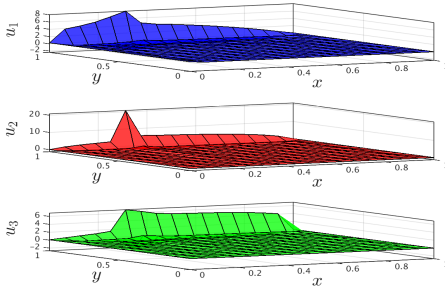
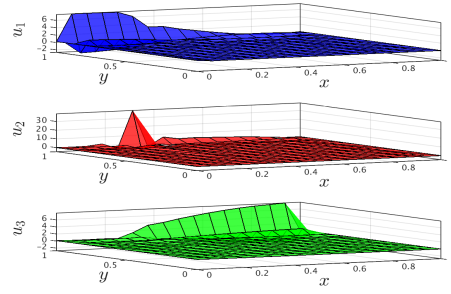
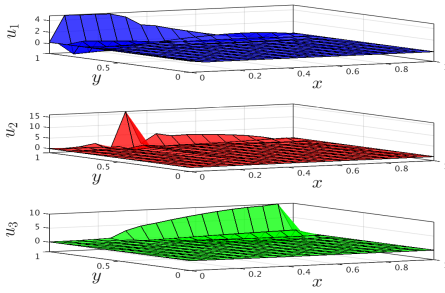
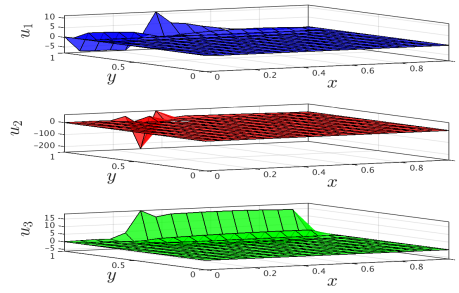
(a) Perturbation approach,  $\epsilon = 10^{-3}$ .(b) SUPG,  $\epsilon = 10^{-3}$ .(c) GLS,  $\epsilon = 10^{-3}$ .(d) SGS,  $\epsilon = 10^{-3}$ .

Figure 5.9: Numerical approximations for the boundary value problem associated with Equation (5.12) obtained using a mesh consisting of  $n = 16$  elements in each spatial dimension and a diffusion parameter of  $\epsilon = 10^{-3}$ , for the proposed stabilized scheme (top-left), the Streamline Upwind Petrov-Galerkin (top-right), Galerkin Least-Squares (bottom-left), and Sub-Grid Scale (bottom-right) methods. The corresponding classical results are depicted in Figure 5.6(c) and the perturbation approach results are repeated from Figure 5.6(d).

locally adaptive, properly handling variable element sizes or unstructured meshes. Finally, there is no need to pre-compute, adapt, or change the mesh at any stage of the computation. This flexibility also removes the need for ordering or scaling of the system of differential equations prior to discretization.

For future work it is intended to evaluate the effectiveness of the assessed stabilization technique on irregular domains discretized by unstructured meshes in order to exploit the full potential offered by the geometric flexibility of the finite element method. Although the present chapter mainly focused on constant diffusion and space dependent convection and reaction coefficients in the steady state regime, variable diffusion coefficients, time dependency of the transport coefficients, and non-linearity will be investigated in steady and transient states.

Devising a strategy to apply the stabilization technique to multidimensional configurations without the need to use multiple discretization sizes decoupling the problem at hand would be a landmark progress which would allow eliminating the risk of introducing any excessive artificial diffusion. Pursuing the derivation, implementation, and assessment of such a strategy is one of the most imperative tasks to be carried out in further work. Such a strategy would endow the stabilization technique with the desirable property of being invariant under rotation of the coordinate axes.

In this chapter, the effect of the stabilization technique on the general properties of the system of algebraic equations after discretization has not been addressed. In particular, the spectral properties of this system may guide one to more effective strategies to solve it, especially when using iterative methods combined with preconditioning techniques. This will be the subject of forthcoming work.

## Chapter 6

# Stabilized Two-dimensional Strain-Gradient Plasticity

---

### Abstract

This chapter addresses the stability of a two-dimensional crystal plasticity model based on dislocation transport involving multiple slip systems at the continuum scale. The dislocation transport model considered is generic, covering most cases of models presented in the literature. Dislocation transport is coupled with mechanical quasi-static equilibrium. The practical implementation of this coupling is detailed. It is shown that the dislocation transport problem requires the solution of systems of coupled convection-diffusion differential equations, even when only a single slip system is considered. When additional slip systems are active it is possible to establish a coupling between them depending on the physical assumptions adopted. The form of the natural boundary conditions of the dislocation transport problem, and the non-linearity of the dislocation transport equations require a highly flexible and versatile stabilization technique able to obtain physically meaningful results. The previously developed stabilization technique will be applied for this purpose. This is the subject of this chapter, showing that the proposed stabilization approach successfully renders strictly positive, smooth and spurious oscillations free numerical approximations.

**keywords.-** Stain-gradient plasticity, Numerical instability, Stabilized finite element method, Convection-diffusion-reaction equations.

---

## 6.1 Introduction

In this last chapter the full potential of the developed stabilization technique is exploited by coupling mechanical equilibrium with dislocation transport in order to obtain a non-local strain-gradient crystal plasticity theory able to take into account size effects.

This coupling of the mechanical equilibrium and the dislocation transport problems follows a well established approach developed for small-strain plasticity problems in which dislocations are represented as line defects able to move only on specific glide planes [28].

In the present implementation, the possibility of activating multiple glide planes is considered. On each of these glide planes two edge dislocation densities will be considered, yielding two transient coupled partial differential equations involving convective and diffusive terms. The implementation allows for interactions between different slip systems, i.e. inter-glide systems coupling. This makes the stabilization technique developed for systems of coupled convection-diffusion-reaction equations well suited for this particular problem.

The form of the natural boundary conditions of the dislocation transport problem (e.g. no dislocation flux through impenetrable boundaries), its application to multi-phase materials with distinct properties, and the non-linear nature of the dislocation transport equations with non-homogeneous and time dependent transport coefficients, all require a highly flexible and versatile stabilization technique using either the advective or divergence form of the partial differential equations to discretize.

The aforementioned implementation is described in detail through this chapter. Section 6.2 presents the dislocation transport equations extended from a single slip system in one dimension towards the two-dimensional multiple slip systems case. The effect of the mechanics on the dislocation transport problem is elucidated at the end of this section. Subsequently, Section 6.3 explains the way in which the dislocation transport effect is taken into account in the mechanical problem, which is discretized using a standard finite element scheme. The interaction between the mechanical and transport problems is thereby complete and Section 6.4 describes in full detail its algorithmic implementation. Section 6.5 presents a case study to assess the effectiveness of the stabilization technique in producing numerically well behaved approximations free of spurious oscillations. This section also presents the results of such a computational assessment, and at the same time discusses the advantages and drawbacks of the presented stabilization technique, with suggestions for future improvements. Finally Section 6.6 closes the chapter by discussing the main conclusions and outlines future work.

## 6.2 Two-dimensional dislocation transport

First, the extension from one-dimensional single slip system dislocation transport towards two-dimensional dislocation transport on multiple slip systems is carried out.

Considering a crystalline material having  $n_s$  active slip systems, the positive and negative (edge) dislocation densities conservation equations on the  $k$ -th glide plane can be written as

$$\frac{\partial \rho_+^{(k)}}{\partial t} + \nabla \cdot \Phi_+^{(k)} = s_+^{(k)}, \quad (6.1)$$

$$\frac{\partial \rho_-^{(k)}}{\partial t} + \nabla \cdot \Phi_-^{(k)} = s_-^{(k)}, \quad (6.2)$$

with the corresponding fluxes given by

$$\Phi_+^{(k)} = \left[ +C_0^{(k)} \rho_+^{(k)} - \sum_{k=1}^{n_s} \mathbf{S}^{(kl)} \left( C_2^{(l)} \rho_+^{(l)} \nabla \rho_+^{(l)} + C_3^{(l)} \rho_+^{(l)} \nabla \rho_-^{(l)} \right) \cdot \mathbf{s}^{(l)} \right] \mathbf{s}^{(k)}, \quad (6.3)$$

$$\Phi_-^{(k)} = \left[ -C_0^{(k)} \rho_-^{(k)} - \sum_{k=1}^{n_s} \mathbf{S}^{(kl)} \left( C_2^{(l)} \rho_-^{(l)} \nabla \rho_-^{(l)} + C_3^{(l)} \rho_-^{(l)} \nabla \rho_+^{(l)} \right) \cdot \mathbf{s}^{(l)} \right] \mathbf{s}^{(k)}. \quad (6.4)$$

where  $\mathbf{s}^{(k)}$  is the unit vector parallel to the Burgers vector in the  $k$ -th glide plane, i.e.  $\mathbf{b}^{(k)} = b^{(k)} \mathbf{s}^{(k)}$  with  $b^{(k)} = \|\mathbf{b}^{(k)}\|_2$ . This unit vector is graphically represented in Figure 6.1. This convention allows to incorporate different phases, with slip systems having different Burgers vector lengths. This also applies to the other coefficients, the definitions of which for each glide system read as

$$C_0^{(k)} = \frac{b^{(k)} \tau^{(k)}}{B^{(k)}}, \quad \text{and} \quad C_1^{(k)} = \frac{\bar{G} (b^{(k)})^2}{12 B^{(k)}}. \quad (6.5)$$

After introducing the parameters used to switch in the generic formulation between the Dogge and Groma models, between constant and variable length scales, including or excluding crossed interactions within a particular glide plane, the constants appearing in Equations (6.3-6.4) are given by

$$C_2^{(k)} = (b'_1 + b'_2) C_1^{(k)} \mathcal{L}^{(k)}, \quad \text{and} \quad C_3^{(k)} = (b'_1 - b'_2) C_1^{(k)} \mathcal{L}^{(k)}. \quad (6.6)$$

Two additional constants are defined, which will be used further on

$$C_4^{(k)} = b'_1 C_1^{(k)} \mathcal{L}^{(k)}, \quad \text{and} \quad C_5^{(k)} = b'_2 C_1^{(k)} \mathcal{L}^{(k)}. \quad (6.7)$$

The coupling between different glide systems is taken into account through the  $\mathbf{S}^{(kl)}$  *projection matrix* whose form has been proposed in a variety of ways depending on the modelling assumptions [85]. Taking the identity matrix for this, implies decoupling of the different slip systems. With these conventions it is possible to define the total and geometrically necessary dislocations densities by adding and subtracting the positive

and negative dislocations densities. Their fluxes are given by

$$\Phi_{\rho}^{(k)} = \left[ C_0^{(k)} \kappa^{(k)} - \sum_{k=1}^{n_s} \mathbf{S}^{(kl)} \left( C_4^{(l)} \rho^{(l)} \nabla \rho^{(l)} + C_5^{(l)} \kappa^{(l)} \nabla \kappa^{(l)} \right) \cdot \mathbf{s}^{(l)} \right] \mathbf{s}^{(k)}, \quad (6.8)$$

$$\Phi_{\kappa}^{(k)} = \left[ C_0^{(k)} \rho^{(k)} - \sum_{k=1}^{n_s} \mathbf{S}^{(kl)} \left( C_5^{(l)} \rho^{(l)} \nabla \kappa^{(l)} + C_4^{(l)} \kappa^{(l)} \nabla \rho^{(l)} \right) \cdot \mathbf{s}^{(l)} \right] \mathbf{s}^{(k)}. \quad (6.9)$$

Finally, the *resolved stress* on the  $k$ -th slip system  $\tau^{(k)}$  appearing in Equation 6.5 is defined as

$$\tau^{(k)} = \mathbf{m}^{(k)} \cdot \boldsymbol{\sigma} \cdot \mathbf{s}^{(k)}, \quad (6.10)$$

with  $\mathbf{m}^{(k)}$  being the unit vector normal to the glide plane of the  $k$ -th slip system. This vector is also graphically represented in Figure 6.1. The stress tensor  $\boldsymbol{\sigma}$  constitutes the mechanical influence on the dislocation transport problem, directly acting as a convective driving force causing positive and negative dislocations to flow in mutually opposite directions.

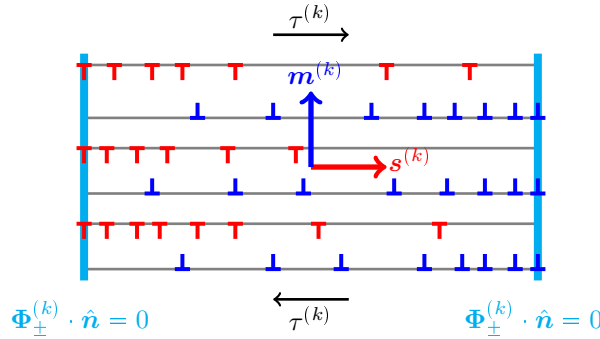


Figure 6.1: Positive and negative dislocations in independent glide planes of the same slip system, bounded by impenetrable barriers.

## 6.3 Mechanical equilibrium

Once the dislocations densities on each slip system are determined it is possible to compute their fluxes. The flux of geometrically necessary dislocations density  $\Phi_{\kappa}^{(k)}$  is of particular interest since it allows to determine the *plastic slip rate* on each slip system through the *Orowan relation*

$$\dot{\gamma}_p^{(k)} = b^{(k)} \mathbf{s}^{(k)} \cdot \Phi_{\kappa}^{(k)}. \quad (6.11)$$

With the slip rates, a *plastic strain rate* on each slip system  $\dot{\epsilon}_p^{(k)}$  can be computed next. Summing all the plastic strain rates of all slip systems, the total plastic strain rate is given by

$$\dot{\epsilon}_p = \frac{1}{2} \sum_{k=1}^{n_s} \dot{\gamma}_p^{(k)} \left( \mathbf{m}^{(k)} \otimes \mathbf{s}^{(k)} + \mathbf{s}^{(k)} \otimes \mathbf{m}^{(k)} \right). \quad (6.12)$$



By considering the deformation process to be quasi-static for small strains, the total strain can be written as the sum of an elastic and a plastic contribution

$$\boldsymbol{\epsilon} = \boldsymbol{\epsilon}_e + \boldsymbol{\epsilon}_p. \quad (6.13)$$

Using the linear elastic constitutive relation, the stress is related to the elastic strain by

$$\boldsymbol{\sigma} = \mathbf{D}\boldsymbol{\epsilon}_e. \quad (6.14)$$

Substituting Equation (6.13) in (6.14) and using  $\boldsymbol{\epsilon} = 1/2 [\nabla \mathbf{u} + (\nabla \mathbf{u})^T] = \nabla^s \mathbf{u}$ , the stress tensor is rewritten as

$$\boldsymbol{\sigma} = \mathbf{D}(\nabla^s \mathbf{u} - \boldsymbol{\epsilon}_p). \quad (6.15)$$

For static equilibrium, the governing equilibrium equation given by

$$\nabla \cdot \boldsymbol{\sigma} = \mathbf{f}, \quad (6.16)$$

with  $\mathbf{f}$  the body forces. After multiplication by a weighting function  $\mathbf{v}^T$ , integration over the whole spatial domain, integration by parts of the left hand side, and reorganization of terms, the classical weighted residual statement results

$$\int_{\Omega} \nabla \mathbf{v}^T \boldsymbol{\sigma} d\Omega = \int_{\Omega} \mathbf{v}^T \mathbf{f} d\Omega + \int_{\Gamma} \mathbf{v}^T \mathbf{t} d\Gamma, \quad (6.17)$$

where  $\mathbf{t} = \boldsymbol{\sigma} \cdot \hat{\mathbf{n}}$  are the tractions applied on the boundary  $\Gamma$  with  $\hat{\mathbf{n}}$  its unit normal vector.

Substitution of Equation (6.15) into Equation (6.17) allows taking into account the plastic strain, i.e. the effect of dislocation transport, in the weighted residual statement. After passing the plasticity term to the right hand side the following weak form is obtained

$$\int_{\Omega} \nabla \mathbf{v}^T \mathbf{D} \nabla^s \mathbf{u} d\Omega = \int_{\Omega} \mathbf{v}^T \mathbf{f} d\Omega + \int_{\Gamma} \mathbf{v}^T \mathbf{t} d\Gamma + \int_{\Omega} \nabla \mathbf{v}^T \mathbf{D} \boldsymbol{\epsilon}_p d\Omega, \quad (6.18)$$

where the plastic strain is acting as an internal force caused by an additional internal strain, similarly to thermal strains induced by temperature changes.

Note that once the displacement field  $\mathbf{u}$  is determined after taking into account external forces, plastic strain and boundary conditions; the stress field  $\boldsymbol{\sigma}$  can be recovered by using Equation (6.15).

## 6.4 Algorithmic coupling of transport and equilibrium problems

The previous two sections have addressed the dislocation transport problem and the mechanical equilibrium problem. The couplings of the two problems are contained in Equations (6.10) and (6.18) respectively. The present section describes in detail the

coupling of both problems by showing their integration from an algorithmic perspective.

Here and in the rest of this chapter, all mechanical actions will be imposed through prescribed displacements at the boundary denoted by  $\hat{\mathbf{u}} = \mathbf{u}(\Gamma)$ . When displacements are not explicitly prescribed on some parts of the boundary, they are considered as traction-free boundaries.

Even though the mechanical equilibrium problem is static, the dislocation transport problem with which it interacts, Equations (6.1-6.2), is intrinsically transient. Therefore it will be assumed that all mechanical actions are applied slowly enough to render inertia forces negligible, i.e. the mechanical problem remains static at every time instance. On the contrary, the time-dependent character of the transport dislocation equations is fully taken into account. External actions in the mechanical problem will be introduced through the boundary conditions, i.e. displacements on the boundary, at the specified time instance  $t$  and denoted by  $\hat{\mathbf{u}}^{(t)} = \mathbf{u}(\Gamma, t)$ . For simplicity, the displacements on the boundary at any given time  $\hat{\mathbf{u}}^{(t)}$  will be given by a predefined steady state boundary displacement, denoted by  $\hat{\mathbf{u}}^{(\infty)}$ , multiplied by a scalar time function  $f(t)$ , thus

$$\hat{\mathbf{u}}^{(t)} = f(t)\hat{\mathbf{u}}^{(\infty)}. \quad (6.19)$$

In addition to the external loading through  $\hat{\mathbf{u}}^{(t)}$ , the plastic strain at a given time instance  $\epsilon_p^{(t)}$  has to be resolved and supplied to the mechanical problem. This allows to determine the displacement field  $\mathbf{u}^{(t)}$  according to Equation (6.18), and compute the stress field  $\boldsymbol{\sigma}^{(t)}$  with Equation (6.15). The obtained stress field is then projected onto each glide system according to Equation (6.10) and passed to the dislocation transport problem, Equations (6.1-6.2), through the constants defined by Equations (6.3-6.5). Once the dislocations densities at the next time instance are obtained, they can be used to evaluate the flux of geometrically necessary dislocations. Using the Orowan relation, Equation (6.11), together with Equation (6.12) the total plastic slip rate is obtained and used to compute the total plastic slip at the next time instance as

$$\epsilon_p^{(t+\Delta t)} = \epsilon_p^{(t)} + \Delta t \dot{\epsilon}_p, \quad (6.20)$$

This updated plastic slip, together with the new displacements on the boundary  $\hat{\mathbf{u}}^{(t+\Delta t)}$ , is used according to Equation (6.18) to update the displacement field. This incremental process is summarized in Algorithm 1.

## 6.5 Computational assessment

The main purpose of the present section is to assess the effectiveness of the stabilization technique for systems of coupled convection-diffusion-reaction equations in two-dimensional configurations for a coupled dislocation transport - mechanical equilibrium problem. This is done by considering a characteristic problem which best elucidates the behaviour in a simple manner, even though it does not exploit all the capabilities of the developed implementation.

---

**Given:**

Boundary displacements at final time:  $\hat{\mathbf{u}}^{(\infty)} = \mathbf{u}(\Gamma, T_f)$ .

Initial fields on the whole domain:  $\boldsymbol{\epsilon}_p^{(0)} = \boldsymbol{\epsilon}_p(\Omega, t = 0)$ , and  $\boldsymbol{\rho}^{(0)} = \boldsymbol{\rho}(\Omega, t = 0)$ .

**Initialize:**

Boundary displacements at initial time:  $\hat{\mathbf{u}}^{(0)} = f(t = 0)\hat{\mathbf{u}}^{(\infty)}$ .

Initial stress fields:  $\boldsymbol{\sigma}^{(0)} \Leftarrow [\hat{\mathbf{u}}^{(0)}, \boldsymbol{\epsilon}_p^{(0)}]$ .

Resolved stress on each glide system:  $\tau^{(k)} \Leftarrow [\boldsymbol{\sigma}^{(0)}]$ .

---

**Time marching:**

**for**  $n = 0, 1, 2, \dots, [T_f / \Delta t]$  **do**

**Compute:**

Dislocation field:  $\boldsymbol{\rho}^{(n+1)} \Leftarrow [\boldsymbol{\rho}^{(n)}, \tau^{(k)}]$ .

Plastic slip rate:  $\dot{\boldsymbol{\epsilon}}_p \Leftarrow [\boldsymbol{\rho}^{(n+1)}]$ .

Plastic strain:  $\boldsymbol{\epsilon}_p^{(n+1)} = \boldsymbol{\epsilon}_p^{(n)} + \Delta t \dot{\boldsymbol{\epsilon}}_p$ .

Stress field:  $\boldsymbol{\sigma}^{(n+1)} \Leftarrow [\hat{\mathbf{u}}^{(n+1)}, \boldsymbol{\epsilon}_p^{(n+1)}]$ .

Resolved stress on each glide system:  $\tau^{(k)} \Leftarrow [\boldsymbol{\sigma}^{(n+1)}]$ .

**end for**

---

---

Algorithm 1: Algorithmic implementation of the interaction between the mechanical equilibrium and dislocation transport problems.

### 6.5.1 Problem description

A simple shear problem, applied to a unit square geometry, is analysed using fully kinematic boundary conditions. The prescribed displacements of the bottom and top edges in the steady state are: on the bottom edge  $\hat{\mathbf{u}}^{(\infty)} (0 \leq x \leq 1, y = 0) = [0, 0]^T$  and on the top edge  $\hat{\mathbf{u}}^{(\infty)} (0 \leq x \leq 1, y = 1) = [d, 0]^T$ . On the left and right edges periodic boundary conditions are imposed for all time instances, i.e.  $\hat{\mathbf{u}}^{(t)} (x = 1, 0 \leq y \leq 1) = \hat{\mathbf{u}}^{(t)} (x = 0, 0 \leq y \leq 1)$ . Note that the prescribed displacements only depend on the parameter  $d$ . A graphical representation is show in Figure 6.2.

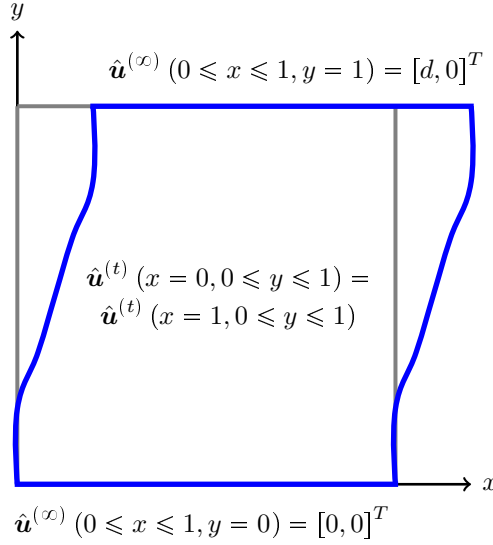


Figure 6.2: Kinematic boundary conditions.

Departing from the undeformed configuration, the steady state boundary displacements  $\hat{\mathbf{u}}^{(\infty)}$  are reached through constant increments until half of the final simulation time  $T_f$  is attained. After this stage  $\hat{\mathbf{u}}^{(\infty)}$  is kept constant, allowing the dislocation transport problem to reach a steady state condition once relaxation of the mechanical problem is achieved. The time function multiplying the mechanical steady state boundary conditions, used in Equation (6.19), therefore reads

$$f(t) = \begin{cases} \frac{2}{T_f}t, & 0 < t < \frac{T_f}{2} \\ 1, & \frac{T_f}{2} \leq t < T_f. \end{cases} \quad (6.21)$$

Although the developed implementation is able to handle multiple slip systems, the presented test is performed activating only a single slip system. The slip system is aligned vertically, i.e. its Burgers vector is parallel to the  $y$ -axis. Neither annihilation nor nucleation is considered, i.e.  $s_+^{(k)} = s_-^{(k)} = 0$  in Equations (6.1-6.2), but uniformly distributed dislocation densities are assumed as the initial conditions. Dislocations are not allowed to flow out the spatial domain, i.e.  $\Phi_{\pm}^{(k)} \cdot \hat{\mathbf{n}} = 0$  on the whole domain boundary.

The material properties are identical to those used in previous chapters and are comparable to those used in [85, 86]. The domain considered has unit edge length  $L = 1 \mu m$ , and a single phase has been used in the computational domain. Its properties are:  $h = 0.1 \mu m$ ,  $b = 0.3 nm$ ,  $B = 10^{-4} Pa s$ ,  $\nu = 1/3$ ,  $G = 25 GPa$ . The initial condition was chosen as  $\rho_{\pm}^{(0)} = 200 \mu m^{-2}$ .

The Groma model, with variable length scale and not taking into account interaction among dislocations of different signs has been used as in [85, 86] to enable a comparative analysis. Taking  $d = 0.01 \mu m$ , the results presented here are comparable to those presented in [85, 86] with the maximum applied shear strain.

For compactness, only results on a single mesh are presented and discussed, although it is important to remark that many simulations with different discretizations, have been carried out to support the conclusions. Because the same space restrictions, classical and stabilized results are only compared for the case of dislocation densities, such comparison provides enough numerical evidence of the necessity of the stabilization technique to approach the problem at hand using a moderately refined discretization.

## 6.5.2 Results

The results presented are obtained using a uniform mesh with  $n_x = n_y = 32$  quadrilateral elements in each direction. A bilinear element, using Lagrange polynomials as interpolation functions, is thereby adopted. The final time has been set as  $T_f = 10^3 \mu s$  using a time step  $\Delta t = 10^{-1} \mu s$  with a fully implicit time integration scheme.

Figure 6.3 illustrates the discretization used in the deformed configuration (with a magnification factor of 10). A pronounced distortion close to the top and bottom edges can be observed, differing notoriously from the distortion in the rest of the spatial domain. This heterogeneity of the strain field is consistent with well known results already presented in the literature [85, 86]. Such heterogeneity will be elucidated more clearly after observing the plots depicting the shear stress. These plots are shown in Figure 6.4. On the left, the shear stress field onto the active glide system in the entire spatial domain at the last time instance is presented, while on the right its cross-section on the central vertical line ( $x = 1/2$ ,  $0 \leq y \leq 1$ ) is depicted at ten equally spaced time instances in order to illustrate its time evolution.

The shear stress is not uniform on the whole spatial domain, as would be the case if only the mechanical boundary conditions are taken into account. This variability is caused by the effect of the dislocation transport problem on the mechanical equilibrium problem. The non-uniform spatial distribution of the shear stress and the mechanical distortion, both occur precisely in the regions where the dislocation densities form boundary layers. This is confirmed in Figure 6.5, depicting the positive and negative dislocation densities in the entire spatial domain at the last time instance (left), together with their time evolution on the middle vertical line (right). It is important to remark that Figure 6.5 shows that all the numerical approximations of the dislocation densities are strictly positive and free of any spurious oscillation when using the stabilization technique and whose results are depicted at the top row. This is no

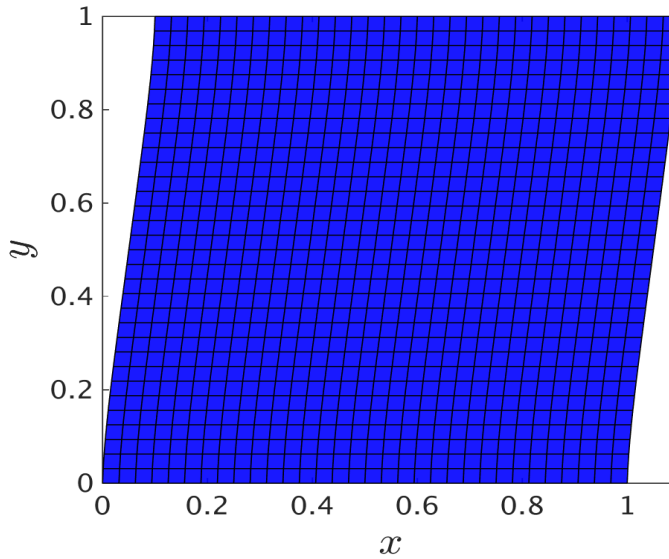


Figure 6.3: Final deformation at the last time instance amplified ten times.

longer true when the stabilization technique is not used. The plots displayed at the bottom row corresponds to the numerical approximation of the dislocation densities for the same problem but without the use of the stabilization technique. The spurious oscillations and non-negative values of the dislocations densities make these approximations useless. Therefore, the ability of the stabilization technique to render well behaved numerical approximations is thereby confirmed. Moreover, this example also confirms the necessity of the stabilization technique in order to handle this problem with a computationally affordable discretization.

Finally, Figure 6.6 shows the plastic slip  $\gamma_p$ , for the last time instance on the whole spatial domain (left) and its time evolution on the central vertical line (right). Note that the plastic slip  $\gamma_p$  at the bottom and top edges ( $y = 0$ , and  $y = 1$ ) do not vanish completely as theoretically assumed through the no-flux boundary conditions in the dislocation transport problem. This quantity is obtained through the accumulation of the plastic slip rate  $\dot{\gamma}_p$  which results from Equation (6.11) using the flux of geometrically necessary dislocation density. This flux, as all the dislocation fluxes, are supposed to vanish at the boundary, but this is only rigorously true in the strong form of the partial differential equation prior to its numerical discretization. The depicted dislocation flux is obtained in a post-processing stage from the dislocation densities approximated at the nodes composing the finite element discretization. This post-processing computation involves the spatial derivatives of the degrees-of-freedom. The evaluation of these derivatives, and therefore of the dislocation fluxes, implies the loss of one order of accuracy in their numerical approximation. This effect is reflected in the fact that fluxes, especially on the boundary, cannot be exactly recovered after discretization via the weak form. Since this is the case for all of the plastic slip rates

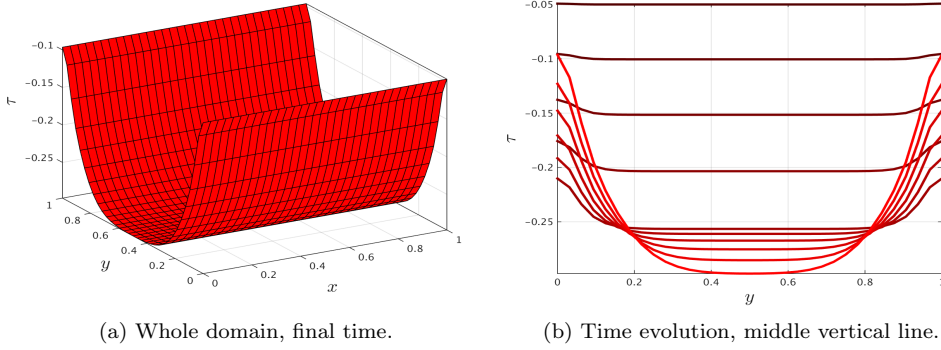


Figure 6.4: Spatial distribution of the shear stress. On the whole spatial domain at final time on the left. On the right the darkest line corresponds to the earliest time instance while the brightest line to the last time instance.

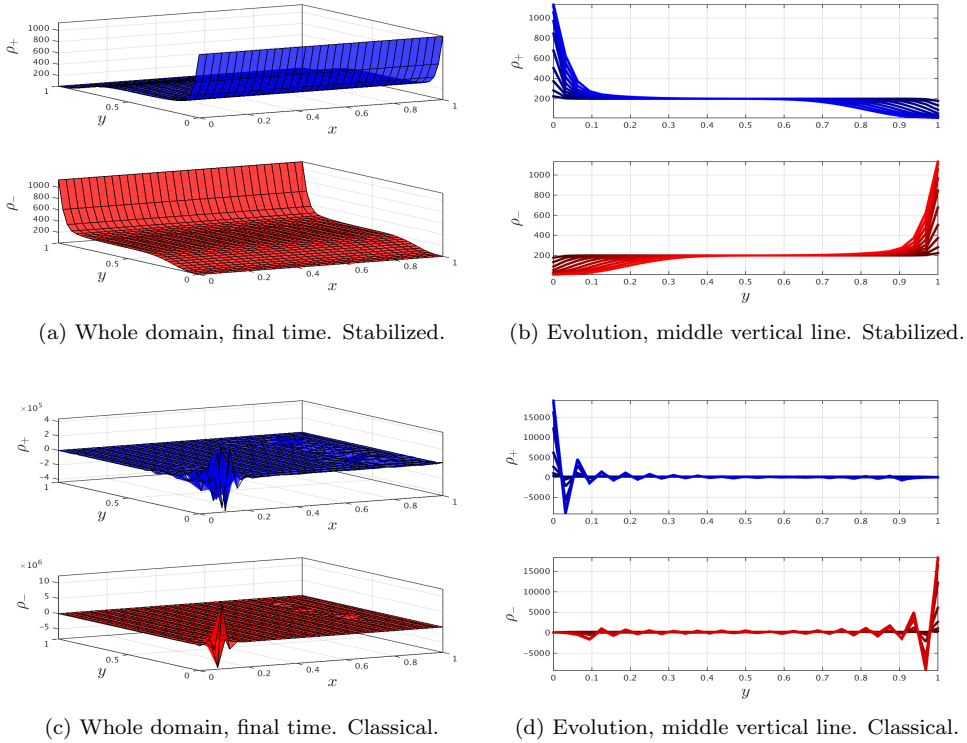


Figure 6.5: Spatial distribution of the dislocations densities. On the whole spatial domain at final time on the left. On the right the darkest line corresponds to the earliest time instance while the brightest line to the last time instance. Stabilized results are displayed at the top row and classical at the bottom row.

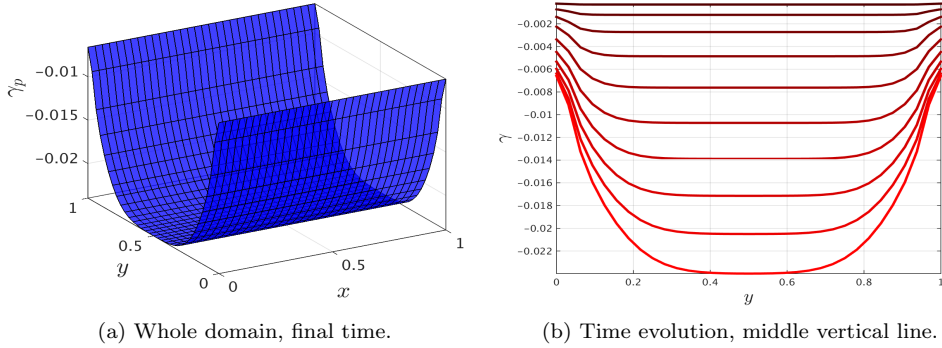


Figure 6.6: Spatial distribution of the plastic slip. On the whole spatial domain at final time on the left. On the right the darkest line corresponds to the earliest time instance while the brightest line to the last time instance.

$\dot{\gamma}_p$  computed for each time instance, this deviation from zero is accumulated in the total plastic slip  $\gamma_p$ . It has been confirmed (based on numerical simulations not shown here) that this approximation error can be reduced through mesh refinement, even though the reduction appears to be only linear.

## 6.6 Conclusions and outlook

In this chapter a two-dimensional crystal plasticity model based on dislocation transport involving multiple slip systems has been outlined. The transport model is made generic through the use of switching parameters allowing to encompass the vast majority of models already presented in the literature [21, 31, 85, 86].

The continuum dislocation transport model has been coupled with the mechanical equilibrium problem assuming quasi-static conditions following a well established framework [28]. The coupling of these two problems has been explained in detail in this chapter.

The dislocation transport problem requires the solution of systems of coupled convection-diffusion differential equations even when working with a single slip system. When additional slip systems are considered, each contributes with two additional transport equations which are coupled through interaction terms. Using a particular form of the projection matrix, the coupling between different slip systems can be changed or fine-tuned.

These two different types of coupling make the stabilization technique for coupled convection-diffusion-reaction equations appealing, since traditional stabilization techniques can not cope with this challenging problem, not to mention the computationally unaffordable mesh refining strategy.



The previously developed stabilization technique is proven to effectively render strictly positive, smooth and free of spurious oscillations numerical approximations of the dislocation densities when applied to the strain-gradient crystal plasticity problem when activating several slip systems. Even more, it is able to properly capture the boundary layers caused by the convection dominated character of the transport equations at hand. This approximation is carried out using a computationally affordable discretization. Although not shown in this chapter, numerical assessments performed using different discretizations allow to claim that the drawback of having non-vanishing normal fluxes across the domain boundaries can be reduced by refining the discretization. Note however that the use of equal-order approximation schemes could be advantageous in order to cope with this numerical error.

Although the test presented here does not exploit the full potential of the developed multiple slip strain-gradient crystal plasticity implementation, it is important to remark that the computational code fulfils the main objective of this work. It is capable to treat multiple slip systems with distinct properties, it incorporates various modelling options allowing to select either the Dogge or the Groma model with constant or variable length scale respectively, and it allows taking into account or neglecting interactions between dislocations of different signs.

Comparison of the results obtained by altering the model parameters is now easy and affordable due to the flexibility, versatility and robustness of the computational implementation of stabilized multiple slip strain-gradient crystal plasticity. This assessment, comparison and analysis is however beyond the scope of this work and will be future work.

# Chapter 7

## Conclusions and Outlook

This thesis deals with the numerical stabilization of convection-diffusion-reaction equations. Of particular interest are the convection dominated equations arising in continuum dislocation transport, which in turn allow the description of the plastic behaviour of crystalline materials. The objectives pursued in this work, as introduced in Chapter 1, have been fulfilled in a stepwise manner. A robust and general, but at the same time versatile and flexible, stabilization technique for multi-dimensional systems of coupled convection-diffusion-reaction equations has been developed, analysed and extensively tested through several numerical assessments. Its application to the convection dominated continuum dislocation transport equations has also been exposed in this thesis. It has been shown to be effective in providing smooth and well behaved numerical approximations without incurring extraordinary computational resources.

### 7.1 Results discussion

This section highlights the main results obtained during the development of this thesis chapter by chapter.

- **Chapter 2.** After presenting the development of a perturbation-based stabilization technique for the single one-dimensional convection-diffusion-reaction equation, a rigorous proof of its effectiveness in rendering unconditionally stable numerical approximations with respect to the space discretization has been provided for the convection-diffusion case, via the fulfilment of the discrete maximum principle. It was also demonstrated and confirmed by numerical assessments that the stabilized solution is consistent with the discretized partial differential equation, since it converges to the classical Bubnov-Galerkin solution if the mesh Péclet number is sufficiently small. The corresponding proofs for the diffusion-reaction and the general convection-diffusion-reaction cases can be obtained in a similar manner. Furthermore, it has been demonstrated that the stabilization technique is applicable irrespective of whether the advective or the divergence form is used for the spatial discretization, making it highly flexible and general.
- **Chapter 3.** In this chapter the stabilization technique has been extended to the case of a system of coupled differential equations. It was furthermore numerically

demonstrated through a detailed computational assessment that the extension to the case of systems of equations effectively inherits the desirable features of the stabilization technique for the single equation case. The most remarkable ones are its ability to stabilize both the divergence or advective form of the differential equation, and its element-wise operation, that allows accommodating spatially heterogeneous transport coefficients.

- **Chapter 4.** The favourable effect and consistency of the stabilization technique when dealing with the non-linear and coupled continuum dislocation transport system of equations in the transient regime has been extensively illustrated. Additionally its versatility and flexibility has been made evident by elaborating and computationally assessing it using different modelling assumptions and length scales.
- **Chapter 5.** Here the stabilization technique has been further extended to multi-dimensional domains and three numerical examples have been successfully stabilized. While presenting and discussing these results, the behaviour of the extended stabilization technique was analysed and it was confirmed that, as in the one-dimensional case, apart of successfully yielding smooth numerical approximations which are free of spurious oscillations, it is consistent as well.
- **Chapter 6.** In this chapter the modelling of plasticity in crystalline materials considering potentially multiple slip systems has been illustrated. The stabilized continuum dislocation transport problem has been coupled to the mechanical equilibrium problem. The non-linearity, the strongly coupled character and the special boundary conditions used for the continuum dislocation transport equations are the most prominent difficulties which most traditional stabilization techniques are unable to deal with. The proposed stabilization scheme has been successfully applied to these equations using a simplified single slip system configuration. Its effectiveness in stabilizing the classical Bubnov-Galerkin scheme has been demonstrated in the numerical simulation performed. These results allow envisioning the use of the developed technique for simulating two-dimensional multi-slip crystal plasticity problems with an affordable computational effort, while keeping the ability to render accurate and physically meaningful numerical approximations.

## 7.2 Further developments

Although the main objectives of this thesis have been successfully fulfilled, some issues remain unresolved and some others arose while carrying out this research project. They can be separated into two categories. The first one concerns numerically related issues, while the second category encompasses aspects related to the plasticity modelling of crystalline materials. They are listed in two separate sections in what follows.

### 7.2.1 Numerical methods

- **Unstructured meshes.** In the numerical assessments presented here for two-dimensional problems, only structured meshes with square finite elements and

linear Lagrange polynomials interpolation functions have been used. The use of unstructured meshes and other types of finite elements, possibly with higher order interpolation functions, could also be explored.

- **Alternative discretization schemes.** Notwithstanding the fact that the present stabilization technique has been developed and applied only within the finite element context, its generality allows to claim it could be successfully used in the context of the finite difference, finite volume or spectral methods. Testing its effectiveness for such numerical schemes represents an interesting challenge.
- **High performance computing.** During this work, little attention has been paid to implementing the algorithms used in the numerical assessments with the most cutting edge tools of scientific computing. The use of more sophisticated and efficient methods for the solution of non-linear systems of algebraic equations, more accurate and efficient time integration schemes and the use of preconditioning techniques could be pursued in order to speed up the computations.
- **Numerical analysis.** Although the ability of the presented stabilization technique to render smooth and well behaved numerical approximations has been explicitly demonstrated via the fulfilment of the discrete maximum principle, a more detailed numerical analysis could provide valuable information about its effectiveness from the mathematical point of view. It could also provide useful insight for further improvement. Of particular interest is the effect the stabilization has on the spectral properties of the linear system generated by the discretization process. Understanding how the eigenvalues of the discretized differential operator are modified by the stabilization technique will provide useful insight from an operational perspective.

## 7.2.2 Crystal plasticity

- **Nucleation and annihilation.** All continuum dislocation transport problems addressed in this work lacked nucleation and annihilation of dislocations. It is expected that taking into account these phenomena does not pose any additional difficulty from the numerical stability perspective. Thus the incorporation of these mechanisms could be included in further developments.
- **Multi-slip systems.** Although the theory for handling multiple slip systems has been developed in this manuscript and the corresponding code is implemented and ready for use, its thorough evaluation is still pending and should be pursued soon.
- **Boundary conditions.** The boundary condition of no flux of dislocations through the boundaries has precisely in part motivated the development of a stabilization technique able to work with either the divergence or advective form of the discretized partial differential equation. Nevertheless, no other type of boundary condition has been considered for the dislocation transport problem during this research project. Even though the treatment of Dirichlet and periodic

boundary conditions should not represent any serious difficulty from the numerical stability perspective, their implementation and testing are also intended as a further development.

- **Multi-grain structures.** All continuum dislocation transport problems elaborated in this work consider the idealized situation when a single crystal is taken into account. In order to handle more realistic problems with higher scientific interest the simulation and study of multi-grains configurations will be addressed.
- **Multi-phase materials.** For simplicity in the assessment of the stabilization technique, only single phase materials have been considered in the numerical simulations presented. The use of multi-phase materials is supposed to not affect the numerical stability because of the element-wise operation of the stabilization technique.

# Bibliography

- [1] Abrahamson L.R., Keller H.B., and Kreiss H.O. 1974. *Difference approximation for singular perturbations of systems of ordinary differential equations*. Numerische Mathematik, **22**, 367-391.
- [2] Ajzoul T., Chaussavoine C., and Amouroux M. 1995. *Finite element analysis of a transient nonlinear heat transfer problem*. Computers and Chemical Engineering, **19**, 423-436.
- [3] Ashwin P., Coombes S., and Nicks R. 2016. *Mathematical Frameworks for Oscillatory Network Dynamics in Neuroscience*, Journal of Mathematical Neuroscience **6:2**.
- [4] Bause M. and Schwegler K. 2012. *Analysis of stabilized higher-order finite element approximation of nonstationary and nonlinear convection-diffusion-reaction equations*, Computer Methods in Applied Mechanics and Engineering, **209-212**, 184-196.
- [5] Bause M. and Schwegler K. 2013. *Higher order finite element approximation of systems of convection-diffusion-reaction equations with small diffusion*, Journal of Computational and Applied Mathematics, **246**, 52-64.
- [6] Bhargava S.C. 1989. *Generalized Lotka-Volterra equations and the mechanism of technological substitution*, Technological Forecasting and Social Change, **35**, 319-326.
- [7] Brooks A.N., and Hughes T.J.R. 1982. *Streamline upwind/Petrov-Galerkin formulations for convection dominated flows with particular emphasis on the incompressible Navier-Stokes equations*. Computer Methods in Applied Mechanics and Engineering, **32**, 199-259.
- [8] Canuto C., Hussaini M.Y., Quarteroni A., and Zang T.A. 2006. *Spectral methods. Fundamentals in single domains*, Scientific Computation, Springer-Verlag, Berlin Heidelberg.
- [9] Cecchi M.M. and Pirozzi M.A. 2005. *High order finite difference numerical methods for time-dependent convection-dominated problems*, Applied Numerical Mathematics, **55**, 334-356.
- [10] Chen D., Hong Y., Trivedi K.S. 2001. *Second-order stochastic fluid models with fluid-dependent flow rates*, Performance and Evaluation, **49**, 341-358.
- [11] Cheng W. and Temam R. 2002. *Numerical approximation of one-dimensional stationary diffusion equations with boundary layers*, Computers & Fluids, **31**, 453-466.
- [12] Ciarlet P.G., and Raviart P.-A. 1972. *Maximum principle and uniform convergence for the finite element method*. Computer Methods in Applied Mechanics and Engineering, **2**, 17-31.
- [13] Codina R. 1998. *Comparison of some finite element methods for solving the diffusion-convection-reaction equation*, Computer Methods in Applied Mechanics and Engineering, **156**, 185-210.
- [14] Codina R. 2000. *On stabilized finite element methods for linear systems of convection-diffusion-reaction equations*, Computational methods in applied mechanics and engineering, **188**, 6182.

- [15] Codina R. and Soto O. 1999. *Finite element implementation of two-equation and algebraic stress turbulence models for steady incompressible flows*, International Journal for Numerical Methods in Fluids, **30**, 309-333.
- [16] Contreras F.R.L., Lyra P.R.M., Souza M.R.A., and Carvalho D.K.E. 2016 *A cell-centered multipoint flux approximation method with a diamond stencil coupled with a higher order finite volume method for the simulation of oil-water displacements in heterogeneous and anisotropic petroleum reservoirs*, Computers & Fluids, **127**, 1-16.
- [17] Cortés J.C., Jódar L., Sala R., and Sevilla-Peris P. 2005. *Exact and numerical solution of Black-Scholes matrix equation*, Applied Mathematics and Computation, **160**, 607-613.
- [18] Cowin S.C. 1999. *Bone poroelasticity*, Journal of Biomechanics, **32**, 217-238.
- [19] Crouzeix M. 1980. *Une méthode multipas implicite-explicite pour l'approximation des équations d'évolution paraboliques*. Numerische Mathematik, **35**, 257-276.
- [20] Djaka K.S., Taupin V., Berbenni S., and Fressengeas C. 2015. *A numerical spectral approach to solve the dislocation density transport equation*, Modelling and Simulation in Materials Science and Engineering, **23**, 65008-65034.
- [21] Dogge M.M.W., Peerlings R.H.J., and Geers M.G.D. 2015. *Extended modelling of dislocation transport-formulation and finite element implementation*, Advanced Modeling and Simulation in Engineering Science, **2:29**.
- [22] Donea J. and Giuliani S. 1974. *Finite Element Analysis of Steady-State Nonlinear Heat Transfer Problems*. Nuclear Engineering and Design, **30**, 205-213.
- [23] Donea J. and Huerta A. 2003. *Finite element methods for flow problems*, John Wiley and Sons, Chichester.
- [24] Elman H., Silvester D., and Wathen A. 2005. *Finite elements and fast iterative solvers: with applications in incompressible fluid dynamics*. Oxford University Press, Oxford.
- [25] Farrell P., Hegarty A., Miller J.M., O'Riordan E., and Shishkin G.I. 2000. *Robust computational techniques for boundary layers*, Champan & Hall/CRC, Boca Raton, Florida.
- [26] Ferziger J. and Perić M. 1996. *Computational methods for fluid dynamics*, Springer Verlag, Berlin Heidelberg.
- [27] Franca L.P., and Dutra Do Carmo E.G. 1988. *The Galerkin gradient least-squares method*. Computer Methods in Applied Mechanics and Engineering, **74**, 41-54.
- [28] van der Giessen E. and Needleman A. 1995. *Discrete dislocation plasticity: a simple planar model*, Modelling and Simulation in Material Science and Engineering, **3**, 689-735.
- [29] Gracia J.L. and Lisbona F.J. 2007. *A uniformly convergent scheme for a system of reaction-diffusion equations*, Journal of Computational and Applied Mathematics, **206**, 1-16.
- [30] Gribaudo M. and Gaeta R. 2006. *Efficient steady-state analysis of second-order fluid stochastic Petri nets*, Performance Evaluation, **63**, 1032-1047.
- [31] Groma I. 1997. *Link between the microscopic and mesoscopic length-scale description of the collective behavior of dislocations*, Physical Review B, **56**, 5807-5813.
- [32] Groma I., Csikor F.F., and Zaiser M. 2003. *Spatial correlations and higher-gradient terms in a continuum description of dislocation dynamics*. Acta Materialia, **51**, 1271-1281.
- [33] Hauke G. 2001. *A simple subgrid stabilized method for the advection-diffusion-reaction equation*. Computer Methods in Applied Mechanics and Engineering, **191**, 2925-2947.
- [34] Hernández H., Massart T.J., Peerlings R.H.J., and Geers M.G.D. 2015. *Towards an unconditionally stable numerical scheme for continuum dislocation transport*, Modelling and Simulation in Materials Science and Engineering, **23**, No. 8.

- [35] Hernández H., Massart T.J., Peerlings R.H.J., and Geers M.G.D. 2017. *A stabilization technique for coupled convection-diffusion-reaction equations*. Ready for submission to the International Journal for Numerical Methods in Engineering.
- [36] Hirschberger C.B., Peerlings R.H.J., Brekelmans W.A.M., and Geers M.G.D. 2011. *On the role of dislocation conservation in single-slip crystal plasticity*. Modelling and simulation in Materials Science and Engineering, **19**, 085002.
- [37] Hodgkin A.L. and Huxley A.F. 1952. *A quantitative description of membrane current and its application to conduction and excitation in nerve*, The Journal of Physiology. **117**, 500-544.
- [38] Hughes T.J.R. 1977. *Unconditionally Stable Algorithms for Nonlinear Heat Conduction*. Computer Methods in Applied Mechanics and Engineering, **10**, 135-139.
- [39] Hughes T.J.R. 1995. *Multiscale phenomena: Green's function, the Dirichlet-to-Neumann formulation, subgrid scale models, bubbles and the origins of stabilized formulations*. Computer Methods in Applied Mechanics and Engineering, **127**, 387-401.
- [40] Hughes T.J.R., Franca L.P., and Hulbert G.M. 1989. *A new nite element formulation for computational uid dynamics: VIII. The Galerkin/least-squares method for advective-diffusive equations*. Computer Methods in Applied Mechanics and Engineering, **73**, 173-189.
- [41] Hughes T.J.R., and Tezduyar T.E. 1984. *Finite Element Methods for First-Order Hyperbolic Systems with Particular Emphasis on the Compressible Euler Equations*. Computer Methods in Applied Mechanics and Engineering, **45**, 217-284.
- [42] Hull D., and Bacon D.J. 2001. *Introduction to Dislocations*. Butterworth-Heinemann, Oxford.
- [43] Idelsohn S., Nigro N., Storti M., and Buscaglia G. 1996. *A Petrov-Galerkin Formulation for Advection-Reaction-Diffusion Problems*. Computer Methods in Applied Mechanics and Engineering, **136**, 27-46.
- [44] John V., and Schmeier E. 2008. *Finite element methods for time-dependent convection-diffusion-reaction equations with small diffusion*. Computer Methods in Applied Mechanics and Engineering, **198**, 475-494.
- [45] Kan-On Y., and Mimura M. 1998. *Singular perturbation approach to a 3-component reaction-diffusion system arising in population dynamics*, SIAM Journal of Mathematical Analysis, **29**, 1519-1536.
- [46] Keating E., and Zyvoloski G. 2009. *A stable and efficient numerical algorithm for unconfined aquifer analysis*. Ground Water, **47**, 569-579.
- [47] Kellogg R.B. Linss T., and Stykes M. 2008. *A finite difference method on layer-adapted meshes for an elliptic reaction-diffusion system in two dimensions*. Mathematics of Computation, **264**, 2085-2096.
- [48] Kellogg R.B. Madden N., and Stykes M. 2007. *A parameter-robust numerical method for a system of reaction-diffusion equations in two dimensions*. Numerical Methods for Partial Differential Equations, DOI 10.1002/num.20265.
- [49] Khoshghalb A., Khalili N., and Selvadurai A.P.S. 2010. *A three-point time discretization technique for parabolic partial differential equations*. International Journal for Numerical and Analytical Methods in Geomechanics, **35**, 406-418.
- [50] Kords C. 2013. *On the role of dislocation transport in the constitutive description of crystal plasticity*. PhD. Thesis. Rheinisch-Westfälischen Technischen Hochschule Aachen.
- [51] Martínez J.M. 2000. *Practical quasi-Newton methods for solving nonlinear systems*. Journal of Computational and Applied Mathematics, **124**, 97-121.



- [52] Matthews S., O’Riordan E., and Shishkin G.I. 2001. *A numerical method for a system of singularly perturbed reaction-diffusion equations*. Journal of Computational and Applied Mathematics, **145**, 151-166.
- [53] Miller J.J.H., O’Riordan E., and Shishkin G.I. 1996. *Fitted numerical methods for singular perturbation problems. Error estimates in the maximum norm for linear problems in one and two dimensions*, World Scientific, Singapore.
- [54] O’Riordan E., and Stynes M. 2009. *Numerical analysis of a strongly coupled system of two singularly perturbed convection-diffusion problems*, Advances in Computational Mathematics, **30**, 101-121.
- [55] O’Riordan E., Stynes J., and Stynes M. 2009. *An iterative numerical algorithm for a strongly coupled system of singularly perturbed convection-diffusion problems*, In Margenov S., Vulkov L.G., and Waśniewski J. Eds. Numerical Analysis and Its Applications, volume 5434 of the series Lecture Notes in Computer Science, 104-115. Springer-Verlag, Berlin Heidelberg.
- [56] Oñate E., Miquel J., and Hauke G. 2005. *Stabilized formulation for the advection-diffusion-absorption equation using finite calculus and linear finite elements*. Computer Methods in Applied Mechanics and Engineering, **195**, 3926-3946.
- [57] Oñate E., Miquel J., and Zárata F. 2007. *Stabilized solution the multidimensional advection-diffusion-absorption equation using linear finite elements*. Computer and Fluids, **36**, 92-112.
- [58] Ohlberger M. and Rohde C. 2002. *Adaptive finite volume approximations for weakly coupled convection dominated parabolic systems*, IMA Journal of Numerical Analysis, **22**, 253-280.
- [59] Ortega J.M., and Rheinboldt W.C. 1970. *Iterative solution of nonlinear equations in several variables*. Academic Press, San Diego.
- [60] Parvazinia M., and Nassehi V. 2010. *Using bubble functions in the multi-scale finite element modeling of the convection-diffusion-reaction equation*. International Communications in Heat and Mass Transfer, **37**, 125-130.
- [61] Patel K.S. and Mehra M. 2015. *High-order compact finite difference method for BlackScholes PDE*, In Agrawal P.N., Mohapatra R.N., Singh U., and Srivastava H.M. Eds. Mathematical analysis and its applications, Roorkee, India, December 2014, volume 143 of the series Springer Proceedings in Mathematics & Statistics, 393-403. Springer India, New Delhi.
- [62] Protter M.H., and Weinberger H.F. 1984. *Maximum principles in differential equations*, Springer Verlag, New-York.
- [63] Quarteroni A., Sacco R. and Saleri F. 2007. *Méthodes Numériques*. Springer-Verlag Italia, Milan.
- [64] Rheinboldt W.C. 1998. *Methods for solving systems of nonlinear equations*. Society for Industrial and Applied Mathematics, Philadelphia.
- [65] Richtmyer R. and Morton K. 1967. *Difference methods of initial-value problems*, Interscience Publishers, New York.
- [66] Roters F., Eisenlohr P., Hantcherli L., Tjahjanto D.D., Bieler T.R., and Raabe D. 2010. *Overview of constitutive laws, kinematics, homogenization and multiscale methods in crystal plasticity finite-element modeling: Theory, experiments, applications*. Acta Materialia, **58**, 1152-1211.
- [67] Saad Y. 2000. *Iterative Methods for Sparse Linear Systems*. Society for Industrial and Applied Mathematics, Philadelphia.
- [68] Seal D.C., Tang Q., Xu Z., and Christlieb A.J. 2015. *An explicit high-order single-stage single-step positivity-preserving finite difference WENO method for the compressible Euler equations*, Journal of Scientific Computing, 1-20.

- [69] Shampine L.F. and Thompson R.J. 1970. *Difference methods for nonlinear first-order hyperbolic systems of equations*, Mathematics of Computation, **24**, 45-56.
- [70] Showalter R.E. and D.B. Visarraga D.B. 2004. *Double-diffusion models from a highly-heterogeneous medium*, Journal of Mathematical Analysis and Applications, **295**, 191-210.
- [71] Showalter R.E. and Walkington N.J. 1991. *Micro-structure models of diffusion in fissured media*, Journal of Mathematical Analysis and Applications, **155**, 1-20.
- [72] Sjögreen B. 2012. *High order finite difference and finite methods for advection on the sphere*, Journal of Scientific Computing. **51**, 703-732.
- [73] Smith G.D. 2004. *Numerical Solution of Partial Differential Equations. Finite Difference Methods*. Oxford University Press, Oxford.
- [74] Spalding D.B. 1972. *A novel finite difference formulation for differential expressions involving both first and second derivatives*, International Journal for Numerical Methods in Engineering, **4**, 551-559.
- [75] Tadmor E. 2012. *A Review of Numerical Methods for Nonlinear Partial Differential Equations*. Bulletin of the American Mathematical Society, **49**, 507-554.
- [76] Toro E. 1999. *Riemann solvers and numerical methods for fluid dynamics. A Practical Introduction*, Springer Verlag, Berlin Heidelberg.
- [77] van der Vorst H. 1992. *Bi-CGSTAB: A Fast and Smoothly Converging Variant of Bi-CG for the Solution of Non-symmetric Linear Systems*. SIAM Journal on Scientific and Statistical Computing, **13**, 631-644.
- [78] van der Vorst H. 2003. *Iterative Krylov Methods for Large Linear Systems*. Cambridge University Press, Cambridge.
- [79] Varadhan S.J., Beaudoin A.J., Acharya A., and Fressengeas C. 2006. *Dislocation transport using an explicit Galerkin/least-squares formulation*. Modelling and simulation in Materials Science and Engineering, **14**, 1245-1270.
- [80] Varga R. 1963. *Matrix Iterative Analysis*. Prentice Hall, Englewood Cliffs.
- [81] Versteeg H. and Malalasekera W. 1995. *An introduction to computational fluid dynamics: The finite volume method*, Prentice Hall, London.
- [82] Wesseling P. 2001. *Principles of computational fluid dynamics*, volume 29 of the Series in Computational Mathematics, Springer Verlag, Berlin Heidelberg.
- [83] Wesseling P. 1973. *On the construction of accurate difference schemes for hyperbolic partial differential equations*, Journal of Engineering Mathematics, **7**, 19-31.
- [84] Wu J. 2008. *Spatial structure: Partial differential equations models*, In Brauer F., van den Driessche P., and Wu J. Eds. Mathematical Epidemiology, volume 1945 of the series Lecture Notes in Mathematics, 191-203. Springer-Verlag, Berlin Heidelberg.
- [85] Yefimov S. and van der Giessen E. 2005. *Multiple slip in a strain-gradient plasticity model motivated by a statistical-mechanics description of dislocations*, International Journal of Solids and Structures, **45**, 3375-3394.
- [86] Yefimov S., Groma I. and van der Giessen E. 2004. *A comparison of a statistical-mechanics based plasticity model with discrete dislocation plasticity calculations*, Journal of the Mechanics and Physics of Solids, **52**, 279-300.
- [87] Zienkiewicz O.C., and Taylor R.L. 2000. *The finite element method Vol. 3: Fluid dynamics*. Butterworth-Heinemann, Oxford.



# Acknowledgments

---

I would like to thank the financial support granted by the European Commission through the two *Erasmus Mundus* grants I received. The first one in order to complete the *Master of Science in Computational Mechanics* and the second in the framework of the *Joint Doctorate in Simulation in Engineering and Entrepreneurship Development* programs. Without such funding the completion of my post-graduate studies would not have been possible.

I want to thank my thesis supervisors, M.G.D Geers, T.J. Massart, and R.H.J. Peerlings, for the opportunity to carry out this work. I highly appreciate their advice and support during these four years. Throughout my career I will be deeply grateful.

I would also like to thank Professors H. Deconinck, G. Degrez, J.G.M. Kuerten, and R. Svendsen, firstly for taking part in my defence committee but mainly for their careful evaluation of this work. Without any doubt their comments, observations and suggestions have substantially improved the quality of this dissertation.

I would like to thank the people who offered me their friendship in Brussels, Nele Van Campfort, Cesyen Cedeño, Mahdi Hatami, Marta Moltedo, Guy Paulus, Gerrit Pierreux, Dominique Pierson, Batoma Sosso, Alexis Tugilimana, and Roland Wintiba. I did enjoy a lot the time I shared with all of them, in the laboratory, in the swimming training and competitions, or just going for a drink or having a meal together. I feel fortunate to have them as friends.

I also thank my friends in Eindhoven Ümit Arabul, Andrés Arias, Priscilla Brandão, Lorenza Henao, Mirosława Lewinska, Awital Mannheim, Siavash Maraghechi, Johanna Melke, Tommaso Ristori, Varun Shah, and Luv Sharma. It has been a pleasure to share time and talks with all them. I would also like to thank the Nayade swimming team, especially Rolijn van Vught and Rik op het Veld who make the training sessions more encouraging.

Mi agradecimiento más profundo es a mi familia, empezando por mis hermanas Ana y Carmen y mis padres Mónico y María Elena, por estar siempre ahí apoyándome y dándome palabras de aliento para salir adelante. A pesar de todas las dificultades que hemos pasado juntos he podido alcanzar mis metas que hago también tuyas; espero que esto los haga sentir orgullosos.



# Curriculum Vitae

---

Héctor Hernández was born in Irapuato, Mexico, on March 1st, 1984. He obtained his Bachelor Degree in Civil Engineering from the University of Guanajuato with the thesis “Numerical simulation of potential and fluid flow”. He has worked during two years in the Research Centre of Mathematics in Guanajuato, Mexico, developing and applying numerical methods for industrial applications. Subsequently, he completed an Erasmus Mundus Master of Science in Computational Mechanics in Swansea University in the United Kingdom and Ecole Centrale de Nantes in France with the thesis “Deflated Krylov Sub-space Methods for the Poisson Pressure Equation”. In 2013, he started an Erasmus Mundus Joint Doctorate Program in the Université libre de Bruxelles (ULB) and Eindhoven University of Technology, which this thesis is the final result of.